TWO HIGHER ORDER ELASTICITY THEORIES: THEIR VARIATIONAL FORMULATIONS AND APPLICATIONS

A Dissertation

by

SUNG KYOON PARK

Submitted to the Office of Graduate Studies of
Texas A&M University
in partial fulfillment of the requirements for the degree of

DOCTOR OF PHILOSOPHY

December 2006

Major Subject: Mechanical Engineering

TWO HIGHER ORDER ELASTICITY THEORIES: THEIR VARIATIONAL FORMULATIONS AND APPLICATIONS

A Dissertation

by

SUNG KYOON PARK

Submitted to the Office of Graduate Studies of
Texas A&M University
in partial fulfillment of the requirements for the degree of

DOCTOR OF PHILOSOPHY

Approved by:

Chair of Committee,	Xin-Lin Gao
Committee Members,	Terry S. Creasy
	Jyhwen Wang
	Anastasia H. Muliana
Head of Department,	Dennis L. O'Neal

December 2006

Major Subject: Mechanical Engineering

ABSTRACT

Two Higher Order Elasticity Theories: Their Variational Formulations and Applications.

(December 2006)

Sung Kyoon Park, B.E., Kookmin University, Korea;

M.S., Hanyang University, Korea

Chair of Advisory Committee: Dr. Xin-Lin Gao

Classical elasticity cannot be used to explain effects related to material microstructures due to its lack of a material length scale parameter. To mitigate this deficiency, higher order elasticity theories have been developed. Two simple higher order theories and their applications are studied in this research. One is a modified couple stress theory and the other is a simplified strain gradient theory, each of which contains only one material length scale parameter in addition to the classical elastic constants. Variational formulations are provided for these two theories by using the principle of minimum total potential energy. In both cases, the governing equations and complete boundary conditions are determined simultaneously for the first time. Also, the displacement form is explicitly derived for each theory for the first time.

The modified couple stress theory is applied to solve a simple shear problem, to develop a new Bernoulli-Euler beam model, and to derive the constitutive relations for hexagonal honeycomb structures, while the simplified strain gradient theory is used to solve the pressurized thick-walled cylinder problem. All these models/solutions are obtained for the first time and supplement their counterparts in classical elasticity.

Numerical results obtained from the newly developed models and derived solutions and their comparisons with their counterpart results in classical elasticity reveal that the higher order theory based models and solutions have the capacity to account for microstructural effects; their counterparts in classical elasticity do not have the same capability. Nevertheless, the former are shown to recover the latter if the microstructural effects are suppressed or ignored.

To my beloved family and God

ACKNOWLEDGMENTS

I would like to thank my advisor, Dr. Xin-Lin Gao, who has academically inspired me to make my own contributions, financially supported me to pursue my dreams, and patiently trained me to be as perfect as I can be. Without his brilliant guidance, insightful instructions and strong encouragement, it would not have been possible for me to complete any part of my dissertation research.

I would also like to express my great appreciation to Dr. Terry Creasy, Dr. Jyhwen Wang and Dr. Anastasia Muliana for serving on my advisory committee and offering me valuable advice and academic support.

The financial support from the U.S. National Science Foundation is also deeply appreciated.

I am also indebted to Dr. Sung Kyu Ha, my M.Sc. advisor at Hanyang University. Without his great help, I could not have come to the United States. Also, I wish to thank Dr. Dong Hoon Choi, who was the head of the iDOT Center in Hanyang University. His precious advice helped me become very sincere for my religion and my study. I also thank Dr. Tae Won Kim who told me about his valuable experience as a Ph.D. student in the U.K.

I am very grateful to Dr. Seung Ik Baek who was always available to help me both as a generous senior and as an excellent scholar. Also, I would like to thank Dr. Ravindran Parag who technically helped me a lot and showed me great kindness.

I also wish to give my special thanks to Dr. Ke Li who helped me both academically and personally even though he got to know me only for a short period of time. Thanks are also due to my first office mate, Mr. Heng Gu, who kindly helped me with many things.

Special thanks are also expressed to my senior schoolmates in HSCL at Hanyang University and my great friends Beverly and Sung Sik in Canada. Their academic and personal help is really appreciated.

I deeply thank my Korean friends and colleagues at Texas A&M University and in

the Korean community families in St. Mary Church. Both of these two groups helped me spiritually and physically when I was in trouble.

Most of all, I would like to give thanks to my lovely mother and father for their endless support and encouragement, to my older brothers and their families for their cheers for me, to my wife, Sun Suk, for her spiritual support, patience and love, and to our baby, “Grace”, from the bottom of my heart.

Finally, my thanks go to the stronger supporter who always exists in my mind.

TABLE OF CONTENTS

Page

CHAPTER Page

LIST OF FIGURES

FIGURE Page

FIGURE Page

CHAPTER I

INTRODUCTION

The classical elasticity theory is well established and has been successfully used to solve many engineering problems. However, this theory is significantly limited by its inability to account for microstructural features of materials due to a lack of any internal material length scale parameter. To describe material responses at the micron and nanometer scales, higher order elasticity theories have been developed.

The contributions by Toupin, Mindlin and Koiter in the early 1960's are instrumental in the development of higher order elasticity theories. In particular, the seminal works by Mindlin and his associates have motivated many subsequent studies. Higher order theories contain internal material length scale parameters in addition to classical elastic constants (Appendix A). The experimental determination of these additional, micro structure-dependent material parameters has proved to be very challenging. Hence, simple higher order elasticity theories involving only one material length scale parameter are highly desirable. Two such theories have recently been proposed by Altan and Aifantis (1997) and Yang et al. (2002). However, systematic and complete mathematical formulations for these two higher order elasticity theories have not been reported in the literature. In addition, the two theories have been applied to solve – heuristically or rigorously – only a few problems. This motivated the research reported in the dissertation.

The rest of this dissertation is organized as follows. In Chapters II, III and IV, a variational formulation and applications of a modified couple stress theory are presented. Chapter V provides a variational formulation of a simplified strain gradient theory and its application to solving a pressurized cylinder problem. The dissertation concludes in Chapter VI. More specific accomplishments in each chapter are detailed below.

In Chapter II, a variational formulation is provided for a modified couple stress

---

This dissertation follows the style and format of Proceedings of the Royal Society of London, Series A-Mathematical Physical and Engineering Sciences.

theory by using the principle of minimum total potential energy, which leads to the simultaneous determination of the equilibrium equations and the boundary conditions. Also, the displacement form of the modified couple stress theory, which is desired for solving many problems, is obtained to supplement the existing stress-based formulation. All equations/expressions are presented in tensorial forms that are coordinate-invariant. As a direct application of the newly obtained displacement form of the theory, a simple shear problem is analytically solved. The solution contains a material length scale parameter and can capture the boundary layer effect, which differs from that based on classical elasticity. The numerical results reveal that the length scale parameter (related to material microstructures) can have a significant effect on material responses.

In Chapter III, a new model for the bending of a Bernoulli-Euler beam is developed using the modified couple stress theory. A variational formulation based on the principle of minimum total potential energy is employed. The new model contains an internal material length scale parameter and can capture the size effect, unlike the classical Bernoulli-Euler beam model. The former reduces to the latter in the absence of the material length scale parameter. As a direct application of the new model, a cantilever beam problem is solved. It is found that the bending rigidity of the cantilever beam predicted by the newly developed model is larger than that predicted by the classical beam model. The difference between the deflections predicted by the two models is very significant when the beam thickness is small, but is diminishing with the increase of the beam thickness. A comparison shows that the predicted size effect agrees fairly well with that observed experimentally.

In Chapter IV, the modified couple stress theory is applied to study mechanical responses of regular honeycomb structures. A finite difference scheme and a homogenization method based on a structural analysis are used to determine effective elastic constants and the constitutive relations for the hexagonal honeycomb structures. A total of six material constants are determined in the current work, including two length scale parameters. This differs from what was reported by Wang and Stronge (1999) using a micropolar elasticity theory.

In Chapter V, a variational formulation is provided for a simplified strain gradient elasticity theory based on the principle of minimum total potential energy, which leads to the simultaneous determination of the governing equations and the complete boundary conditions for the first time. Also, the displacement form of the simplified strain gradient theory is derived here and directly used to solve the problem of a pressurized thick-walled cylinder. A comparison with Lamé's solution in classical elasticity shows that the newly derived strain gradient solution contains an additional material length scale parameter and can account for the microstructural effects, while Lamé's solution does not have the same capability.

In Chapter VI, an overall summary of the dissertation research is provided together with relevant remarks.

CHAPTER II

VARIATIONAL FORMULATION OF A MODIFIED COUPLE STRESS THEORY AND ITS APPLICATION TO A SIMPLE SHEAR PROBLEM*

2.1. INTRODUCTION

Lacking an internal material length scale parameter, classical elasticity and plasticity cannot be used to interpret the size effect observed in numerous tests at micron and nanometer scales. However, higher-order (non-local) continuum theories contain material length scale parameters and are capable of explaining microstructure related size (and other) effects. Couple stress theories represent one class of such higher-order theories.

The classical couple stress elasticity theory (e.g., Toupin, 1962, 1964; Mindlin and Tiersten, 1962; Mindlin, 1963; Koiter, 1964) contains four material constants (two classical and two additional) for isotropic elastic materials. The two additional constants are related to the underlying microstructure of the material and are inherently difficult to determine (e.g., Yang and Lakes, 1982; Lam et al., 2003). Hence, there has been a need to develop higher-order theories involving only one additional material length scale parameter.

One such elasticity theory has been proposed by Yang et al. (2002) through modifying the classical couple stress theory. Compared to the classical theory, the modified theory has two advantages: the couple stress tensor being symmetric, and only one internal length scale parameter involved. These features make the modified couple stress theory easier to use. For example, a new model for the bending of a Bernoulli-Euler beam has recently been developed in Park and Gao (2006) using this modified theory, which is presented in Chapter III. However, some important aspects of the

* To appear in Zeitschrift fur Angewandte Mathematik und Physik (accepted September 2006).

modified couple stress theory were not covered in Yang et al. (2002). For instance, the boundary conditions were not derived, and the displacement form of the theory was not considered in Yang et al. (2002). Therefore, further studies are still needed to better understand and apply the modified couple stress theory.

In response to this need, a variational formulation of the modified couple stress theory is presented in Section 2.2 using the principle of minimum total potential energy, which leads to the simultaneous determination of the equilibrium equations and the boundary conditions. This complements the original work of Yang et al. (2002), where the boundary conditions were not derived. Also, the displacement form of the governing equations is developed in Section 2.3, which supplements the formulation of Yang et al. (2002). As a direct application of the newly obtained displacement form of the modified couple stress theory, a simple shear problem is analytically solved in Section 2.4. Sample numerical results are also presented there to illustrate the new solution, which contains an internal material length scale, and to compare it with the classical elasticity based solution. The chapter concludes with a summary in Section 2.5.

2.2. VARIATIONAL FORMULATION

Following Yang et al. (2002), the strain energy density w for an isotropic elastic material is taken to be a function of both strain (conjugated with stress) and curvature (conjugated with couple stress):

$$w = w(\boldsymbol{\varepsilon}, \boldsymbol{\chi}) = \frac{1}{2}\lambda(\mathrm{tr}\boldsymbol{\varepsilon})^2 + \mu\left(\boldsymbol{\varepsilon} : \boldsymbol{\varepsilon} + l^2 \boldsymbol{\chi} : \boldsymbol{\chi}\right), \tag{2.1}$$

where λ and μ are the Lamé constants, l is a material length scale parameter, and $\boldsymbol{\varepsilon}$, $\boldsymbol{\chi}$ are, respectively, the strain and curvature tensors given by

$$\boldsymbol{\varepsilon} = \frac{1}{2}\left[\nabla \mathbf{u} + (\nabla \mathbf{u})^{\mathrm{T}}\right], \tag{2.2}$$

$$\boldsymbol{\chi} = \frac{1}{2}\left[\nabla \boldsymbol{\theta} + (\nabla \boldsymbol{\theta})^{\mathrm{T}}\right], \tag{2.3}$$

with $\mathbf{u}$ being the displacement vector and $\boldsymbol{\theta}$ the rotation vector defined as

$$\boldsymbol{\theta} = \frac{1}{2}\mathrm{curl}\,\mathbf{u}\,. \tag{2.4}$$

Clearly, Eq. (2.3) shows that $\boldsymbol{\chi}$, called the symmetric curvature tensor in [8], is symmetric with $\boldsymbol{\chi}^{\mathrm{T}} = \boldsymbol{\chi}$. Then, the strain energy U in the region Ω of a deformed isotropic elastic body can be written as

$$U = \int_{\Omega} w\,dv = \frac{1}{2}\int_{\Omega} (\boldsymbol{\sigma} : \boldsymbol{\varepsilon} + \mathbf{m} : \boldsymbol{\chi})\,dv, \tag{2.5}$$

where $\boldsymbol{\sigma}$ and $\mathbf{m}$ are, respectively, the stress tensor (conjugated to $\boldsymbol{\varepsilon}$) and the deviatoric part of the couple stress tensor (conjugated to $\boldsymbol{\chi}$) given by

$$\boldsymbol{\sigma} = \lambda\,\mathrm{tr}(\boldsymbol{\varepsilon})\mathbf{I} + 2\mu\boldsymbol{\varepsilon}, \tag{2.6}$$

$$\mathbf{m} = 2\mu l^2 \boldsymbol{\chi}. \tag{2.7}$$

It is seen from Eqs. (2.3) and (2.7) that $\mathbf{m}$ involved in Eq. (2.5) is symmetric with $\mathbf{m}^{\mathrm{T}} = \mathbf{m}$, which differs from that in the classical couple stress theory (e.g., Koiter, 1964) and subsequently leads to a modified couple stress theory.

The work done by external forces on the deformed elastic body occupying region Ω is

$$W = \int_{\Omega} (\mathbf{f}\cdot\mathbf{u} + \mathbf{y}\cdot\boldsymbol{\theta})\,dv + \int_{\partial\Omega} (\mathbf{t}\cdot\mathbf{u} + \mathbf{c}\cdot\boldsymbol{\theta})\,da, \tag{2.8}$$

where $\mathbf{f}$, $\mathbf{y}$, $\mathbf{t}$ and $\mathbf{c}$ are, respectively, the body force, body couple, traction and surface couple, and $\partial\Omega$ is the surface of Ω.

From Eqs. (2.5) and (2.8) it follows that the total potential energy Π is

$$\Pi = U - W = \frac{1}{2}\int_{\Omega} (\boldsymbol{\sigma} : \boldsymbol{\varepsilon} + \mathbf{m} : \boldsymbol{\chi})\,dv - \int_{\Omega} (\mathbf{f}\cdot\mathbf{u} + \mathbf{y}\cdot\boldsymbol{\theta})\,dv - \int_{\partial\Omega} (\mathbf{t}\cdot\mathbf{u} + \mathbf{c}\cdot\boldsymbol{\theta})\,da. \tag{2.9}$$

Taking the first variation of Π gives

$$\delta\Pi = \int_{\Omega} (\boldsymbol{\sigma} : \delta\boldsymbol{\varepsilon} + \mathbf{m} : \delta\boldsymbol{\chi})\,dv - \int_{\Omega} (\mathbf{f}\cdot\delta\mathbf{u} + \mathbf{y}\cdot\delta\boldsymbol{\theta})\,dv - \int_{\partial\Omega} (\mathbf{t}\cdot\delta\mathbf{u} + \mathbf{c}\cdot\delta\boldsymbol{\theta})\,da. \tag{2.10}$$

Using Eqs. (2.2) and (2.3) and noting the symmetry of $\boldsymbol{\sigma}$, $\mathbf{m}$, $\boldsymbol{\varepsilon}$ and $\boldsymbol{\chi}$ will yield

$$\int_{\Omega} (\boldsymbol{\sigma} : \delta\boldsymbol{\varepsilon} + \mathbf{m} : \delta\boldsymbol{\chi})\,dv = \int_{\Omega} \left[\mathrm{div}(\boldsymbol{\sigma}^{\mathrm{T}}\delta\mathbf{u}) - (\mathrm{div}\boldsymbol{\sigma})\cdot\delta\mathbf{u} + \mathrm{div}(\mathbf{m}^{\mathrm{T}}\delta\boldsymbol{\theta}) - (\mathrm{div}\mathbf{m})\cdot\delta\boldsymbol{\theta}\right] dv, \tag{2.11}$$

which, upon applying the divergence theorem, becomes

$$\int_\Omega (\boldsymbol{\sigma} : \delta\boldsymbol{\varepsilon} + \mathbf{m} : \delta\boldsymbol{\chi})\, dv = \int_{\partial\Omega} \left[(\boldsymbol{\sigma}\mathbf{n})\cdot\delta\mathbf{u} + (\mathbf{m}\mathbf{n})\cdot\delta\boldsymbol{\theta}\right] da - \int_\Omega \left[(\mathrm{div}\boldsymbol{\sigma})\cdot\delta\mathbf{u} + (\mathrm{div}\mathbf{m})\cdot\delta\boldsymbol{\theta}\right] dv, \tag{2.12}$$

where $\mathbf{n}$ is the unit (outward) vector normal to the surface. Substituting Eq. (2.12) into Eq. (2.10) then results in

$$\delta\Pi = -\int_\Omega (\mathrm{div}\boldsymbol{\sigma} + \mathbf{f})\cdot\delta\mathbf{u}\, dv - \int_\Omega (\mathrm{div}\mathbf{m} + \mathbf{y})\cdot\delta\boldsymbol{\theta}\, dv + \int_{\partial\Omega} (\boldsymbol{\sigma}\mathbf{n} - \mathbf{t})\cdot\delta\mathbf{u}\, da + \int_{\partial\Omega} (\mathbf{m}\mathbf{n} - \mathbf{c})\cdot\delta\boldsymbol{\theta}\, da. \tag{2.13}$$

Using Eq. (2.4) gives

$$\int_\Omega (\mathrm{div}\mathbf{m} + \mathbf{y})\cdot\delta\boldsymbol{\theta}\, dv = \frac{1}{2}\int_\Omega \mathrm{curl}(\mathrm{div}\mathbf{m} + \mathbf{y})\cdot(\delta\mathbf{u})\, dv - \frac{1}{2}\int_\Omega \mathrm{div}\left[(\mathrm{div}\mathbf{m} + \mathbf{y})\times(\delta\mathbf{u})\right] dv, \tag{2.14}$$

which, after applying the divergence theorem, becomes

$$\int_\Omega (\mathrm{div}\mathbf{m} + \mathbf{y})\cdot\delta\boldsymbol{\theta}\, dv = \frac{1}{2}\int_\Omega \mathrm{curl}(\mathrm{div}\mathbf{m} + \mathbf{y})\cdot(\delta\mathbf{u})\, dv - \frac{1}{2}\int_{\partial\Omega} \mathbf{n}\cdot\left[(\mathrm{div}\mathbf{m} + \mathbf{y})\times(\delta\mathbf{u})\right] da. \tag{2.15}$$

Inserting Eq. (2.15) into Eq. (2.13) leads to

$$\delta\Pi = -\int_\Omega \left[\mathrm{div}\boldsymbol{\sigma} + \frac{1}{2}\mathrm{curl}(\mathrm{div}\mathbf{m} + \mathbf{y}) + \mathbf{f}\right]\cdot\delta\mathbf{u}\, dv - \int_{\partial\Omega}\left[\mathbf{t} - \boldsymbol{\sigma}\mathbf{n} - \frac{1}{2}\mathbf{n}\times(\mathrm{div}\mathbf{m} + \mathbf{y})\right]\cdot\delta\mathbf{u}\, da$$
$$- \int_{\partial\Omega} (\mathbf{c} - \mathbf{m}\mathbf{n})\cdot\delta\boldsymbol{\theta}\, da. \tag{2.16}$$

Note that the rotation vector $\boldsymbol{\theta}$ on the surface can be decomposed into two components as (e.g., Koiter, 1964)

$$\boldsymbol{\theta} = \boldsymbol{\theta}^{\mathrm{n}} + \boldsymbol{\theta}^{\mathrm{t}} \equiv (\boldsymbol{\theta}\cdot\mathbf{n})\mathbf{n} + (\mathbf{I} - \mathbf{n}\otimes\mathbf{n})\boldsymbol{\theta}, \tag{2.17}$$

where $\boldsymbol{\theta}^{\mathrm{n}}$ is the normal component along $\mathbf{n}$ direction, and $\boldsymbol{\theta}^{\mathrm{t}}$ is the projection component tangential to the surface. Taking the first variation of the two components defined in Eq. (2.17) gives

$$\delta\boldsymbol{\theta}^{\mathrm{n}} = (\delta\boldsymbol{\theta}\cdot\mathbf{n})\mathbf{n} + (\boldsymbol{\theta}\cdot\delta\mathbf{n})\mathbf{n} + (\boldsymbol{\theta}\cdot\mathbf{n})\delta\mathbf{n}, \tag{2.18a}$$

$$\delta\boldsymbol{\theta}^{\mathrm{t}} = \delta\boldsymbol{\theta} - (\delta\boldsymbol{\theta}\cdot\mathbf{n})\mathbf{n} - (\boldsymbol{\theta}\cdot\delta\mathbf{n})\mathbf{n} - (\boldsymbol{\theta}\cdot\mathbf{n})\delta\mathbf{n}. \tag{2.18b}$$

Using Eq. (2.18a) yields

$$\int_{\partial\Omega}(\mathbf{c}-\mathbf{mn})\cdot\delta\boldsymbol{\theta}^{\mathrm{n}}\,da=\int_{\partial\Omega}\left[(\mathbf{c}-\mathbf{mn})\cdot\mathbf{n}\right](\mathbf{n}\cdot\delta\boldsymbol{\theta})\,da \\ +\int_{\partial\Omega}\left\{\left[(\mathbf{c}-\mathbf{mn})\cdot\mathbf{n}\right](\boldsymbol{\theta}\cdot\delta\mathbf{n})+\left[(\mathbf{c}-\mathbf{mn})\cdot\delta\mathbf{n}\right](\boldsymbol{\theta}\cdot\mathbf{n})\right\}da. \tag{2.19}$$

The use of Eq. (2.4) leads to

$$\int_{\partial\Omega}\left[(\mathbf{c}-\mathbf{mn})\cdot\mathbf{n}\right](\mathbf{n}\cdot\delta\boldsymbol{\theta})\,da \\ =\frac{1}{2}\int_{\partial\Omega}\mathbf{n}\cdot\mathrm{curl}\left[(\mathbf{c}\cdot\mathbf{n}-\mathbf{m}:\mathbf{n}\otimes\mathbf{n})\delta\mathbf{u}\right]da-\frac{1}{2}\int_{\partial\Omega}\left[\mathbf{n}\times\nabla(\mathbf{c}\cdot\mathbf{n}-\mathbf{m}:\mathbf{n}\otimes\mathbf{n})\right]\cdot\delta\mathbf{u}\,da. \tag{2.20}$$

By Stoke's theorem,

$$\int_{\partial\Omega}\mathbf{n}\cdot\mathrm{curl}\left[(\mathbf{c}\cdot\mathbf{n}-\mathbf{m}:\mathbf{n}\otimes\mathbf{n})\delta\mathbf{u}\right]da=\oint_{\Gamma}\left[(\mathbf{c}\cdot\mathbf{n}-\mathbf{m}:\mathbf{n}\otimes\mathbf{n})\delta\mathbf{u}\right]\cdot\mathbf{v}\,dl, \tag{2.21}$$

where $\mathbf{v}$ is the unit vector tangential to the closed curve Γ that bounds $\partial\Omega$ whose unit outward normal is $\mathbf{n}$. Using Eqs. (2.20) and (2.21) in Eq. (2.19) then gives

$$\int_{\partial\Omega}(\mathbf{c}-\mathbf{mn})\cdot\delta\boldsymbol{\theta}^{\mathrm{n}}\,da=\frac{1}{2}\oint_{\Gamma}\left[(\mathbf{c}\cdot\mathbf{n}-\mathbf{m}:\mathbf{n}\otimes\mathbf{n})\delta\mathbf{u}\right]\cdot\mathbf{v}\,dl-\frac{1}{2}\int_{\partial\Omega}\left[\mathbf{n}\times\nabla(\mathbf{c}\cdot\mathbf{n}-\mathbf{m}:\mathbf{n}\otimes\mathbf{n})\right]\cdot\delta\mathbf{u}\,da \\ +\int_{\partial\Omega}\left\{\left[(\mathbf{c}-\mathbf{mn})\cdot\mathbf{n}\right](\boldsymbol{\theta}\cdot\delta\mathbf{n})+\left[(\mathbf{c}-\mathbf{mn})\cdot\delta\mathbf{n}\right](\boldsymbol{\theta}\cdot\mathbf{n})\right\}da. \tag{2.22}$$

Similarly, applying Eq. (2.18b) results in

$$\int_{\partial\Omega}(\mathbf{c}-\mathbf{mn})\cdot\delta\boldsymbol{\theta}^{\mathrm{t}}\,da=\int_{\partial\Omega}\left[\mathbf{c}-(\mathbf{c}\cdot\mathbf{n})\mathbf{n}-\mathbf{mn}+(\mathbf{m}:\mathbf{n}\otimes\mathbf{n})\mathbf{n}\right]\cdot\delta\boldsymbol{\theta}\,da \\ -\int_{\partial\Omega}\left\{\left[(\mathbf{c}-\mathbf{mn})\cdot\mathbf{n}\right](\boldsymbol{\theta}\cdot\delta\mathbf{n})+\left[(\mathbf{c}-\mathbf{mn})\cdot\delta\mathbf{n}\right](\boldsymbol{\theta}\cdot\mathbf{n})\right\}da. \tag{2.23}$$

From Eqs. (2.17), (2.22) and (2.23) it then follows that

$$\int_{\partial\Omega}(\mathbf{c}-\mathbf{mn})\cdot\delta\boldsymbol{\theta}\,da=\frac{1}{2}\oint_{\Gamma}\left[(\mathbf{c}\cdot\mathbf{n}-\mathbf{m}:\mathbf{n}\otimes\mathbf{n})\delta\mathbf{u}\right]\cdot\mathbf{v}\,dl-\frac{1}{2}\int_{\partial\Omega}\left[\mathbf{n}\times\nabla(\mathbf{c}\cdot\mathbf{n}-\mathbf{m}:\mathbf{n}\otimes\mathbf{n})\right]\cdot\delta\mathbf{u}\,da \\ +\int_{\partial\Omega}\left[\mathbf{c}-(\mathbf{c}\cdot\mathbf{n})\mathbf{n}-\mathbf{mn}+(\mathbf{m}:\mathbf{n}\otimes\mathbf{n})\mathbf{n}\right]\cdot\delta\boldsymbol{\theta}\,da. \tag{2.24}$$

Inserting Eq. (2.24) into Eq. (2.16) then gives

$$\delta\Pi=-\int_{\Omega}\left[\mathrm{div}\boldsymbol{\sigma}+\frac{1}{2}\mathrm{curl}(\mathrm{div}\mathbf{m}+\mathbf{y})+\mathbf{f}\right]\cdot\delta\mathbf{u}\,dv-\frac{1}{2}\oint_{\Gamma}\left[(\mathbf{c}\cdot\mathbf{n}-\mathbf{m}:\mathbf{n}\otimes\mathbf{n})\delta\mathbf{u}\right]\cdot\mathbf{v}\,dl \\ -\int_{\partial\Omega}\left\{\mathbf{t}-\frac{1}{2}\mathbf{n}\times\nabla(\mathbf{c}\cdot\mathbf{n})-\boldsymbol{\sigma}\mathbf{n}-\frac{1}{2}\mathbf{n}\times\left[\mathrm{div}\mathbf{m}-\nabla(\mathbf{m}:\mathbf{n}\otimes\mathbf{n})+\mathbf{y}\right]\right\}\cdot\delta\mathbf{u}\,da \\ -\int_{\partial\Omega}\left[\mathbf{c}-(\mathbf{c}\cdot\mathbf{n})\mathbf{n}-\mathbf{mn}+(\mathbf{m}:\mathbf{n}\otimes\mathbf{n})\mathbf{n}\right]\cdot\delta\boldsymbol{\theta}\,da. \tag{2.25}$$

By applying the principle of total minimum potential energy, i.e., $\delta\Pi = 0$ for the

stable equilibrium, and the fundamental lemma of the calculus of variation (e.g., Gao and Mall, 2001), the governing (equilibrium) equations are obtained as

$$\mathrm{div}\boldsymbol{\sigma} + \frac{1}{2}\mathrm{curl}(\mathrm{div}\mathbf{m} + \mathbf{y}) + \mathbf{f} = \mathbf{0} \tag{2.26}$$

for all points in Ω, and the boundary conditions as

$$\left.\begin{aligned} &\boldsymbol{\sigma}\mathbf{n} + \frac{1}{2}\mathbf{n}\times\left[\mathrm{div}\mathbf{m} - \nabla(\mathbf{m}:\mathbf{n}\otimes\mathbf{n}) + \mathbf{y}\right] = \mathbf{t} - \frac{1}{2}\mathbf{n}\times\nabla(\mathbf{c}\cdot\mathbf{n}) \quad \text{or} \quad \mathbf{u} = \bar{\mathbf{u}}, \\ &\mathbf{m}\mathbf{n} - (\mathbf{m}:\mathbf{n}\otimes\mathbf{n})\mathbf{n} = \mathbf{c} - (\mathbf{c}\cdot\mathbf{n})\mathbf{n} \quad \text{or} \quad \boldsymbol{\theta} = \bar{\boldsymbol{\theta}} \end{aligned}\right\} \tag{2.27a,b}$$

for all points on ∂Ω that is smooth, and

$$\frac{1}{2}\left[(\mathbf{m}:\mathbf{n}\otimes\mathbf{n})_{+} - (\mathbf{m}:\mathbf{n}\otimes\mathbf{n})_{-}\right] = \frac{1}{2}\left[(\mathbf{c}\cdot\mathbf{n})_{+} - (\mathbf{c}\cdot\mathbf{n})_{-}\right] \quad \text{or} \quad \mathbf{u}\cdot\mathbf{v} = \bar{\mathrm{u}}^{\mathrm{v}} \tag{2.27c}$$

for all points along Γ**,** which is an edge between two smooth boundary surfaces, with one denoted as "+" and the other as "–". In Eqs. (2.27a–c), the overbar represents the prescribed value, and the superscript "v" stands for the component along the tangential direction with the unit vector **v** (i.e., $\bar{\mathrm{u}}^{\mathrm{v}} \equiv \bar{\mathbf{u}}\cdot\mathbf{v}$).

It can be readily shown that the equilibrium equations given in Eq. (2.26) are the same as those provided in Yang et al. (2002) based on the conservation of momenta, which was used earlier by Koiter (1964). Also, the boundary conditions (B.C.'s) obtained in Eqs. (2.27a–c) are the same as those derived by Koiter (1964) for the classical couple stress theory using the virtual work principle and index notation. These B.C.'s were not derived for the modified couple stress theory in Yang et al. (2002), where they were simply quoted from Koiter (1964). The only difference between the B.C.'s derived here in Eqs. (2.27a–c) and those listed in Yang et al (2002) is that $\boldsymbol{\theta}^{\mathrm{t}}$ there is now replaced by **θ** in Eq. (2.27b). Note that the material length scale parameter *l* is involved in the modified couple stress theory (see Eqs. (2.26) and (2.27a–c)) through **m** (see Eq. (2.7)).

For isotropic elastic materials in the absence of couple stress, body couple and surface couple, i.e., $l = 0$, $\mathbf{y} = \mathbf{0}$ and $\mathbf{c} = \mathbf{0}$, Eqs. (2.26) and (2.27a–c) reduce to

$$\begin{aligned} &\mathrm{div}\boldsymbol{\sigma} + \mathbf{f} = \mathbf{0} \qquad \text{in } \Omega, \\ &\mathbf{t} = \boldsymbol{\sigma}\mathbf{n} \quad \text{or} \quad \mathbf{u} = \bar{\mathbf{u}} \quad \text{on } \partial\Omega, \end{aligned} \tag{2.28}$$

where $\boldsymbol{\sigma}$ (= $\boldsymbol{\sigma}^{\mathrm{T}}$) is the Cauchy stress tensor satisfying Eq. (2.6). Eq. (2.28), together with Eqs. (2.2) and (2.6), defines the boundary value problem (in its general form) in classical elasticity (e.g., Little, 1973; Slaughter, 2002).

2.3. DISPLACEMENT FORM

To supplement the stress-based formulation presented in the preceding section and that in Yang et al. (2002), the displacement form of the modified couple stress theory is derived below in this section.

Using Eqs. (2.2) – (2.4) in Eqs. (2.6) and (2.7) gives

$$\boldsymbol{\sigma} = \lambda(\mathrm{div}\mathbf{u})\mathbf{I} + \mu[\nabla\mathbf{u} + (\nabla\mathbf{u})^{\mathrm{T}}], \tag{2.29}$$

$$\mathbf{m} = \frac{1}{2}\mu l^2\left\{\nabla(\mathrm{curl}\,\mathbf{u}) + [\nabla(\mathrm{curl}\,\mathbf{u})]^{\mathrm{T}}\right\}. \tag{2.30}$$

It follows from Eq. (2.29) that

$$\mathrm{div}\boldsymbol{\sigma} = (\lambda + 2\mu)\nabla(\mathrm{div}\mathbf{u}) - \mu\,\mathrm{curl}(\mathrm{curl}\,\mathbf{u}), \tag{2.31}$$

where use has been made of the identity $\nabla^2\mathbf{u} = \nabla(\mathrm{div}\mathbf{u}) - \mathrm{curl}(\mathrm{curl}\,\mathbf{u})$.

Similarly, taking divergence on Eq. (2.30) yields

$$\mathrm{div}\,\mathbf{m} = \frac{1}{2}\mu l^2\left\{\nabla^2(\mathrm{curl}\,\mathbf{u}) + \mathrm{div}[\nabla(\mathrm{curl}\,\mathbf{u})]^{\mathrm{T}}\right\}, \tag{2.32}$$

which becomes, after taking curl and using the identity $\mathrm{curl}\{\mathrm{div}[\nabla(\mathrm{curl}\mathbf{u})]^{\mathrm{T}}\} = \mathrm{div}\{\mathrm{curl}[\nabla(\mathrm{curl}\,\mathbf{u})]\}$,

$$\mathrm{curl}(\mathrm{div}\,\mathbf{m}) = \frac{1}{2}\mu l^2\left\{\mathrm{curl}[\nabla^2(\mathrm{curl}\,\mathbf{u})] + \mathrm{div}\,\mathrm{curl}[\nabla(\mathrm{curl}\,\mathbf{u})]\right\}. \tag{2.33}$$

Using the identity $\mathrm{curl}[\nabla(\mathrm{curl}\,\mathbf{u})] = \mathbf{0}$ (e.g., Slaughter, 2002) in Eq. (2.33) gives

$$\mathrm{curl}(\mathrm{div}\,\mathbf{m}) = \frac{1}{2}\mu l^2\,\mathrm{curl}\left[\nabla^2(\mathrm{curl}\,\mathbf{u})\right]. \tag{2.34}$$

Substituting Eqs. (2.31) and (2.34) into Eq. (2.26) then results in

$$(\lambda + 2\mu)\nabla(\mathrm{div}\mathbf{u}) - \mu\,\mathrm{curl}\left[\mathrm{curl}\,\mathbf{u} - \left(\frac{l}{2}\right)^2\nabla^2(\mathrm{curl}\,\mathbf{u})\right] + \frac{1}{2}\mathrm{curl}\,\mathbf{y} + \mathbf{f} = \mathbf{0} \tag{2.35}$$

as the equilibrium equations in terms of the displacement $\mathbf{u}$. Clearly, the material length

scale parameter l is explicitly involved in Eq. (2.35) (the governing equations) in addition to the two elastic constants λ and μ. This differs from that in the stress-based formulation discussed in Section 2.2.

For isotropic elastic materials without couple stress and body couple, $l = 0$ and $\mathbf{y} = \mathbf{0}$ and Eq. (2.35) reduces to

$$(\lambda + 2\mu)\nabla(\text{div}\mathbf{u}) - \mu\,\text{curl}(\text{curl}\mathbf{u}) + \mathbf{f} = \mathbf{0}, \tag{2.36}$$

which are the well-known Navier equations in classical elasticity (e.g., Little, 1973). A comparison of the displacement formulation with the stress formulation in classical elasticity can be found in Gao and Rowlands (2000).

The equilibrium equations given in Eq. (2.35) together with the boundary conditions listed in Eqs. (2.27a–c) define the boundary value problem in the displacement formulation of the modified couple stress theory. This formulation was not considered in Yang et al. (2002).

2.4. SIMPLE SHEAR PROBLEM

As a direct application of the displacement form of the modified couple stress theory obtained in the preceding section, a simple shear problem is solved here. Due to its simplicity, this problem (or its variants) has recently been studied analytically or computationally as a benchmark problem (e.g., Teneketzis Tenek and Aifantis, 2001; Diebels and Steeb, 2002; Horstemeyer et al., 2003; Tekoglu and Onck, 2005).

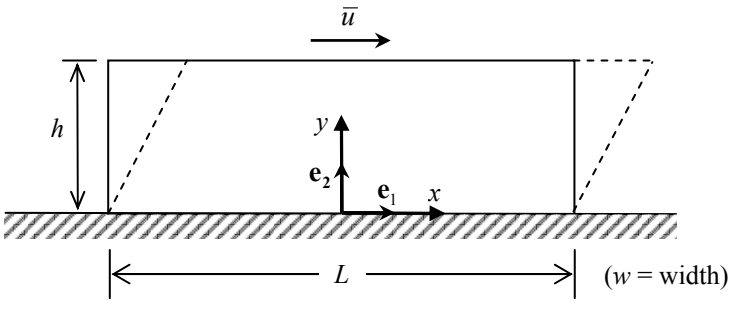

Fig. 2.1. Simple shear problem.

Consider a block of width w, length L, and height h undergoing a simple shear deformation, as shown in Fig. 2.1. Assume that w and L are much larger than h such that they both can be viewed as infinite. The prescribed displacement $\bar{u}$ (at $y = h$) is induced by a shear force acting on the top surface $y = h$. The Cartesian coordinate system shown in the figure will be used in the formulation below.

The displacement $\mathbf{u}$ in the block is taken to be

$$\mathbf{u} = u(y)\mathbf{e}_1, \tag{2.37}$$

where $u(y) = \mathbf{u} \cdot \mathbf{e}_1$ is the only non-vanishing component of the displacement vector. It follows from Eq. (2.37) that

$$\mathrm{div}\mathbf{u} = 0, \quad \mathrm{curl}\mathbf{u} = -\frac{du}{dy}\mathbf{e}_3. \tag{2.38}$$

Using Eq. (2.38) in Eq. (2.35), the displacement form of the governing equations, then gives, in the absence of body force and body couple (i.e., $\mathbf{f} = \mathbf{0}$ and $\mathbf{y} = \mathbf{0}$),

$$\mathrm{curl}(\mathrm{curl}\mathbf{u}) - \frac{l^2}{4}\mathrm{curl}[\nabla^2(\mathrm{curl}\mathbf{u})] = \mathbf{0}, \tag{2.39}$$

where

$$\mathrm{curl}(\mathrm{curl}\mathbf{u}) = \begin{vmatrix} \mathbf{e}_1 & \mathbf{e}_2 & \mathbf{e}_3 \\ \partial/\partial x & \partial/\partial y & \partial/\partial z \\ 0 & 0 & -u' \end{vmatrix} = -\frac{d^2u}{dy^2}\mathbf{e}_1, \tag{2.40}$$

$$\mathrm{curl}\left[\nabla^2(\mathrm{curl}\mathbf{u})\right] = \begin{vmatrix} \mathbf{e}_1 & \mathbf{e}_2 & \mathbf{e}_3 \\ \partial/\partial x & \partial/\partial y & \partial/\partial z \\ 0 & 0 & -u''' \end{vmatrix} = -\frac{d^4u}{dy^4}\mathbf{e}_1. \tag{2.41}$$

Substituting Eqs. (2.40) and (2.41) into Eq. (2.39) leads to

$$\frac{d^2u}{dy^2} - \left(\frac{l}{2}\right)^2 \frac{d^4u}{dy^4} = 0 \tag{2.42}$$

as the governing equation for determining $u(y)$. The general solution of this homogeneous fourth-order ordinary differential equation (with $l \neq 0$) can be readily obtained as

$$u(y) = C_1 + C_2 y + C_3 e^{\frac{2}{l}y} + C_4 e^{-\frac{2}{l}y}, \tag{2.43}$$

where $C_1 - C_4$ are four integration constants to be determined from boundary conditions.

Using Eq. (2.37) in Eq. (2.2) gives

$$\boldsymbol{\varepsilon} = \frac{1}{2}\frac{du}{dy}\left(\mathbf{e}_1 \otimes \mathbf{e}_2 + \mathbf{e}_2 \otimes \mathbf{e}_1\right), \tag{2.44}$$

which shows that tr($\boldsymbol{\varepsilon}$) = 0. Then, it follows from Eqs. (2.6) and (2.44) that

$$\boldsymbol{\sigma} = \mu\frac{du}{dy}\left(\mathbf{e}_1 \otimes \mathbf{e}_2 + \mathbf{e}_2 \otimes \mathbf{e}_1\right). \tag{2.45}$$

The boundary conditions of the current problem are, based on Eqs. (2.27a,b),

$$\mathbf{u}\big|_{y=0} = \mathbf{0}, \tag{2.46a}$$

$$\boldsymbol{\theta}\big|_{y=0} = \mathbf{0}, \tag{2.46b}$$

$$\mathbf{u}\big|_{y=h} = \bar{u}\,\mathbf{e}_1, \tag{2.46c}$$

$$\boldsymbol{\theta}\big|_{y=h} = \mathbf{0}, \tag{2.46d}$$

where the rotation $\boldsymbol{\theta}$ is obtained from Eqs. (2.4) and (2.38) as

$$\boldsymbol{\theta} = \frac{1}{2}\mathrm{curl}\mathbf{u} = -\frac{1}{2}\frac{du}{dy}\mathbf{e}_3. \tag{2.47}$$

Note that there is no edge here because of the assumed $w \to \infty$ and $L \to \infty$. This excludes the boundary conditions listed in Eq. (2.27c).

Using Eqs. (2.4), (2.37), (2.38) and (2.43) in Eqs. (2.46a-d) then gives

$$C_1 + C_3 + C_4 = 0, \tag{2.48a}$$

$$C_2 + \frac{2}{l}C_3 - \frac{2}{l}C_4 = 0, \tag{2.48b}$$

$$C_1 + C_2 h + C_3 e^{\frac{2}{l}h} + C_4 e^{-\frac{2}{l}h} = \bar{u}, \tag{2.48c}$$

$$C_2 + \frac{2}{l}C_3 e^{\frac{2}{l}h} - \frac{2}{l}C_4 e^{-\frac{2}{l}h} = 0. \tag{2.48d}$$

Solving this system of four linear algebraic equations for $C_1 - C_4$ yields

$$C_1 = \frac{\bar{u}\left(e^{-\frac{2}{l}h} + e^{\frac{2}{l}h} - 2\right)}{2\left[-2 + \left(1+\frac{h}{l}\right)e^{-\frac{2}{l}h} + \left(1-\frac{h}{l}\right)e^{\frac{2}{l}h}\right]}, \tag{2.49a}$$

$$C_2 = \frac{\bar{u}\left(e^{-\frac{2}{l}h} - e^{\frac{2}{l}h}\right)}{l\left[-2 + \left(1+\frac{h}{l}\right)e^{-\frac{2}{l}h} + \left(1-\frac{h}{l}\right)e^{\frac{2}{l}h}\right]}, \tag{2.49b}$$

$$C_3 = \frac{\bar{u}\,(1-e^{-\frac{2}{l}h})}{2\left[-2 + \left(1+\frac{h}{l}\right)e^{-\frac{2}{l}h} + \left(1-\frac{h}{l}\right)e^{\frac{2}{l}h}\right]}, \tag{2.49c}$$

$$C_4 = \frac{\bar{u}\,(1-e^{\frac{2}{l}h})}{2\left[-2 + \left(1+\frac{h}{l}\right)e^{-\frac{2}{l}h} + \left(1-\frac{h}{l}\right)e^{\frac{2}{l}h}\right]}. \tag{2.49d}$$

The substitution of Eqs. (2.49a-d) into Eq. (2.43) will then give the closed-form expression of $u(y)$, thereby completing the solution of the simple shear problem based on the modified couple stress theory. Clearly, this solution contains a material length scale parameter (l) and hence has the capacity to account for microstructure-related effects. When $l = 0$ (i.e., in the absence of couple stress), Eq. (2.42) reduces to

$$\frac{d^2u}{dy^2} = 0, \tag{2.50}$$

whose solution is given by

$$u(y) = d_1 + d_2 y, \tag{2.51}$$

with d_1 and d_2 being two integration constants. The two needed boundary conditions are now simply (see Eqs. (2.28) and (2.37))

$$u\big|_{y=0} = 0, \quad u\big|_{y=h} = \bar{u}. \tag{2.52}$$

Using Eq. (2.51) in Eq. (2.52) then yields

$$u(y) = \frac{\bar{u}}{h} y \tag{2.53}$$

as the non-vanishing displacement component in the block. The substitution of Eq. (2.53) into Eqs. (2.37), (2.44) and (2.45) finally gives the complete classical elasticity solution of the simple shear problem shown in Fig. 2.1 as

$$\mathbf{u} = \frac{\bar{u}}{h} y \mathbf{e}_1, \quad \boldsymbol{\varepsilon} = \frac{\bar{u}}{2h} (\mathbf{e}_1 \otimes \mathbf{e}_2 + \mathbf{e}_2 \otimes \mathbf{e}_1), \quad \boldsymbol{\sigma} = \mu \frac{\bar{u}}{h} (\mathbf{e}_1 \otimes \mathbf{e}_2 + \mathbf{e}_2 \otimes \mathbf{e}_1). \tag{2.54}$$

Clearly, this classical elasticity solution, involving only the shear modulus μ, does not contain any material length scale parameter. Also, the non-zero shear strain and shear stress components are constant throughout the thickness, as seen from Eq. (2.54).

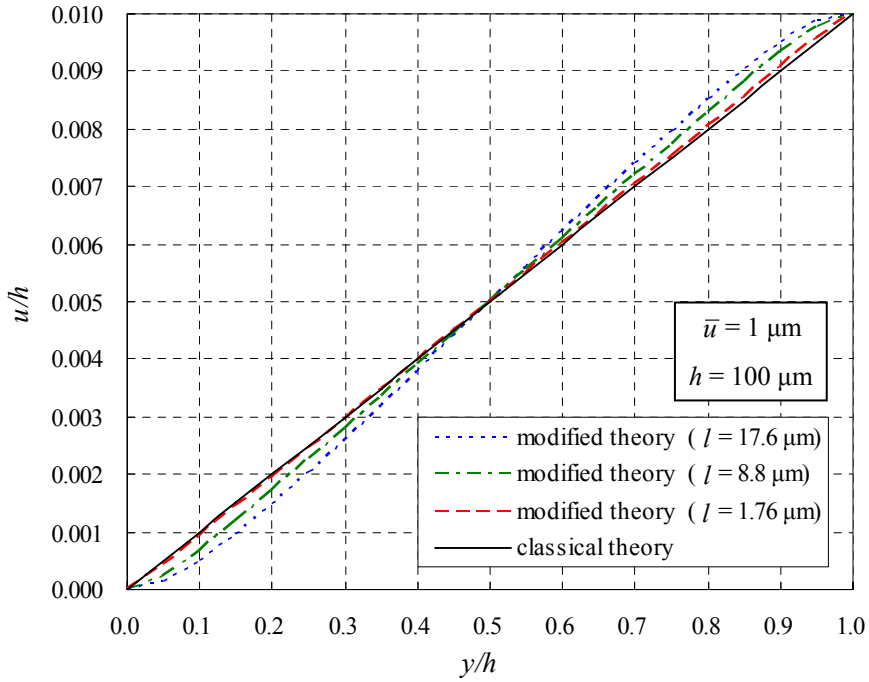

Fig. 2.2. Displacement in the block.

To demonstrate the newly derived solution, some numerical results are obtained and shown in Figs. 2.2 and 2.3, where the classical elasticity solution given in Eq. (2.54) is also displayed for comparison. For illustration purpose, the material properties for the

block are taken to be E = 1.44 GPa, ν = 0.38, l = 17.6 μm, which are typical for an epoxy (Lam et al., 2003; Park and Gao, 2006). To see the influence of material microstructure (as represented by l), two other cases with different values of l (i.e., l = 8.8 μm and l = 1.76 μm) are also included in this parametric study. The geometric parameters used here are h = 100 μm, $\bar{u}$ = 1 μm.

It is seen from Figs. 2.2 and 2.3 that the boundary layer (or sticking) effect, which was also observed in the molecular dynamics simulations of Horstemeyer et al. (2003), can be captured by the present solution, while the classical elasticity based solution does not have the same capability. Also, it can be observed that the influence of the microstructure (through l) can be significant: the larger the value of l, the larger the difference between the predictions by the present solution and by the classical elasticity solution. These trends are similar to those observed by Teneketzis Tenek and Aifantis (2001) using a different gradient elasticity theory.

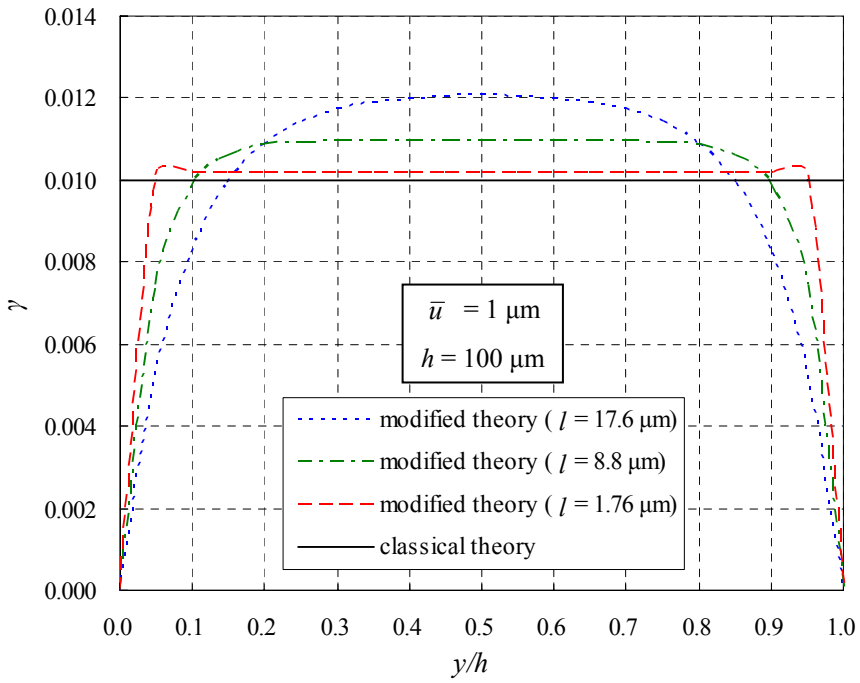

Fig. 2.3. Shear strain in the block ($\gamma = 2\varepsilon_{12}$).

2.5. SUMMARY

A variational formulation based on the principle of minimum total potential energy is presented for the modified couple stress theory proposed by Yang et al. (2002), which leads to the simultaneous determination of the equilibrium equations and the boundary conditions. This complements the original work of Yang et al., where the boundary conditions were not derived. To supplement the stress-based formulation in Yang et al. (2002), the governing equations in terms of displacement are also derived, which can be applied to solve problems that favor a displacement formulation. All equations are expressed in tensorial forms and hence are coordinate-invariant.

By applying the newly obtained displacement form of the modified couple stress theory, a simple shear problem is analytically solved. The closed-form solution derived contains a material length scale parameter and can capture the boundary layer effect, while the classical elasticity solution does not have the same capability. The numerical results quantitatively show that the influence of the length scale parameter (related to material microstructures) on mechanical responses of materials can be significant.

CHAPTER III

BERNOULLI-EULER BEAM MODEL BASED ON THE MODIFIED COUPLE STRESS THEORY*

3.1. INTRODUCTION

Thin (cantilever) beams have found important applications in micro- and nano-scale measurements such as those in biosensors and atomic force microscopes (e.g., Pereira, 2001; Pei et al., 2004). In these applications, the beam thickness is typically on the order of microns, and the size effect (i.e., the thinner, the stiffer) is often observed (e.g., Lam et al., 2003; McFarland and Colton, 2005). Lacking an internal material length scale parameter, classical beam models cannot be used to interpret this microstructure-dependent size effect and, therefore, need to be extended by using higher-order (non-local) continuum theories that contain additional material length scale parameters.

The classical couple stress elasticity theory elaborated by Koiter (1964) and others including Toupin (1962), Mindlin and Tiersten (1962) and Mindlin (1963) is a higher-order continuum theory that contains four material constants (two classical and two additional) for isotropic elastic materials. This theory has been applied to model the pure bending of a circular cylinder by Anthoine (2000). Beam bending models based on other non-local elasticity theories have also been reported. For example, the higher-order model for Bernoulli-Euler beams developed by Papargyri-Beskou et al. (2003) is based on the gradient elasticity theory with surface energy of Vardoulakis and Sulem (1995), which involves four elastic constants (two classical and two non-classical). This strain gradient beam model has been studied further by Vardoulakis and Giannakopoulos (2006). The non-local Bernoulli-Euler beam model proposed by Peddieson et al. (2003) using a constitutive equation due to Eringen (1983) also contains two additional material

* Published in Park, S.K. and Gao, X.-L., 2006, Journal of Micromechanics and Microengineering **16**, 2355-2359.

constants. Considering the difficulties in determining the microstructure related length scale parameters (e.g., Yang and Lakes, 1982; Lam et al., 2003) and the approximate nature of beam theories, it is desirable to have non-local beam models that involve only one additional material length scale parameter.

A modified couple stress theory has recently been proposed by Yang et al. (2002), in which the couple stress tensor is symmetric and only one internal material length scale parameter is involved, unlike those in the classical couple stress theory mentioned above. A variational formulation of this modified couple stress theory has subsequently been provided by Park and Gao (2006), which is presented in Chapter II.

The objective of this chapter is to develop a new non-local model for Bernoulli-Euler beams using the minimum total potential energy principle and the concepts of the modified couple stress theory of Yang et al. (2002). The rest of the chapter is organized as follows. In Section 3.2, the strain energy density function is constructed by using the modified couple stress theory and the displacement field typical for a Bernoulli-Euler beam. The principle of minimum total potential energy is then used to obtain the governing equation and boundary conditions for the beam. The resulting beam model contains an internal material length scale parameter and can capture the size effect. To illustrate the newly developed model, a cantilever beam problem is solved in Section 3.3, and the differences between the new beam model and the classical Bernoulli-Euler beam theory are quantitatively shown. The predictions are also compared to and verified by the existing experimental data. The chapter concludes with a summary in Section 3.4.

3.2. FORMULATION

According to the modified couple stress theory of Yang et al. (2002), the strain energy density is a function of both strain (conjugated with stress) and curvature (conjugated with couple stress). It then follows that the strain energy U in a deformed isotropic linear elastic material occupying region Ω is given by

$$U = \frac{1}{2}\iiint_{\Omega} \left(\boldsymbol{\sigma} : \boldsymbol{\varepsilon} + \mathbf{m} : \boldsymbol{\chi} \right) dv, \tag{3.1}$$

where the stress tensor, $\boldsymbol{\sigma}$, strain tensor, $\boldsymbol{\varepsilon}$, deviatoric part of the couple stress tensor, $\mathbf{m}$, and symmetric curvature tensor, $\boldsymbol{\chi}$, are, respectively, defined by

$$\boldsymbol{\sigma} = \lambda \operatorname{tr}(\boldsymbol{\varepsilon})\mathbf{I} + 2\mu\boldsymbol{\varepsilon}, \tag{3.2}$$

$$\boldsymbol{\varepsilon} = \frac{1}{2}\left[\nabla\mathbf{u} + (\nabla\mathbf{u})^{\mathrm{T}}\right], \tag{3.3}$$

$$\mathbf{m} = 2\mu l^2 \boldsymbol{\chi}, \tag{3.4}$$

$$\boldsymbol{\chi} = \frac{1}{2}\left[\nabla\boldsymbol{\theta} + (\nabla\boldsymbol{\theta})^{\mathrm{T}}\right], \tag{3.5}$$

with λ and μ being Lamé's constants, l a material length scale parameter, $\mathbf{u}$ the displacement vector, and $\boldsymbol{\theta}$ the rotation vector given by

$$\boldsymbol{\theta} = \frac{1}{2}\operatorname{curl}\mathbf{u}. \tag{3.6}$$

Clearly, both $\boldsymbol{\sigma}$ and $\mathbf{m}$, as respectively defined in Eqs. (3.2) and (3.4), are symmetric, with $\boldsymbol{\sigma} = \boldsymbol{\sigma}^{\mathrm{T}}$ and $\mathbf{m} = \mathbf{m}^{\mathrm{T}}$ due to the symmetry of $\boldsymbol{\varepsilon}$ and $\boldsymbol{\chi}$ given in Eqs. (3.3) and (3.5), respectively. Also, note that the square of the length scale parameter l introduced in Eq. (2.4) is the ratio of the modulus of curvature to the modulus of shear, and l is therefore regarded as a material property measuring the effect of couple stress (Mindlin, 1963).

The work done by external forces is

$$W = \iiint_{\Omega}\left(\mathbf{f}\cdot\mathbf{u} + \mathbf{c}\cdot\boldsymbol{\theta}\right)dv + \iint_{\partial\Omega}\left(\mathbf{t}\cdot\mathbf{u} + \mathbf{s}\cdot\boldsymbol{\theta}\right)da, \tag{3.7}$$

where $\mathbf{f}$, $\mathbf{c}$, $\mathbf{t}$ and $\mathbf{s}$ are, respectively, the body force, body couple, traction and surface couple, and $\partial\Omega$ is the surface of Ω.

Using the coordinate system (x, y, z) shown in Fig. 3.1, where x-axis is coincident with the centroidal axis of the undeformed beam, y-axis is the neutral axis and z-axis is the symmetry axis, the displacement components in a Bernoulli-Euler beam can be represented by (e.g., Shames, 1985)

$$u = -z\psi(x), \quad v = 0, \quad w = w(x), \tag{3.8}$$

where u, v, w are, respectively, the x-, y- and z-components of the displacement vector $\mathbf{u}$, and ψ is the rotation angle of the centroidal axis of the beam given approximately by

$$\psi \approx \frac{dw(x)}{dx} \tag{3.9}$$

for small deformations considered here.

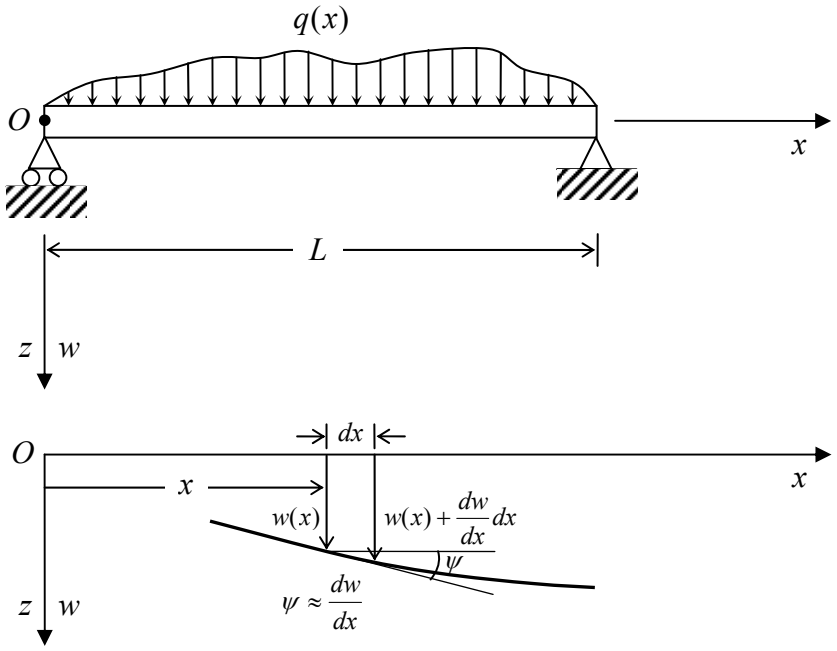

Fig. 3.1. Beam configuration.

From Eqs. (3.3), (3.8) and (3.9) it follows that

$$\varepsilon_{xx} = -z\frac{d^2w(x)}{dx^2}, \quad \varepsilon_{yy} = \varepsilon_{zz} = \varepsilon_{xy} = \varepsilon_{yz} = \varepsilon_{zx} = 0, \tag{3.10}$$

and from Eqs. (3.6), (3.8) and (3.9) that

$$\theta_y = -\frac{dw(x)}{dx}, \quad \theta_x = \theta_z = 0. \tag{3.11}$$

Using Eq. (3.11) in Eq. (3.5) gives

$$\chi_{xy} = -\frac{1}{2}\frac{d^2w(x)}{dx^2}, \quad \chi_{xx} = \chi_{yy} = \chi_{zz} = \chi_{yz} = \chi_{zx} = 0, \tag{3.12}$$

and inserting Eq. (3.10) into Eq. (3.2) yields

$$\sigma_{xx} = \frac{E(1-\nu)}{(1+\nu)(1-2\nu)}\left(-z\frac{d^2w(x)}{dx^2}\right),$$
$$\sigma_{yy} = \sigma_{zz} = \frac{E\nu}{(1+\nu)(1-2\nu)}\left(-z\frac{d^2w(x)}{dx^2}\right), \tag{3.13}$$
$$\sigma_{xy} = \sigma_{yz} = \sigma_{zx} = 0,$$

where E, ν are, respectively, the Young's modulus and Poisson's ratio of the beam material which are related to Lamé's constants λ and μ by (e.g., Timoshenko and Goodier, 1970)

$$\lambda = \frac{E\nu}{(1+\nu)(1-2\nu)}, \tag{3.14a}$$

$$\mu = \frac{E}{2(1+\nu)}. \tag{3.14b}$$

The material constant μ defined in Eq. (3.14b) is also known as the shear modulus (often denoted by G). For a slender beam with a large aspect ratio, the Poisson effect is secondary and may be neglected to facilitate the formulation of a simple beam theory (e.g., Shames, 1985). By setting $\nu = 0$, as was done in classical beam theories (e.g., Shames, 1985), Eq. (3.13) reduces to

$$\sigma_{xx} = -Ez\frac{d^2w(x)}{dx^2}, \quad \text{all other } \sigma_{ij} = 0. \tag{3.15}$$

Similarly, the use of Eq. (3.12) in Eq. (3.4) gives

$$m_{xy} = -\mu l^2 \frac{d^2w(x)}{dx^2}, \quad m_{xx} = m_{yy} = m_{zz} = m_{yz} = m_{zx} = 0, \tag{3.16}$$

where μ is the shear modulus (see Eq. (3.14b)).

Substituting Eqs. (3.10), (3.12), (3.15), and (3.16) into Eq. (3.1) then leads to

$$U = -\frac{1}{2}\int_{x=0}^{L} M_x \frac{d^2w(x)}{dx^2}dx - \frac{1}{2}\int_{x=0}^{L} Y_{xy}\frac{d^2w(x)}{dx^2}dx, \tag{3.17}$$

where the resultant moment M_x and couple moment Y_{xy} are defined, respectively, by

$$M_x = \int_A \sigma_{xx} z\, dA, \tag{3.18a}$$

$$Y_{xy} = \int_A m_{xy}\, dA. \tag{3.18b}$$

By neglecting the body force and body couple, the work done by the external forces in the form of transverse loading $q(x)$ shown in Fig. 3.1 (without surface couple) is obtained from Eq. (3.7) as

$$W = \int_{x=0}^{L} q(x)w(x)\,dx. \tag{3.19}$$

From Eqs. (3.17) and (3.19) it follows that the total potential energy Π in the loaded beam is

$$\Pi = U - W = -\frac{1}{2}\int_{x=0}^{L} (M_x + Y_{xy})\frac{d^2w(x)}{dx^2}dx - \int_{x=0}^{L} q(x)w(x)\,dx. \tag{3.20}$$

Taking the first variation of Π gives

$$\delta\Pi = -(M_x + Y_{xy})\delta w'(x)\Big|_0^L + \left(\frac{dM_x}{dx} + \frac{dY_{xy}}{dx}\right)\delta w(x)\Big|_0^L - \int_0^L \left(\frac{d^2M_x}{dx^2} + \frac{d^2Y_{xy}}{dx^2} + q\right)\delta w(x)dx. \tag{3.21}$$

Applying the principle of minimum total potential energy, i.e., $\delta\Pi = 0$ for the stable equilibrium (e.g., Steigmann, 1992), and the fundamental lemma of the calculus of variation (e.g., Gao and Mall, 2001) then leads to, from Eq. (3.21),

$$\frac{d^2M_x}{dx^2} + \frac{d^2Y_{xy}}{dx^2} + q(x) = 0, \qquad \forall\, x \in (0, L) \tag{3.22}$$

as the governing (equilibrium) equation, and

$$\left.\begin{array}{ll} M_x + Y_{xy} & or \quad \dfrac{dw}{dx} \\ \dfrac{d(M_x + Y_{xy})}{dx} & or \quad w \end{array}\right\} \quad \text{prescibed} \quad \text{at} \quad x = 0 \ \text{and} \ x = L \tag{3.23}$$

as the boundary conditions.

From Eqs. (3.15), (3.16) and (3.18a,b) it follows that

$$M_x = -EI\frac{d^2w(x)}{dx^2}, \tag{3.24a}$$

$$Y_{xy} = -\mu A l^2 \frac{d^2w(x)}{dx^2}. \tag{3.24b}$$

where I is the usual second moment of cross-sectional area defined by

$$I = \int_A z^2 dA. \tag{3.25}$$

Substituting Eqs. (3.24a,b) into Eq. (3.22) then gives

$$(EI + \mu A l^2)\frac{d^4 w(x)}{dx^4} = q(x) \tag{3.26}$$

as the equilibrium equation of the beam in terms of $w(x)$. Furthermore, combining Eqs. (3.24a) and (3.24b) yields

$$M_x + Y_{xy} = -(EI + \mu A l^2)\frac{d^2 w(x)}{dx^2}, \tag{3.27}$$

which shows that the bending deformation of the beam has two contributions: one associated with the normal stress component σ_{xx} (the conventional term; see Eqs. (3.18a) and (3.24a)) and the other associated with the couple stress component m_{xy} (the additional term; see Eqs. (3.18b) and (3.24b)). Equation (3.27) also indicates that the bending rigidity of the beam, ($EI + \mu A l^2$), explicitly depends on l. The value of l is related to and changes with the underlying microstructure of the beam material.

It is seen from Eqs. (3.22)-(3.27) that the current beam model based on the modified couple stress theory contains only one additional material constant, i.e., internal material length scale parameter l, unlike the other non-local beam models reviewed in Section 3.1. Nevertheless, the presence of l enables the incorporation of the material microstructural features in the new model and renders it possible to explain the size effect. This will be demonstrated further in the next section.

Clearly, when the microstructural effect is suppressed by letting $l = 0$, the new model defined by Eqs. (3.22)-(3.27) will reduce to the classical Bernoulli-Euler beam model.

3.3. EXAMPLE: A CANTILEVER BEAM PROBLEM

The Bernoulli-Euler beam model based on the modified couple stress theory of Yang et al. (2002) is developed in the preceding section. In this section, the problem of a cantilever beam with the loading, geometry and cross-sectional shape shown in Fig. 3.2 is solved by directly applying the new model.

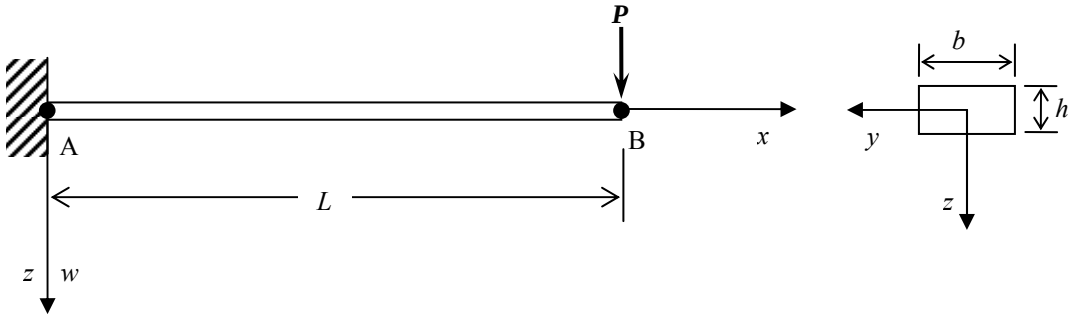

Fig. 3.2. Cantilever beam problem.

Following Eq. (3.23), the boundary conditions of this problem are

$$w\big|_{x=0} = 0\,, \tag{3.28a}$$

$$\left.\frac{dw}{dx}\right|_{x=0} = 0\,, \tag{3.28b}$$

$$(M_x + Y_{xy})\big|_{x=L} = 0\,, \tag{3.28c}$$

$$\left.\frac{d(M_x + Y_{xy})}{dx}\right|_{x=L} = P\,, \tag{3.28d}$$

where P is the magnitude of the applied force. Integrating the governing equation given in Eq. (3.26) four times gives, with $q(x) = 0$ here,

$$(EI + \mu A l^2)\, w(x) = \frac{C_1}{6}x^3 + \frac{C_2}{2}x^2 + C_3 x + C_4\,. \tag{3.29}$$

Using Eqs. (3.28a-d) in Eq. (3.29) will yield, with the help of Eqs. (3.24a,b),

$$C_1 = -P\,,\quad C_2 = PL\,,\quad C_3 = C_4 = 0\,. \tag{3.30}$$

It then follows from Eqs. (3.29) and (3.30) that

$$w(x) = \frac{Px^2}{6(EI + \mu A l^2)}(3L - x) \tag{3.31}$$

as the deflection of the beam at the x cross-section. Knowing $w(x)$, all other quantities will be readily determined using the formulas derived in Section 3.2. It should be mentioned that the beam deflection relation given by Eq. (3.31) is similar to that provided in McFarland and Colton (2005) for a cantilever plate using a different

approach based on the micropolar elasticity theory.

If the microstructural effect, as measured by the internal material length parameter l, is neglected, Eq. (3.31) reduces to

$$w(x) = \frac{Px^2}{6EI}(3L - x), \tag{3.32}$$

which is the well-known deflection formula given by the classical Bernoulli-Euler beam theory for the cantilever beam shown in Fig. 3.2. A comparison of Eqs. (3.31) and (3.32) shows that the classical beam theory predicts a larger deflection than that by the new model based on the modified couple stress theory. This is further illustrated in Fig. 3.3.

Figure 3.3 compares the deflections of the cantilever beam predicted by the new model and by the classical Bernoulli-Euler beam theory. For illustration purpose, the beam considered here is taken to be made of epoxy (Lam et al., 2003) with the following properties: E = 1.44 GPa, ν = 0.38, l = 17.6 μm, with the value of E obtained from Fig. 9 of Lam et al. (2003) (for bending tests) and the value of l determined from their Eq. $(68)_2$ by letting b_h = 24 μm, ν = 0.38, and $l_0 = l_1 = 0$, $l_2 \equiv l$ (see Lam et al. (2003), p. 1484, p. 1506). Here l_0, l_1 and l_2 are the three material length scale parameters involved in the strain gradient elasticity theory proposed by Lam et al. (2003) (see their Eq. (44)), which includes the modified couple stress theory of Yang et al. (2002) as a special case when the dilatation gradient (measured by l_0) and the deviatoric stretch gradient (measured by l_1) effects are ignored. Also, b_h, called a higher-order bending parameter by Lam et al. (2003), is a material constant related to l_0, l_1, l_2 and ν (Poisson's ratio) (see their Eq. $(68)_2$). The value of b_h = 24 μm used here is taken from Lam et al. (2003), where it was obtained from curve fitting the experimental data. The cross-sectional shape is kept to be the same by letting b/h = 2 (see Fig. 3.2) for all cases. The values of P and h have been so chosen that the beam remains elastic everywhere, as was done in Lam et al. (2003).

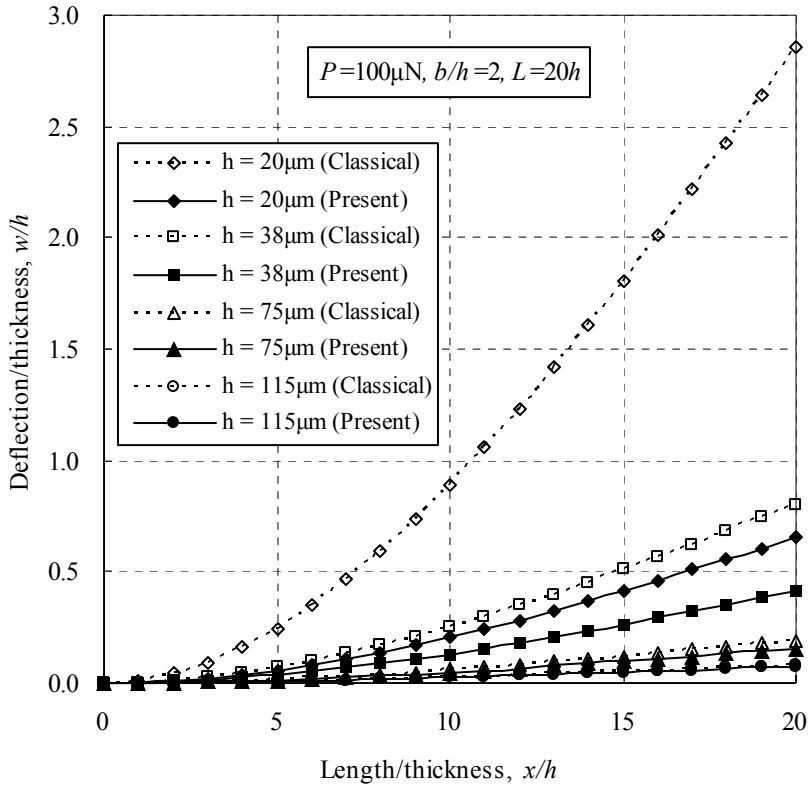

Fig. 3.3. Deflection of the cantilever beam.

Clearly, it is seen from Fig. 3.3 that the deflection predicted by the classical beam theory is larger than that by the new model along the entire length of the cantilever beam and for all cases considered. Figure 3.3 also shows that the difference between the two sets of predicted values is very large when thickness of the beam (h) is on the order of 10 μm but is diminishing when the thickness of the beam becomes larger (h around 100 μm here), thereby indicating that the size effect is only significant at the micron scale. This agrees with the general trends observed in experiments, as shown in Fig. 3.4, where the normalized bending rigidity D' predicted by the present beam model is compared to the experimental data provided in Lam et al. (2003) (see their Fig. 12). The bending tests of Lam et al. (2003) were performed using a Hysitron Triboindenter, with the epoxy beam specimens fabricated through casting. The normalized bending rigidity D' for the plane stress beam (with $\nu = 0$) here is given by

$$D' \equiv \frac{EI + \mu A l^2}{bh^3} = \frac{E}{12}\left[1 + 2\left(\frac{b_h}{h}\right)^2\right], \tag{3.33}$$

where use has been made of Eq. (3.14b) and the following relations:

$$I = \frac{bh^3}{12}, \tag{2.34a}$$

$$A = bh, \tag{2.34b}$$

$$l = \sqrt{\frac{b_h^2}{3(1-\nu)}}, \tag{2.34c}$$

with Eq. (3.34c) obtained from Eq. $(68)_2$ of Lam et al. (2003) using $l_0 = l_1 = 0$, $l_2 \equiv l$ for the modified couple stress theory as mentioned above. Figure 3.4 further illustrates the significant size effect displayed by beams with small thickness (h < 100 μm here): the smaller the thickness (h) is, the larger the normalized bending stiffness (D') is.

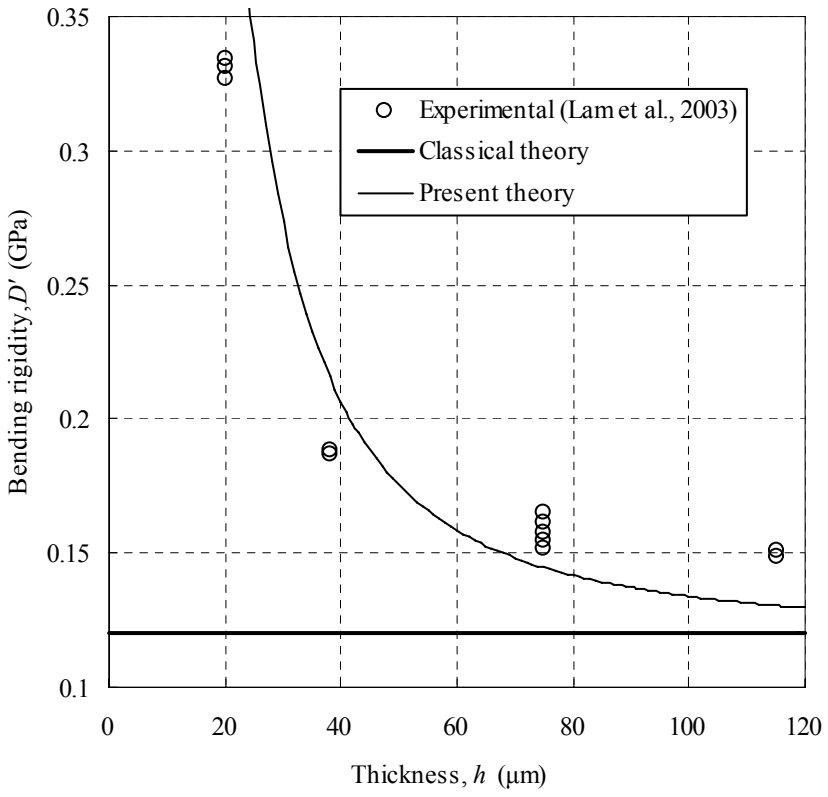

Fig. 3.4. Bending rigidity of the cantilever beam.

It is seen from Fig. 3.4 that this experimentally observed effect is captured fairly well by the new beam model based on the modified couple stress theory of Yang et al. (2002). In contrast, the classical beam theory does not have the same capability, as shown in Fig. 3.4.

3.4. SUMMARY

A new model for the bending of a Bernoulli-Euler beam is developed by using the minimum total potential energy principle and a modified couple stress theory. The model contains an internal material length scale parameter to account for the microstructural effect, unlike that in the classical Bernoulli-Euler beam theory. The inclusion of this additional material constant enables the new model to capture the size effect. When the microstructural effect is neglected, the new model reduces to that of the classical beam theory.

A cantilever beam problem is solved by directly applying the newly developed beam model. The solution is compared to that of the classical beam theory for the same problem. The numerical results show that the deflection of the cantilever beam predicted by the new model is always smaller than that by the classical beam model. The smaller the beam thickness, the larger the difference between the deflection values predicted by the two models. However, the difference is diminishing with the increase of the beam thickness. These predictions confirm the size effect at the micron scale observed in bending tests and compare fairly well with the existing experimental data.

CHAPTER IV

MODELING OF HONEYCOMB STRUCTURES USING THE MODIFIED COUPLE STRESS THEORY

4.1. INTRODUCTION

Cellular materials have found important applications in the aerospace and automobile industries, which include shock absorption, structural reinforcement, weight reduction and thermal isolation (e.g., Gibson and Ashby, 1997). Honeycomb structures with hexagonal cells are most commonly used two-dimensional (2-D) cellular materials (e.g., Jacobs and Kilduff, 2005). Most studies on honeycomb structures are based on classical elasticity and plasticity, as was summarized in Gibson and Ashby (1997) and Li et al. (2005). The latter provided a model for imperfect honeycombs having irregular cell shapes and non-uniform cell wall thickness.

Several studies have been conducted to better understand mechanical responses of honeycomb structures by using higher order elasticity theories. Chen et al. (1998) derived constitutive relations of honeycombs having hexagonal, triangular and square cell shapes using the equivalence of elastic strain energy and a generalized continuum model. Wang and Stronge (1999) used a micropolar elasticity theory to determine stress-strain relations for regular honeycomb structures. The theory of micropolar media was employed by Warren and Byskov (2002) to obtain constitutive relations for 2-D cellular solids with three-fold symmetry. Diebels and Steeb (2003) studied the homogenized responses of 2-D beam network structures using the Cosserat couple stress theory. Constitutive relations for five different types of 2-D cellular solids were derived by Kumar and McDowell (2004) using the micropolar theory and an energy method. However, the modified couple stress theory discussed in Chapter II, which contains only one additional material constant and is simpler than other higher order elasticity theories, has not been used to model honeycomb structures. This motivated the current work.

In this chapter, the modified couple stress theory is applied to determine the effective

elastic constants and the constitutive relations for regular honeycomb structures. In section 4.2, the 3-D modified couple stress theory discussed in Chapter II is reduced to the 2-D form. The constitutive equations for regular honeycombs are obtained in section 4.3, where a finite difference scheme is introduced to discretize expressions involving partial derivatives. In section 4.4, the stress-strain relations are derived using a structural mechanics approach. A summary is provided in the fifth and last section of the chapter.

4.2. TWO-DIMENSIONAL FORM OF THE MODIFIED COUPLE STRESS THEORY

For 2-D deformations in the x_1x_2-plane, the displacement field can be represented by

$$u_1 = u_1(x_1, x_2),\ u_2 = u_2(x_1, x_2)\,. \tag{4.1}$$

Using Eq. (4.1) in Eqs. (2.2)-(2.4) then gives

$$\varepsilon_{11} = u_{1,1}\,,\quad \varepsilon_{22} = u_{2,2}\,,\quad \varepsilon_{12} = \frac{1}{2}(u_{1,2} + u_{2,1})\,, \tag{4.2a}$$

$$\chi_{31} = \frac{1}{2}\theta_{3,1} = \frac{1}{4}(u_{2,1} - u_{1,2})_{,1}\,,\quad \chi_{32} = \frac{1}{2}\theta_{3,2} = \frac{1}{4}(u_{2,1} - u_{1,2})_{,2}\,, \tag{4.2b}$$

where

$$\theta_3 = \frac{1}{2}(u_{2,1} - u_{1,2})\,. \tag{4.3}$$

Also, recall from Chapter II that the equilibrium equations in the modified couple stress theory are

$$\mathrm{div}\boldsymbol{\sigma} + \frac{1}{2}\mathrm{curl}(\mathrm{div}\mathbf{m} + \mathbf{y}) + \mathbf{f} = 0\,, \tag{4.4}$$

where $\boldsymbol{\sigma}$, $\mathbf{m}$, $\mathbf{y}$, and $\mathbf{f}$ are, respectively, the Cauchy stress, couple stress, body couple, and body force, each of which is a function of x_1 and x_2 only.

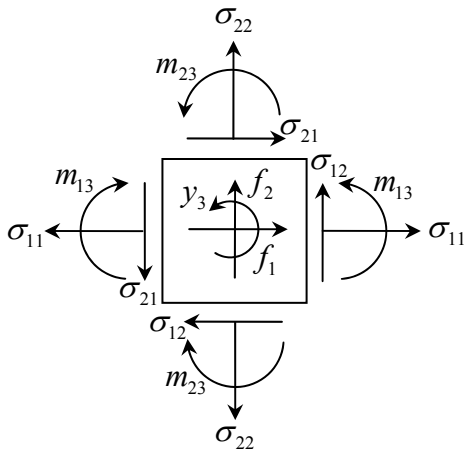

Fig. 4.1. 2-D Cartesian components of the Cauchy stress and the couple stress.

For 2-D deformations, Eq. (4.4) reduces to

$$\sigma_{11,1} + \sigma_{12,2} + \frac{1}{2}(m_{31,12} + m_{32,22}) + \frac{1}{2} y_{3,2} + f_1 = 0\,, \tag{4.5a}$$

$$\sigma_{21,1} + \sigma_{22,2} - \frac{1}{2}(m_{31,11} + m_{32,21}) - \frac{1}{2} y_{3,2} + f_2 = 0\,, \tag{4.5b}$$

$$y_{2,1} - y_{1,2} + f_3 = 0\,. \tag{4.5c}$$

Figure 4.1 shows a 2-D differential element illustrating the components of the Cauchy stress and the couple stress tensors.

The compatibility conditions can be readily obtained from Eqs. (4.2a,b) as

$$\varepsilon_{11,22} + \varepsilon_{22,11} = 2\varepsilon_{12,12}\,, \tag{4.6a}$$

$$\chi_{32,1} - \chi_{31,2} = 0\,. \tag{4.6b}$$

Eqs. (4.2a,b), (4.5a-c) and (4.6a,b) give the explicit expressions of the governing equations of the modified couple stress theory for 2-D deformations in the x_1x_2-plane, which will be used in the formulation below.

4.3. STRESS TRANSFORMATIONS IN HONEYCOMB STRUCTURES

Consider a honeycomb, with hexagonal cells, that is undergoing plane strain deformations (induced, for example, by a concentrated external force acting on a rigid

plate on the top of the honeycomb shown in Fig. 4.2). From the periodicity of the honeycomb structures, the rhombus identified in Fig. 4.3 (enclosed by the dotted lines) can be taken as a repeating unit (or unit cell).

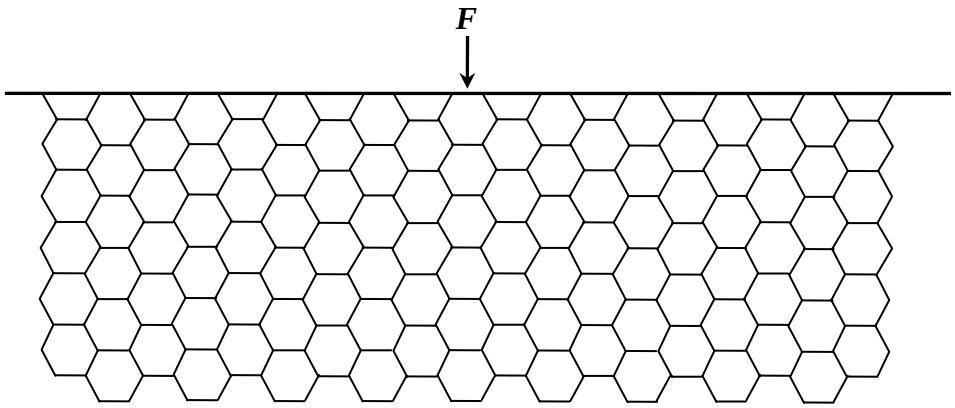

Fig. 4.2. Periodic honeycomb structure.

To facilitate the micromechanical analysis based on the rhombus unit cell, whose adjacent sides are not orthogonal to each other, a system of two non-orthogonal in-plane coordinates (ξ, ζ) is adopted in addition to the Cartesian coordinate system (x_1, x_2), as shown in Fig. 4.4, where θ is the angle between the ξ and ζ axes and α is the angle between the ξ and x_1 axes.

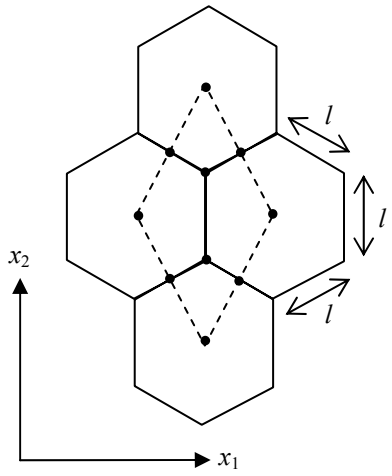

Fig. 4.3. Unit cell of the honeycomb structure.

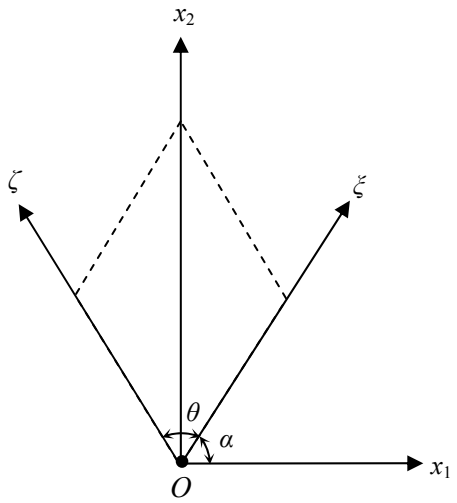

Fig. 4.4. Non-orthogonal coordinate system (ξ, ζ).

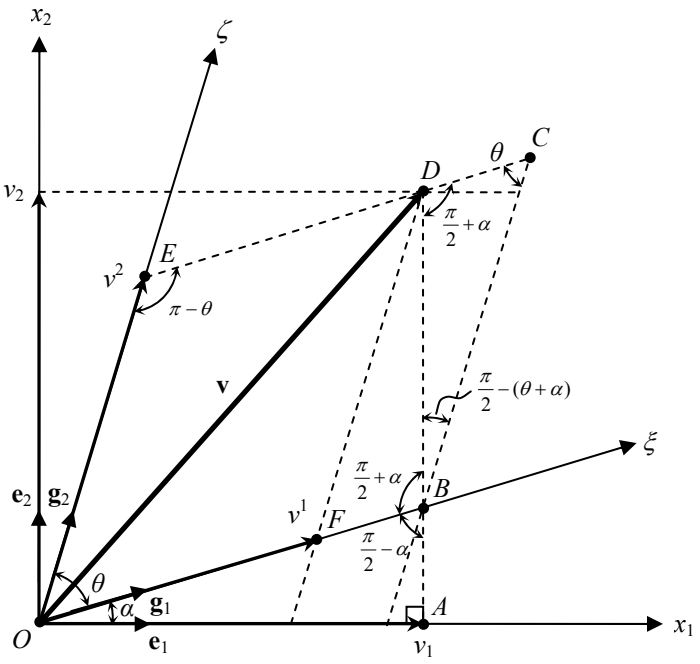

Fig. 4.5 Non-orthogonal coordinate transformation.

The transformation relation between this non-orthogonal coordinate system (ξ, ζ) and the Cartesian coordinate system (x_1, x_2) can be established with the help of Fig. 4.5. An arbitrary vector **v** can be represented in terms of the Cartesian base vectors $\mathbf{e}_1$, $\mathbf{e}_2$ and

the non-orthogonal base vectors $\mathbf{g}_1$, $\mathbf{g}_2$ as

$$\mathbf{v} = v^1\mathbf{g}_1 + v^2\mathbf{g}_2 = v_1\mathbf{e}_1 + v_2\mathbf{e}_2\,, \tag{4.7}$$

where the components with superscripts (i.e., v^1 and v^2) and subscripts (i.e., v_1 and v_2) denote, respectively, the non-orthogonal and the Cartesian components of the same vector **v**.

From the geometrical relations shown in Fig. 4.5, the non-orthogonal components are seen to be given by

$$v^1 = \overline{OF} = \overline{OB} - \overline{CD}\,, \tag{4.8a}$$

$$v^2 = \overline{OE} = \overline{BC}\,. \tag{4.8b}$$

Using the sine law for the triangle BCD yields

$$\overline{OB} = \frac{v_1}{\cos\alpha}\,, \tag{4.9a}$$

$$\overline{CD} = \frac{\cos(\theta+\alpha)}{\sin\theta}\left(v_2 - \frac{\sin\alpha}{\cos\alpha}v_1\right), \tag{4.9b}$$

$$\overline{BC} = \frac{\cos\alpha}{\sin\theta}\left(v_2 - \frac{\sin\alpha}{\cos\alpha}v_1\right). \tag{4.9c}$$

Substituting Eqs. (4.9a-c) into Eqs. (4.8a,b) leads to

$$v^1 = \frac{\sin(\theta+\alpha)}{\sin\theta}v_1 - \frac{\cos(\theta+\alpha)}{\sin\theta}v_2\,, \tag{4.10a}$$

$$v^2 = \overline{BC} = -\frac{\sin\alpha}{\sin\theta}v_1 + \frac{\cos\alpha}{\sin\theta}v_2\,. \tag{4.10b}$$

Therefore, the transformation relations between the two different coordinate systems can be expressed as $\mathbf{v}'=\mathbf{Q}^{\mathrm{T}}\mathbf{v}$, where $\mathbf{v}'$ is the vector **v** in the non-orthogonal (transformed) coordinate system, and $\mathbf{Q}^{\mathrm{T}}$ is the transformation tensor given by

$$\mathbf{Q}^{\mathrm{T}} = \frac{1}{\sin\theta}\begin{bmatrix}\sin(\theta+\alpha) & -\cos(\theta+\alpha)\\ -\sin\alpha & \cos\alpha\end{bmatrix}_{\{\mathbf{e}_1,\mathbf{e}_2\}}. \tag{4.11}$$

It then follows that the coordinate transformation relations are

$$\begin{pmatrix}\xi\\ \zeta\end{pmatrix} = \frac{1}{\sin\theta}\begin{bmatrix}\sin(\theta+\alpha) & -\cos(\theta+\alpha)\\ -\sin\alpha & \cos\alpha\end{bmatrix}\begin{pmatrix}x_1\\ x_2\end{pmatrix}. \tag{4.12}$$

With $\mathbf{Q}^{\mathrm{T}}$ obtained in Eq. (4.11), the Cauchy stress and the couple stress components in the non-orthogonal coordinate system (ξ,ζ) can now be obtained through $\boldsymbol{\sigma}'=\mathbf{Q}^{\mathrm{T}}\boldsymbol{\sigma}\mathbf{Q}$, $\mathbf{m}'=\mathbf{Q}^{\mathrm{T}}\mathbf{m}$ as

$$\sigma_{\xi\xi}=\frac{1}{\sin^2\theta}\left\{\sin^2(\theta+\alpha)\sigma_{11}-2\cos(\theta+\alpha)\sin(\theta+\alpha)\sigma_{12}+\cos^2(\theta+\alpha)\sigma_{22}\right\}, \quad (4.13a)$$

$$\sigma_{\xi\zeta}=\frac{1}{\sin^2\theta}[-\sin(\theta+\alpha)\sin\alpha\,\sigma_{11}+\{\cos(\theta+\alpha)\sin\alpha+\cos\alpha\sin(\theta+\alpha)\}\sigma_{12} -\cos(\theta+\alpha)\cos\alpha\,\sigma_{22}], \quad (4.13b)$$

$$\sigma_{\zeta\zeta}=\frac{1}{\sin^2\theta}(\sin^2\alpha\,\sigma_{11}-2\cos\alpha\sin\alpha\,\sigma_{12}+\cos^2\alpha\,\sigma_{22}), \quad (4.13c)$$

$$m_{\xi 3}=\frac{1}{\sin\theta}\{\sin(\theta+\alpha)m_{13}-\cos(\theta+\alpha)m_{23}\}, \quad (4.13d)$$

$$m_{\zeta 3}=\frac{1}{\sin\theta}(-\sin\alpha\,m_{13}+\cos\alpha\,m_{23}). \quad (4.13e)$$

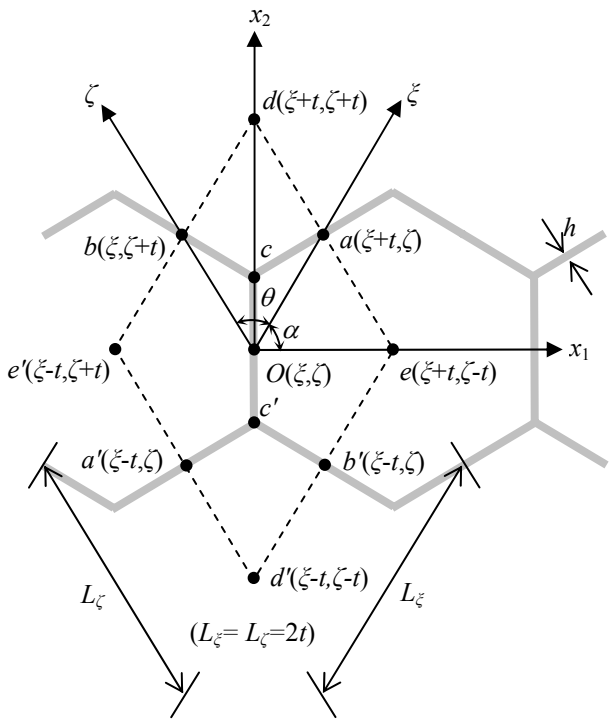

Fig. 4.6. Unit cell with the coordinate systems (ξ, ζ) and (x_1, x_2).

Figure 4.6 shows a rhombus repeating unit (having cell wall thickness h, side lengths L_ξ, L_ζ) with the center O, middle points of each side a, a', b, b', and edge points c, c', d, d', e, e'. Displacement components at those points will be determined below. In Fig 4.6, t is the length between two adjacent points on the boundary of the rhombus unit cell (d-e'-d'-e), which equals half of the side length (L_ξ or L_ζ).

For the repeating unit cell shown in Fig. 4.6, $\theta = 60°$ and $\alpha = 60°$ (see Fig. 4.5). Then, using Eq. (4.12) gives the coordinate transformation relations as

$$\begin{pmatrix} \xi \\ \zeta \end{pmatrix} = \begin{bmatrix} 1 & \frac{1}{\sqrt{3}} \\ -1 & \frac{1}{\sqrt{3}} \end{bmatrix} \begin{pmatrix} x_1 \\ x_2 \end{pmatrix}. \tag{4.14}$$

It follows from Eq. (4.14) that

$$\frac{\partial \xi}{\partial x_1} = 1, \tag{4.15a}$$

$$\frac{\partial \xi}{\partial x_2} = \frac{1}{\sqrt{3}}, \tag{4.15b}$$

$$\frac{\partial \zeta}{\partial x_1} = -1, \tag{4.15c}$$

$$\frac{\partial \zeta}{\partial x_2} = \frac{1}{\sqrt{3}}. \tag{4.15d}$$

By using the chain rule, the components of the stain and curvature tensors can be determined from Eqs. (4.2a,b) and (4.15a-d) as

$$\varepsilon_{11} = \frac{\partial u_1}{\partial x_1} = \frac{\partial u_1}{\partial \xi} - \frac{\partial u_1}{\partial \zeta}, \tag{4.16a}$$

$$\varepsilon_{22} = \frac{\partial u_2}{\partial x_2} = \frac{1}{\sqrt{3}}\left(\frac{\partial u_2}{\partial \xi} + \frac{\partial u_2}{\partial \zeta} \right), \tag{4.16b}$$

$$\gamma_{12} = 2\varepsilon_{12} = \frac{\partial u_1}{\partial x_2} + \frac{\partial u_2}{\partial x_1} = \frac{1}{\sqrt{3}}\left(\frac{\partial u_1}{\partial \xi} + \frac{\partial u_1}{\partial \zeta} \right) + \left(\frac{\partial u_2}{\partial \xi} - \frac{\partial u_2}{\partial \zeta} \right), \tag{4.16c}$$

$$\chi_{13} = \frac{1}{4}\left(\frac{\partial^2 u_2}{\partial x_1^2} - \frac{\partial^2 u_1}{\partial x_1 \partial x_2} \right) = \frac{1}{4}\left(\frac{\partial^2 u_2}{\partial \xi^2} - 2\frac{\partial^2 u_2}{\partial \xi \partial \zeta} + \frac{\partial^2 u_2}{\partial \zeta^2} \right) - \frac{1}{4\sqrt{3}}\left(\frac{\partial^2 u_1}{\partial \xi^2} - \frac{\partial^2 u_1}{\partial \zeta^2} \right), \tag{4.16d}$$

$$\chi_{23}=\frac{1}{4}\left(\frac{\partial^2 u_2}{\partial x_1 \partial x_2}-\frac{\partial^2 u_1}{\partial x_2^2}\right)=\frac{1}{4\sqrt{3}}\left(\frac{\partial^2 u_2}{\partial \xi^2}-\frac{\partial^2 u_2}{\partial \zeta^2}\right)-\frac{1}{12}\left(\frac{\partial^2 u_1}{\partial \xi^2}+2\frac{\partial^2 u_1}{\partial \xi \partial \zeta}+\frac{\partial^2 u_1}{\partial \zeta^2}\right). \quad (4.16e)$$

In order to discretely compute the strain and curvature components given in Eqs. (4.16a-e) in terms of the partial derivatives, a finite difference (FD) scheme is utilized so that the partial derivatives can be approximated by simpler algebraic expressions. By using the FD scheme, the derivatives involved in Eqs. (4.16a-d) can be approximately replaced by

$$\frac{\partial u_1}{\partial \xi}=\frac{u_{1a}-u_{1a'}}{L_\xi}, \quad (4.17a)$$

$$\frac{\partial u_1}{\partial \zeta}=\frac{u_{1b}-u_{1b'}}{L_\zeta}, \quad (4.17b)$$

$$\frac{\partial u_2}{\partial \xi}=\frac{u_{2a}-u_{2a'}}{L_\xi}, \quad (4.17c)$$

$$\frac{\partial u_2}{\partial \zeta}=\frac{u_{2b}-u_{2b'}}{L_\zeta}, \quad (4.17d)$$

$$\frac{\partial^2 u_1}{\partial \xi^2}=\frac{4(u_{1a}-2u_{1O}+u_{1a'})}{L_\xi^2}, \quad (4.17e)$$

$$\frac{\partial^2 u_1}{\partial \zeta^2}=\frac{4(u_{1b}-2u_{1O}+u_{1b'})}{L_\zeta^2}, \quad (4.17f)$$

$$\frac{\partial^2 u_2}{\partial \xi^2}=\frac{4(u_{2a}-2u_{2O}+u_{2a'})}{L_\xi^2}, \quad (4.17g)$$

$$\frac{\partial^2 u_2}{\partial \zeta^2}=\frac{4(u_{2b}-2u_{2O}+u_{2b'})}{L_\zeta^2}, \quad (4.17h)$$

$$\frac{\partial^2 u_1}{\partial \xi \partial \zeta}=\frac{u_{1d}-u_{1e}-u_{1e'}+u_{1d'}}{L_\xi L_\zeta}, \quad (4.17i)$$

$$\frac{\partial^2 u_2}{\partial \xi \partial \zeta}=\frac{u_{2d}-u_{2e}-u_{2e'}+u_{2d'}}{L_\xi L_\zeta}. \quad (4.17j)$$

4.4. STRESS-STRAIN RELATIONS

In this section, the modified couple stress theory will be used to determine effective elastic properties and to establish the stress-strain relations of the honeycomb structure. The methodology follows that of Wang and Stronge (1999) based on a micropolar elasticity theory.

4.4.1. Loading by normal stresses σ_{11} and σ_{22}

When the unit cell is subjected to the normal stresses in the directions of x_1, x_2, its deformed shape (enclosed by the dotted lines) is shown in Fig. 4.7(a). Due to the loading symmetry with respect to the axis x_1, only the upper part of the unit cell shown in Fig. 4.7(b) needs to be considered. The interaction force and deflection at the joint c (see Fig. 4.8) can be obtained using structural mechanics as

$$P_{2c} = 2\sigma_{22} A \sin\tfrac{\theta}{2}, \tag{4.18a}$$

$$\delta_{2c} = \frac{P_{2c}}{AE}\left(\frac{l}{2}\right) = \frac{\sigma_{22}}{E}\left(\frac{l}{2}\right). \tag{4.18b}$$

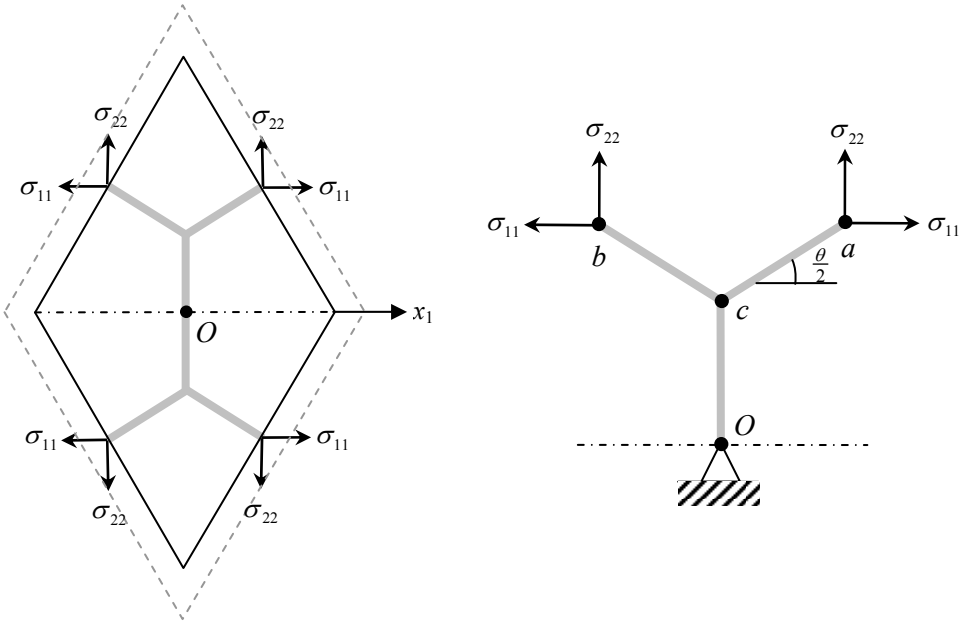

(a) (b)

Fig. 4.7. (a) Unit cell under normal stresses,
(b) Symmetric part of the unit cell under normal stresses.

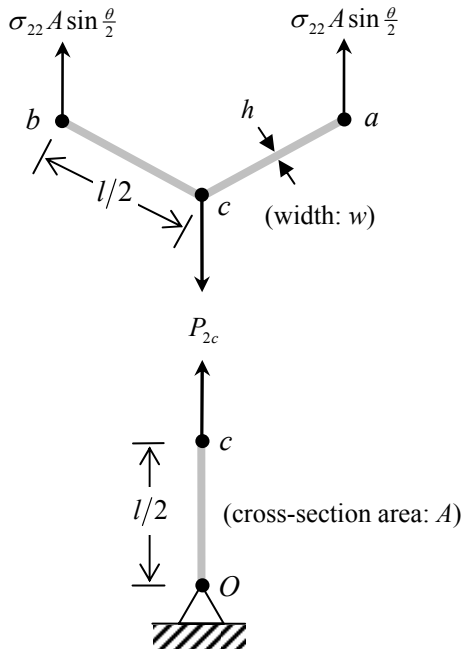

Fig. 4.8. Interaction force at the joint *c* in Fig. 4.7.

Figure 4.9 (a) shows the directions of the deflections $\delta_{\xi\xi}$ and $\delta_{\xi\zeta}$ at point *a* in Fig. (4.7b), which are along the directions of the induced forces $\sigma_{\xi\xi}A$ and $\sigma_{\xi\zeta}A$, respectively. The displacement components at point *a* are given by

$$u_{1a} = \delta_{\xi\xi}\cos\tfrac{\theta}{2} - \delta_{\xi\zeta}\sin\tfrac{\theta}{2}, \tag{4.19a}$$

$$u_{2a} = \delta_{\xi\xi}\sin\tfrac{\theta}{2} + \delta_{\xi\zeta}\cos\tfrac{\theta}{2} + \delta_{2c}. \tag{4.19b}$$

In order to establish the transformation relations between the stress components in the non-orthogonal coordinate system (ξ, ζ) and in the Cartesian coordinate system (x_1, x_2) at the end point *a*, the force equilibrium equations are obtained as

$$\sum F_{\xi\xi} = 0 : -\sigma_{\xi\xi}\Delta A + \sigma_{11}\Delta A\cos^2\tfrac{\theta}{2} + \sigma_{22}\Delta A\sin^2\tfrac{\theta}{2} = 0, \tag{4.20a}$$

$$\sum F_{\xi\zeta} = 0 : -\sigma_{\xi\zeta}\Delta A - \sigma_{11}\Delta A\cos\tfrac{\theta}{2}\sin\tfrac{\theta}{2} + \sigma_{22}\Delta A\sin\tfrac{\theta}{2}\cos\tfrac{\theta}{2} = 0. \tag{4.20b}$$

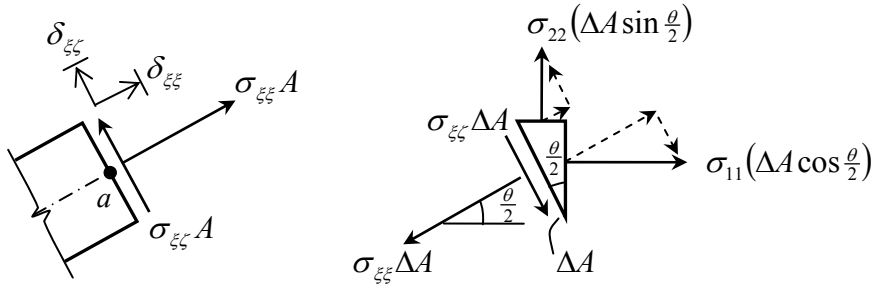

(a) (b)

Fig. 4.9 (a) Force and the deflection directions at point *a* in Fig. 4.7, (b) Internal force equilibrium at point *a*.

By using Eqs. (4.20a,b), the deflections at point *a* can be determined as

$$\delta_{\xi\xi} = \frac{(\sigma_{\xi\xi}A)}{AE}\left(\frac{l}{2}\right) = \frac{l}{2E}(\sigma_{11}\cos^2\tfrac{\theta}{2} + \sigma_{22}\sin^2\tfrac{\theta}{2}), \tag{4.21a}$$

$$\delta_{\xi\zeta} = \frac{(\sigma_{\xi\zeta}A)}{3EI}\left(\frac{l}{2}\right)^3 = \frac{\eta^2 l}{2E}(\sigma_{22}-\sigma_{11})\cos\tfrac{\theta}{2}\sin\tfrac{\theta}{2}, \tag{4.21b}$$

where I is the second moment of the cross-sectional area ($I = wh^3/12$). Inserting Eqs. (4.21a,b) into Eqs. (4.19a,b) gives

$$u_{1a} = \frac{l}{2E}(\sigma_{11}\cos^2\tfrac{\theta}{2} + \sigma_{22}\sin^2\tfrac{\theta}{2})\cos\tfrac{\theta}{2} - \frac{\eta^2 l}{2E}(\sigma_{22}-\sigma_{11})\cos\tfrac{\theta}{2}\sin^2\tfrac{\theta}{2}, \tag{4.22a}$$

$$u_{2a} = \frac{l}{2E}(\sigma_{11}\cos^2\tfrac{\theta}{2} + \sigma_{22}\sin^2\tfrac{\theta}{2})\sin\tfrac{\theta}{2} + \frac{\eta^2 l}{2E}(\sigma_{22}-\sigma_{11})\cos^2\tfrac{\theta}{2}\sin\tfrac{\theta}{2} + \frac{\sigma_{22}l}{2E}. \tag{4.22b}$$

Substituting $\theta = 60°$ into Eqs. (4.22a,b) then yields the displacement components at point *a* as

$$u_{1a} = \frac{\sqrt{3}l}{16E}\left\{(3+\eta^2)\sigma_{11} + (1-\eta^2)\sigma_{22}\right\}, \tag{4.23a}$$

$$u_{2a} = \frac{3l}{16E}\left\{(1-\eta^2)\sigma_{11} + (3+\eta^2)\sigma_{22}\right\}. \tag{4.23b}$$

Due to the symmetry, the displacement components at the other key points on the unit cell shown in Fig. 4.6 can be readily obtained as

$$u_{1b} = -u_{1a}\,, \tag{4.24a}$$

$$u_{2b} = u_{2a}\,, \tag{4.24b}$$

$$u_{1a'} = -u_{1a}\,, \tag{4.24c}$$

$$u_{1b'} = u_{1a}\,, \tag{4.24d}$$

$$u_{2a'} = -u_{2a}\,, \tag{4.24e}$$

$$u_{2b'} = -u_{2a}\,. \tag{4.24f}$$

These indicate that the displacement of the center point O is indeed zero (i.e., $u_{1o} = 0 = u_{2o}$), as expected.

By substituting Eqs. (4.17a-d), (4.23a,b) and (4.24a-f) into Eqs. (4.16a,b), the relations between the normal stresses and normal strains will be obtained as

$$\varepsilon_{11} = \frac{1}{4E}\left\{(3+\eta^2)\sigma_{11} + (1-\eta^2)\sigma_{22}\right\}, \tag{4.25a}$$

$$\varepsilon_{22} = \frac{1}{4E}\left\{(1-\eta^2)\sigma_{11} + (3+\eta^2)\sigma_{22}\right\}, \tag{4.25b}$$

where the slenderness ratio of the cell wall η is defined as $\eta \equiv l/h$, and use has been made of $L_\xi = L_\zeta = \sqrt{3}\,l$ (see Figs. 4.6 and 4.8).

By setting $\sigma_{22} = 0$ in Eq. (4.25a), the effective Young's modulus in the x_1 direction, E_1^*, is obtained as

$$E_1^* = \frac{4}{3+\eta^2}E\,. \tag{4.26}$$

Similarly, by setting $\sigma_{11} = 0$ in Eq. (4.25b), the effective Young's modulus in the x_2 direction, E_2^*, is determined to be

$$E_2^* = \frac{4}{3+\eta^2}E\,. \tag{4.27}$$

The effective Poisson's ratio, ν_{12}^*, is obtained by setting $\sigma_{22} = 0$ in (4.25a,b) and taking the ratio of the resulting expressions, i.e.,

$$\nu_{12}^* = -\frac{\varepsilon_{22}}{\varepsilon_{11}} = \frac{1-\eta^2}{3+\eta^2}\,. \tag{4.28}$$

4.4.2. Loading by shear stresses σ_{12} and σ_{21}

The deformed shape (enclosed by dotted lines) of a unit cell induced by shear stresses $3\sigma_{12}$ and σ_{21} is illustrated in Fig. 4.10(a). Here $3\sigma_{12}$ is used for the purpose of producing a pure shear deformation of the unit cell.

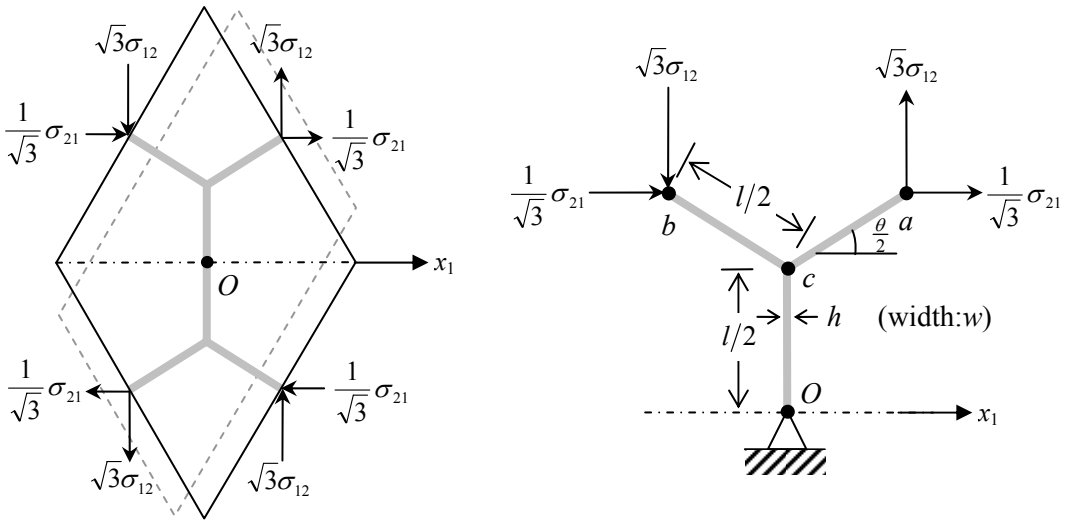

(a) (b)

Fig. 4.10 (a) Unit cell undergoing pure shear,
(b) Symmetric part of the unit cell undergoing pure shear.

Since the deformed shape of the upper part and the lower part of the unit cell is symmetric about the center point *O*, as shown in Fig. 4.10(a), the relations between the shear stress and shear strain components can be established by using only the upper part of the unit cell shown in Fig. 4.10(b).

To calculate the interaction forces at the joint *c*, a free-body diagram (FBD) of member *ca* shown in Fig. 4.11(a) will be used. From this FBD, the equilibrium equations can be written as

$$\sum F_x = 0 : -F_x + \sigma_{\xi\xi} A \cos\tfrac{\theta}{2} - \sigma_{\xi\zeta} A \sin\tfrac{\theta}{2} = 0\,, \tag{4.29a}$$

$$\sum F_y = 0 : -F_y + \sigma_{\xi\xi} A \sin\tfrac{\theta}{2} + \sigma_{\xi\zeta} A \cos\tfrac{\theta}{2} = 0\,, \tag{4.29b}$$

$$\sum M_z = 0 : -\frac{M_c}{2} + \frac{l}{2}\sigma_{\xi\zeta} A = 0\,. \tag{4.29c}$$

The deflections at point *a* in Fig. 4.10(b) are given by

$$\delta_{\xi\xi} = \frac{(\sigma_{\xi\xi} A)}{AE}\left(\frac{l}{2}\right), \tag{4.30a}$$

$$\delta_{\xi\zeta} = \frac{(\sigma_{\xi\zeta} A)}{3EI}\left(\frac{l}{2}\right)^3 . \tag{4.30b}$$

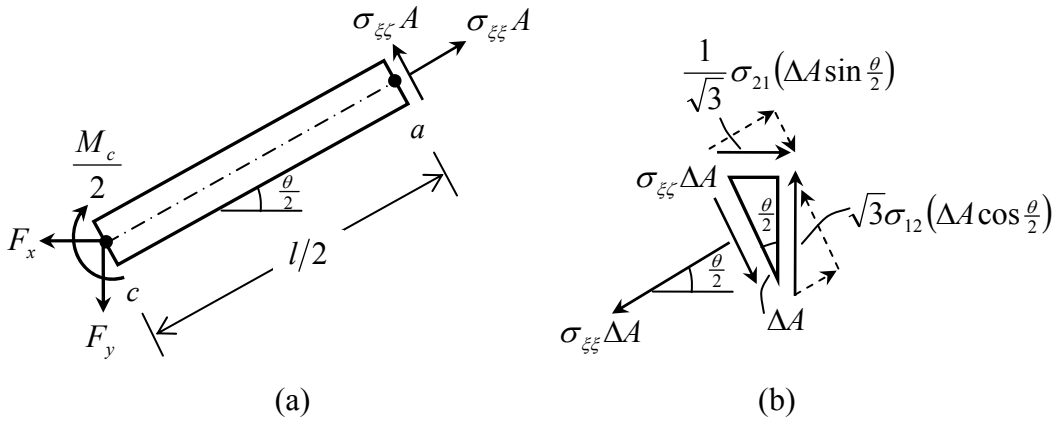

(a) (b)

Fig. 4.11 (a) FBD of member *ca* in Fig. 4.10, (b) Equilibrium at point *a*.

Figure 4.11(b) shows the internal forces at point *a* that are equilibrated. From this FBD, the equilibrium equations are obtained as

$$\sum F_{\xi\xi} = 0 : -\sigma_{\xi\xi}\Delta A + \sqrt{3}\sigma_{12}\Delta A \cos\tfrac{\theta}{2}\sin\tfrac{\theta}{2} + \frac{1}{\sqrt{3}}\sigma_{21}\Delta A \sin\tfrac{\theta}{2}\cos\tfrac{\theta}{2} = 0, \tag{4.31a}$$

$$\sum F_{\xi\zeta} = 0 : -\sigma_{\xi\zeta}\Delta A + \sqrt{3}\sigma_{12}\Delta A \cos^2\tfrac{\theta}{2} - \frac{1}{\sqrt{3}}\sigma_{21}\Delta A \sin^2\tfrac{\theta}{2} = 0 . \tag{4.31b}$$

Solving $\sigma_{\xi\xi}$ and $\sigma_{\xi\zeta}$ from Eqs. (4.31a,b) and inserting the resulting expressions into Eqs. (4.29a-c) will yield

$$F_x = \frac{1}{\sqrt{3}}\sigma_{12} A \sin\tfrac{\theta}{2}, \tag{4.32a}$$

$$F_y = \sqrt{3}\sigma_{12} A \cos\tfrac{\theta}{2}, \tag{4.32b}$$

$$M_c = \frac{\sigma_{12} Al}{\sqrt{3}}(3\cos^2\tfrac{\theta}{2} - \sin^2\tfrac{\theta}{2}) . \tag{4.32b}$$

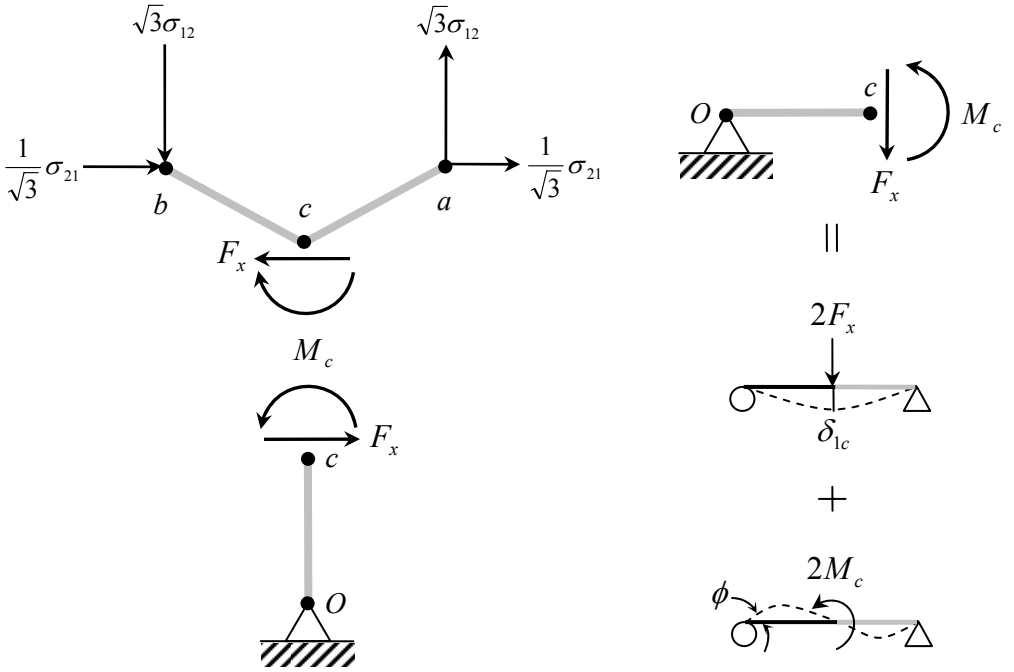

(a) (b)

Fig. 4.12. (a) Interactions at point *c* in Fig. 4.10,
(b) Superposition of two types of deformations of a simply supported beam.

Decomposed forces in member *ca* are shown in Fig. 4.12(a) to calculate the deflection δ_{1c} and rotated angle ϕ at point *c*. The deformation of member *oc* can be analyzed by using the superposition principle, as shown in Fig. 4.12(a). The deflection by the shear force and the rotated angle by the bending moment are, respectively, given by

$$\delta_{1c} = \frac{2F_x l^3}{32EAh^2} = \frac{\eta^2 l}{16\sqrt{3}E}\sigma_{12}\sin\tfrac{\theta}{2}, \tag{4.33a}$$

$$\phi = \frac{M_c l}{EAh^2} = \frac{\eta^2}{\sqrt{3}E}\sigma_{12}(3\cos^2\tfrac{\theta}{2} - \sin^2\tfrac{\theta}{2}). \tag{4.33b}$$

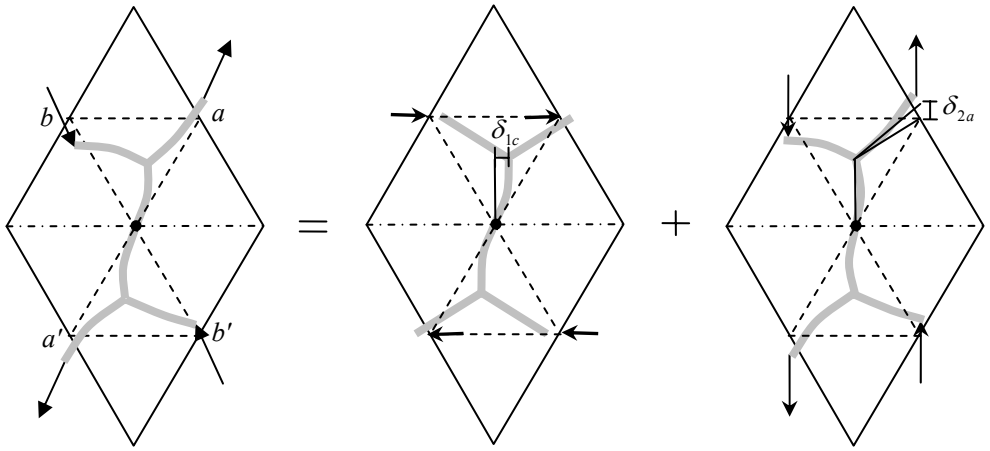

Fig. 4.13. Shear deformation of a unit cell.

The deflection by the bending moment is obtained with the help of the third figure in Fig. 4.13 and Fig. 4.12(b) as

$$\delta_{2a} = \frac{l}{2}\phi . \tag{4.34}$$

The displacement components at point *a* can now be determined as

$$u_{1a} = \delta_{\xi\xi}\cos\tfrac{\theta}{2} - \delta_{\xi\zeta}\sin\tfrac{\theta}{2} + \delta_{1c}, \tag{4.35a}$$

$$u_{2a} = \delta_{\xi\xi}\sin\tfrac{\theta}{2} + \delta_{\xi\zeta}\cos\tfrac{\theta}{2} + \delta_{2a}. \tag{4.35b}$$

Substituting Eqs. (4.30a,b), (4.31a,b) and (4.33-34) into Eqs. (4.35a,b) yields

$$u_{1a} = \frac{2l}{\sqrt{3}E}\sigma_{12}\cos^2\tfrac{\theta}{2}\sin\tfrac{\theta}{2} - \frac{\eta^2 l}{2\sqrt{3}E}\sigma_{12}(3\cos^2\tfrac{\theta}{2} - \sin^2\tfrac{\theta}{2})\sin\tfrac{\theta}{2} + \frac{\eta^2 l}{16\sqrt{3}E}\sigma_{12}\sin\tfrac{\theta}{2}, \tag{4.36a}$$

$$u_{2a} = \frac{2l}{\sqrt{3}E}\sigma_{12}\cos\tfrac{\theta}{2}\sin^2\tfrac{\theta}{2} + \frac{\eta^2 l}{2\sqrt{3}E}\sigma_{12}(3\cos^2\tfrac{\theta}{2} - \sin^2\tfrac{\theta}{2})(\cos\tfrac{\theta}{2} + 1). \tag{4.36b}$$

When $\theta = 60°$, Eqs. (4.36a,b) gives

$$u_{1a} = \frac{l}{32\sqrt{3}E}(24 - 15\eta^2)\sigma_{12}, \tag{4.37a}$$

$$u_{2a} = \frac{l}{4\sqrt{3}E}\left\{\sqrt{3} + 2\eta^2(\sqrt{3}+2)\right\}\sigma_{12}. \tag{4.37b}$$

Due to the symmetry shown in Fig. 4.10 (a), the displacement components at the other key points in the unit cell (see Fig. 4.6) can be readily obtained as

$$u_{1b} = u_{1a}\,, \tag{4.38a}$$

$$u_{2b} = -u_{2a}\,, \tag{4.38b}$$

$$u_{1a'} = -u_{1a}\,, \tag{4.38c}$$

$$u_{2a'} = -u_{2a}\,, \tag{4.38d}$$

$$u_{1b'} = -u_{1a}\,, \tag{4.38e}$$

$$u_{2b'} = u_{2a}\,. \tag{4.38f}$$

Using Eqs. (4.16c) and (4.17a-d) in Eqs. (4.38a-f) then gives the shear stress and shear strain relation as

$$\gamma_{12} = \frac{1}{24E}\left\{16\sqrt{3} + \eta^2(32 + 11\sqrt{3})\right\}\sigma_{12}\,. \tag{4.39}$$

From Eq. (4.39) the effective shear modulus G_{12}^{*} is obtained as

$$G_{12}^{*} = \frac{24E}{16\sqrt{3} + \eta^2(32 + 11\sqrt{3})}\,. \tag{4.40}$$

4.4.3. Loading by couple stress m_{13}

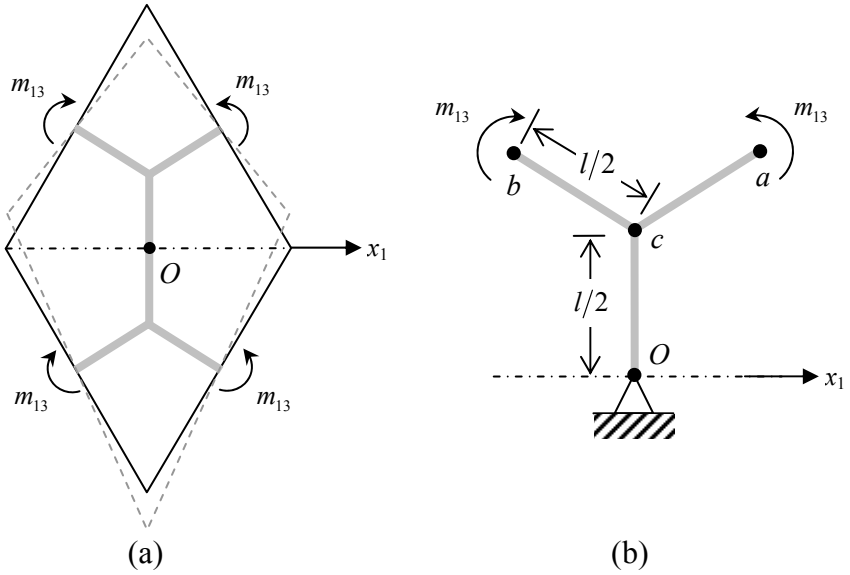

Fig. 4.14. (a) Unit cell under couple stress m_{13},
(b) Upper part of the unit cell under couple stress m_{13}.

The deformed shape (enclosed in the dotted lines) of the unit cell subjected to couple stress m_{13} and the upper part of the unit cell are shown in Fig. 4.14 (a,b). It is clear that there is no interaction force at the joint c because the two bending moments due to the couple stresses are equilibrated at c.

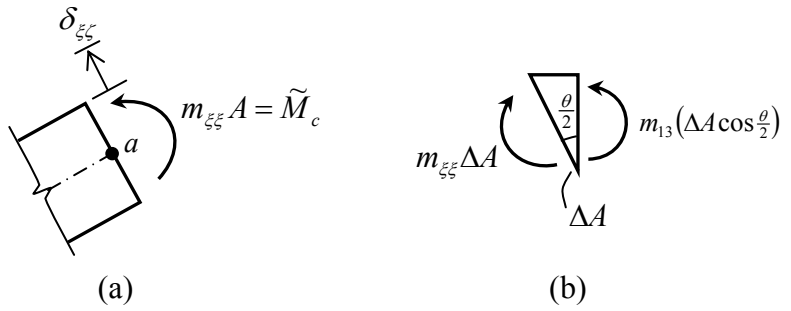

Fig. 4.15. (a) Bending moment and deflection at point a in Fig. 4.14,
(b) Equilibrium at point a.

Fig. 4.15 (a) shows the direction of the deflection $\delta_{\xi\zeta}$ at point a by the bending moment $\tilde{M}_c$ due to the couple stress $m_{\xi\zeta}$. The rotation angle ϕ of member ca is given by

$$\phi = \frac{\tilde{M}_c l}{8EI}. \tag{4.41}$$

From the FBD in Fig. 4.15 (b), the equilibrium requires

$$\sum M_z = 0 : -m_{\xi\xi}\Delta A + m_{13}\Delta A\cos\tfrac{\theta}{2} = 0. \tag{4.42}$$

Let $\tilde{M}_c = m_{\xi\xi}A$. Then, Eq. (4.42) gives

$$\tilde{M}_c = m_{13}\cos\tfrac{\theta}{2}A. \tag{4.43}$$

The displacement components at points d and e in the unit cell shown in Fig. 4.6 can be determined with the help of Fig. 4.16. Note that the edges of the unit cell will move whenever cell walls enclosed in the unit cell deform. To better understand geometrical relations, the three shadowed triangles shown in Fig. 4.16 are detached from the unit cell. The rotation angle ϕ is the same as the angle between the edges of the undeformed unit cell and the deformed unit cell.

From the geometrical relations shown in Fig. 4.16 and the sine law, the displacements at points *d* and *e* can be obtained as

$$\frac{u_{2d}}{\sin\phi} = \frac{\frac{\sqrt{3}}{2}l}{\sin\{\pi - (\frac{\theta}{2} + \phi)\}} = \frac{\frac{\sqrt{3}}{2}l}{\sin\frac{\theta}{2}\cos\phi + \cos\frac{\theta}{2}\sin\phi}, \tag{4.44a}$$

$$\frac{u_{2d'}}{\sin\phi} = \frac{\frac{\sqrt{3}}{2}l}{\sin(\frac{\theta}{2} - \phi)} = \frac{\frac{\sqrt{3}}{2}l}{\sin\frac{\theta}{2}\cos\phi - \cos\frac{\theta}{2}\sin\phi}, \tag{4.44b}$$

$$u_{1e} = -\sqrt{3}l\sin^2\phi, \tag{4.44c}$$

$$u_{2e} = \sqrt{3}l\sin\phi\cos\phi = \frac{l\sin\phi}{\frac{1}{\sqrt{3}\cos\phi}}. \tag{4.44d}$$

By symmetry,

$$u_{1e'} = -u_{1e}, \tag{4.45a}$$

$$u_{2d'} = -u_{2d}. \tag{4.45b}$$

The displacement components at other key points are all zero-valued, i.e.,

$$u_{1a} = u_{1a'} = u_{2a} = u_{2a'} = u_{1b} = u_{1b'} = u_{2b} = u_{2b'} = u_{1d'} = u_{1d} = u_{1O} = u_{2O} = 0. \tag{4.46}$$

When $\theta = 60°$, Eqs. (4.44a,b) give

$$u_{2d} = \frac{l\sin\phi}{\frac{\cos\phi}{\sqrt{3}} + \sin\phi}, \tag{4.47a}$$

$$u_{2d'} = \frac{l\sin\phi}{\frac{\cos\phi}{\sqrt{3}} - \sin\phi}. \tag{4.47b}$$

For the small angle ϕ, Eq. (4.44d) can be replaced by

$$u_{2e} = \frac{l\sin\phi}{\frac{\cos\phi}{\sqrt{3}}}. \tag{4.48}$$

From Eqs. (4.47a,b) and (4.48) an inequality, $u_{2d'} > u_{2e} > u_{2d}$, can be identified, which is used in drawing Fig. 4.16. Based on a linear regression analysis, Eqs. (4.47a,b) and (4.48) can be approximately represented by

$$u_{2d'} \approx \alpha l\phi, \tag{4.49a}$$

$$u_{2e} \approx \beta l\phi, \tag{4.49b}$$

$$u_{2d} \approx \gamma l \phi , \tag{4.49c}$$

where $\alpha = 2.04$, $\beta = 1.72$, $\gamma = 1.52$, and $0° < \phi < 6°$.

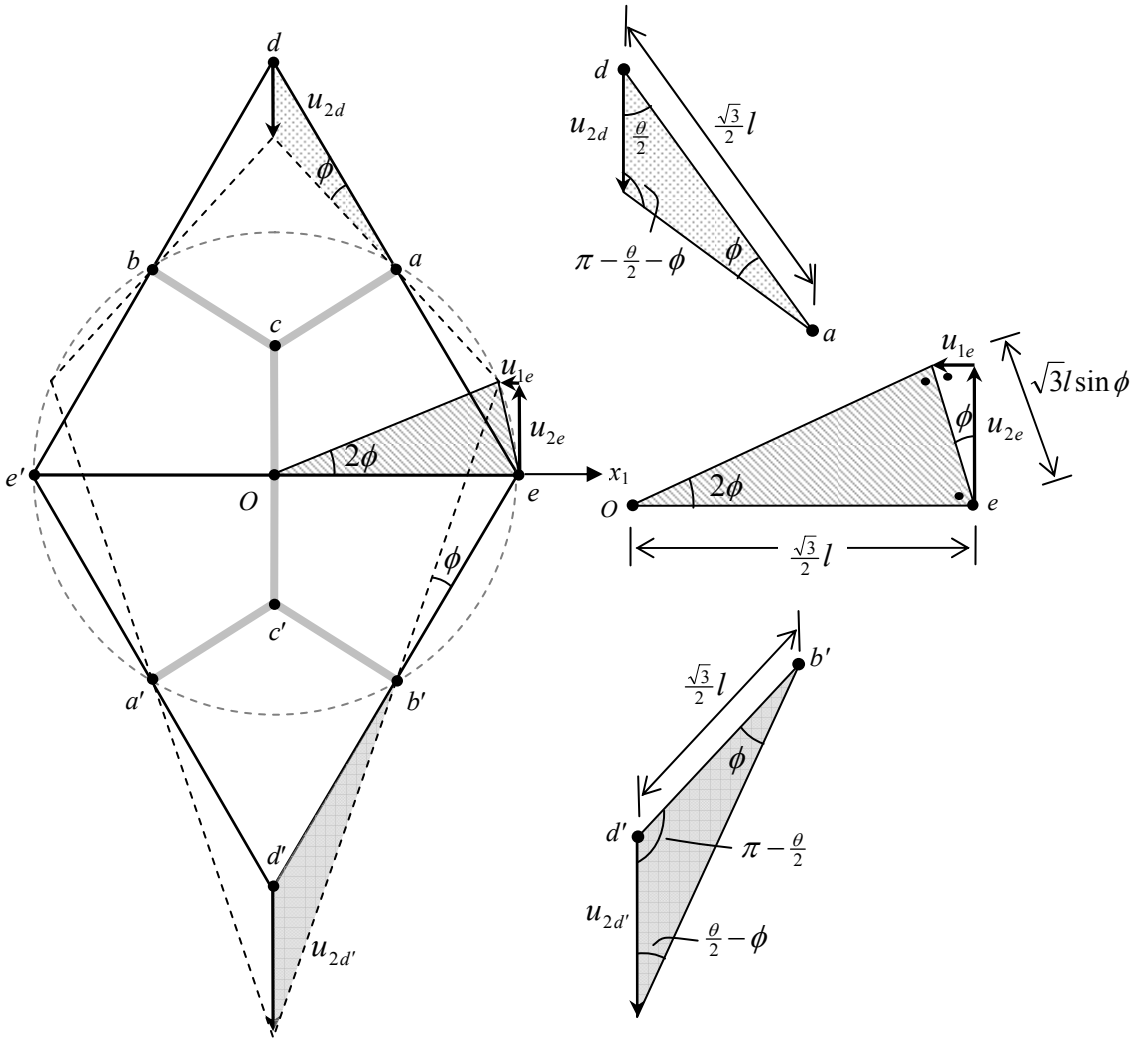

Fig. 4.16. Displacements at the key points induced by couple stress m_{13}.

Substituting Eqs. (4.17e-h,j) and (4.49a-c) into Eq. (4.16d) gives

$$\chi_{13} = \frac{7}{6}\frac{\phi}{l}. \tag{4.50}$$

Using Eqs. (4.41) and (4.43) (with $\theta = 60°$) in Eq. (4.50) then yields

$$\chi_{13} = \frac{7\sqrt{3}}{8E_s h^2} m_{13} . \tag{4.51}$$

The use of Eqs. (2.7) and (4.40) in Eq. (4.51) finally leads to the determination of the material length scale parameter $l_{13}{}^{*}$:

$$l_{13}^{*} = \sqrt{\frac{16\sqrt{3} + \eta^2 (32 + 11\sqrt{3})}{42\sqrt{3}}}\, h . \tag{4.52}$$

4.4.4 Loading by couple stress m_{23}

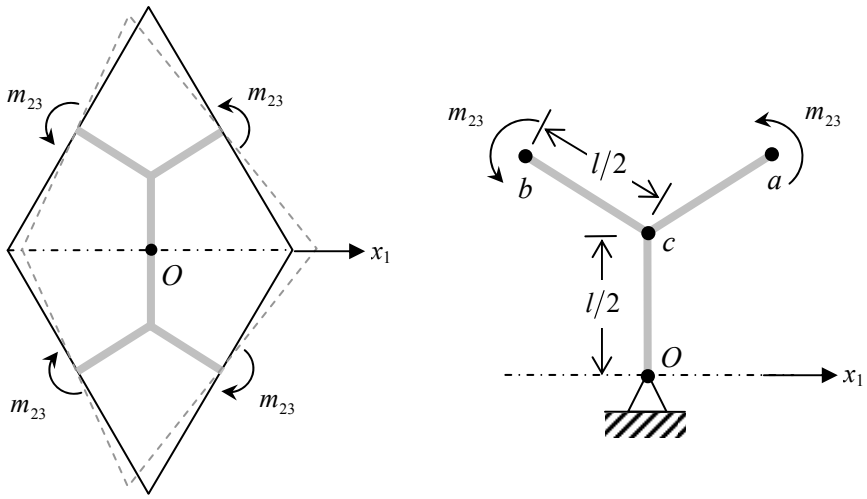

(a) (b)

Fig. 4.17. (a) Unit cell under couple stress m_{23},
(b) Symmetric part of the unit cell under couple stress m_{23}.

When couple stress m_{23} is applied, the deformed shape of the unit cell is shown in Fig. 4.17(a). Because of the symmetric loading with respect to x_1 axis, only the upper part of the unit cell (see Fig. 4.17(b)) needs to be considered to determine the displacements at edge points.

As illustrated in Figs. 4.18 (a,b), an interaction moment exists at the joint c which satisfies the following equilibrium equation based on the FBD shown in Fig. 4.18(b):

$$\sum M_z = 0 : -m_{\xi\xi} \Delta A + m_{23} \Delta A \sin\tfrac{\theta}{2} = 0 . \tag{4.53}$$

It then follows from Eq. (4.53) that

$$\frac{\hat{M}_c}{2} = m_{23} \sin \tfrac{\theta}{2} A\,, \tag{4.54}$$

where $\hat{M}_c \equiv 2m_{\xi\xi} A$ is the reaction moment at point *c*.

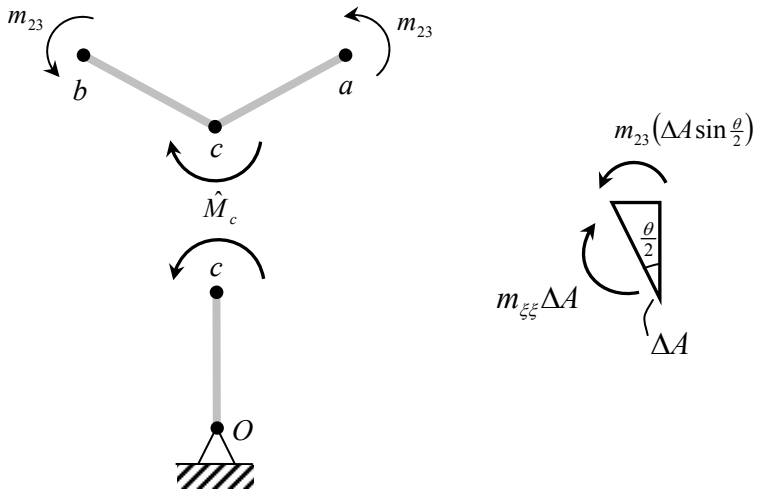

(a) (b)

Fig. 4.18 (a) Interaction moment at point *c* in Fig. 4.17, (b) Equilibrium at point *a*.

Due to the periodicity of the honeycomb, rotations only exist at points *a* and *b* (but no deflection). The rotation angle at point *a* or *b* can be obtained as

$$\phi = \frac{6\frac{\hat{M}_c}{2} l}{Ewh^3}\,. \tag{4.55}$$

Using Eq. (4.54) in Eq. (4.55) gives, with $\theta = 60°$,

$$\phi = \frac{3l}{Eh^2} m_{23}\,. \tag{4.56}$$

Similar to that used in Section 4.4.3, a geometrical approach is taken here to obtain the displacements at points *d*, *d*′, *e* and *e*′.

From the geometry in Fig. 4.19, the displacement components at point *d* are given by

$$u_{1d} = \frac{l \sin \phi}{\frac{1}{\cos \phi}}, \tag{4.57a}$$

$$u_{2d} = \frac{l}{2}\sin^2\phi\,. \tag{4.57b}$$

For a small angle ϕ, Eq. (4.57a) can be approximately represented by

$$u_{1d} = \frac{l\sin\phi}{\cos\phi}\,. \tag{4.58}$$

Using the sine law gives the displacements at points e and e' as

$$\frac{u_{1e}}{\sin\phi} = \frac{\frac{\sqrt{3}}{2}l}{\sin(\frac{\pi}{3}-\phi)}, \tag{4.59a}$$

$$\frac{u_{1e'}}{\sin\phi} = \frac{\frac{\sqrt{3}}{2}l}{\sin(\frac{2\pi}{3}-\phi)}, \tag{4.59b}$$

which, upon the use of trigonometry formulas, become

$$u_{1e} = \frac{l\sin\phi}{\cos\phi - \frac{\sin\phi}{\sqrt{3}}}, \tag{4.60a}$$

$$u_{1e'} = \frac{l\sin\phi}{\cos\phi + \frac{\sin\phi}{\sqrt{3}}}\,. \tag{4.60b}$$

From Eqs. (4.58) and (4.60a,b) an inequality, $u_{1e}>u_{1d}>u_{1e'}$, is identified, which is used in drawing Fig. 4.19. From the symmetry shown in Fig. 4.17(a), the displacement components at point d can be determined as

$$u_{1d'} = u_{1d}\,, \tag{4.61a}$$

$$u_{2d'} = -u_{2d}\,. \tag{4.61b}$$

The displacements at all other key points are zero-valued, i.e.,

$$u_{1a} = u_{1a'} = u_{2a} = u_{2a'} = u_{1b} = u_{1b'} = u_{2b} = u_{2b'} = u_{2e} = u_{2e'} = u_{1O} = u_{2O} = 0\,. \tag{4.62}$$

Based on a linear regression analysis, Eqs. (4.58) and (4.60a,b) can be approximately represented by

$$u_{1e} \approx \alpha' l\phi\,, \tag{4.63a}$$

$$u_{1d} \approx \beta' l\phi\,, \tag{4.63b}$$

$$u_{1e'} \approx \gamma' l\phi\,, \tag{4.63c}$$

where $\alpha' = 1.05$, $\beta'=1.00$, $\gamma'=0.96$, and $0°<\phi<6°$.

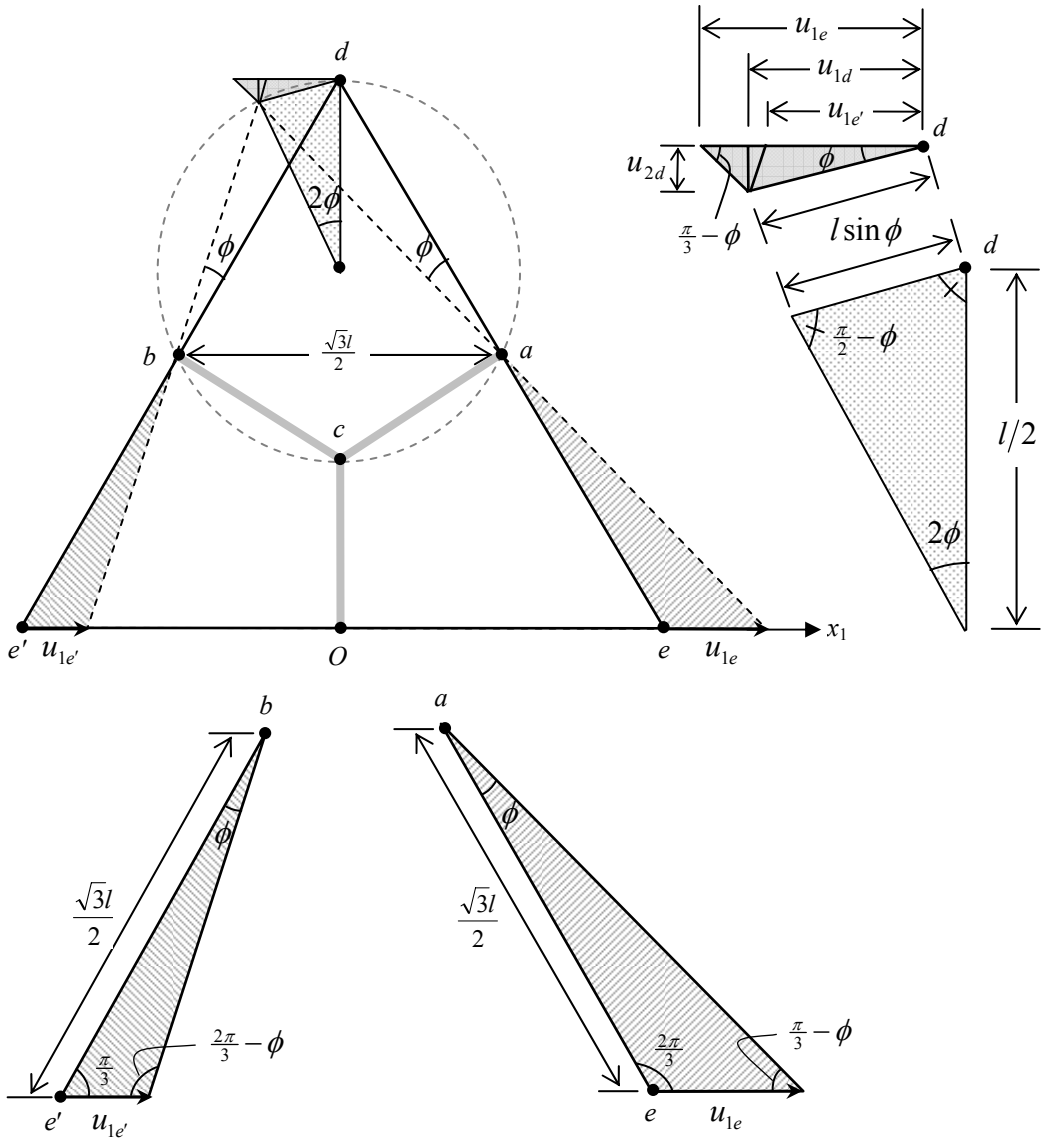

Fig. 4.19. Displacements at the key points induced by couple stress m_{23}.

Substituting Eqs. (4.17e-i) and (4.62a-c) into Eq. (4.16e) gives

$$\chi_{23} = \frac{4.01}{18}\frac{\phi}{l}. \tag{4.64}$$

Inserting Eq. (4.56) into Eq. (4.64) yields

$$\chi_{23} = \frac{4.01}{6Eh^2} m_{23}. \tag{4.65}$$

The use of Eqs. (2.7) and (4.40) in Eq. (4.65) then leads to the determination of the material length scale parameter l_{23}^{*}:

$$l_{23}^{*}=\sqrt{\frac{48+\eta^{2}(33+32\sqrt{3})}{192.48}}\,h\,. \tag{4.66}$$

4.4.5 Constitutive relations

Combining Eqs. (4.25a,b), (4.39), (4.51) and (4.65) finally gives

$$\begin{pmatrix}\varepsilon_{11}\\ \varepsilon_{22}\\ \gamma_{12}\\ \chi_{13}\\ \chi_{23}\end{pmatrix}=\frac{1}{E}\begin{bmatrix}\frac{3+\eta^{2}}{4} & \frac{1-\eta^{2}}{4} & 0 & 0 & 0\\ \frac{1-\eta^{2}}{4} & \frac{3+\eta^{2}}{4} & 0 & 0 & 0\\ 0 & 0 & \frac{16\sqrt{3}+\eta^{2}(32+11\sqrt{3})}{24} & 0 & 0\\ 0 & 0 & 0 & \frac{7\sqrt{3}}{8h^{2}} & 0\\ 0 & 0 & 0 & 0 & \frac{4.01}{6h^{2}}\end{bmatrix}\begin{pmatrix}\sigma_{11}\\ \sigma_{22}\\ \sigma_{12}\\ m_{13}\\ m_{23}\end{pmatrix}, \tag{4.67}$$

which are the stress-strain relations of the periodic honeycomb structure.

Eq. (4.67) can be inverted to obtain

$$\begin{pmatrix}\sigma_{11}\\ \sigma_{22}\\ \sigma_{12}\\ m_{13}\\ m_{23}\end{pmatrix}=E\begin{bmatrix}\frac{\eta^{2}+3}{2(\eta^{2}+1)} & \frac{\eta^{2}-1}{2(\eta^{2}+1)} & 0 & 0 & 0\\ \frac{\eta^{2}-1}{2(\eta^{2}+1)} & \frac{\eta^{2}+3}{2(\eta^{2}+1)} & 0 & 0 & 0\\ 0 & 0 & \frac{24}{16\sqrt{3}+\eta^{2}(32+11\sqrt{3})} & 0 & 0\\ 0 & 0 & 0 & \frac{8h^{2}}{7\sqrt{3}} & 0\\ 0 & 0 & 0 & 0 & \frac{6h^{2}}{4.01}\end{bmatrix}\begin{pmatrix}\varepsilon_{11}\\ \varepsilon_{22}\\ \gamma_{12}\\ \chi_{13}\\ \chi_{23}\end{pmatrix}. \tag{4.68}$$

The coefficient matrix in Eq. (4.68) gives the stiffness matrix of the regular honeycomb structure, which is treated as a homogenized continuum.

4.5. SUMMARY

The constitutive relations for a regular honeycomb structure is derived based on the modified couple stress theory, and the effective elastic constants are determined using a structural mechanics approach and a unit cell. Each cell wall of the unit cell is regarded as a Bernoulli-Euler beam.

Two couple stress loading modes are analyzed to obtain the effective material length scale parameters. Since the rigidity of the deformed unit cell is different for each loading

mode, two effective material length scale parameters are obtained, which differs from the model developed by Wang and Stronge (1999) using a micropolar elasticity theory, where two loading modes are regarded to be the same.

CHAPTER V

VARIATIONAL FORMULATION OF A SIMPLIFIED STRAIN GRADIENT ELASTICITY THEORY AND ITS APPLICATION TO THE PROBLEM OF A PRESSURIZED THICK-WALLED CYLINDER

5.1. INTRODUCTION

Higher order strain gradient elasticity theories containing internal material length scale parameters are capable of explaining microstructure-dependent effects observed at the micron scale (e.g., Lam et al., 2003), unlike the classical elasticity theory that does not include such additional material parameters. Mindlin (1965) developed a general (grade-3) strain gradient elasticity theory that contains 18 independent material constants (with two being the classical Lamé constants) for an isotropic elastic material. The strain gradient theory (grade-2) proposed by Casal (1972) includes 4 elastic constants, with two being the classical Lamé constants and the other two being the material length scale parameters. This theory has been generalized to three-dimensional cases by Vardoulakis and Sulem (1995) and further elaborated by Exadaktylos and Vardoulakis (1998). Due to the difficulties in determining microstructure-dependent length scale parameters (e.g., Lam et al., 2003), strain gradient elasticity theories involving only one additional elastic constant are very desirable.

One such strain gradient model has been suggested by Altan and Aifantis (1992, 1997) by simplifying the strain gradient elasticity theory of Mindlin and Eshel (1968). This simplified model contains three elastic constants, with two being Lamé constants and the third one being a strain gradient coefficient having the dimension of length squared and measuring the material microstructural effects. This model has been applied to analyze a number of problems (Ru and Aifantis, 1993; Aifantis, 1996; Teneketzis Tenek and Aifantis, 2001; Lazopoulos, 2004; Li et al., 2004) due to its simplicity. However, a rigorous, complete mathematical formulation for the model proposed by

Altan and Aifantis (1992, 1997) is still lacking in the literature. This motivated the work presented in this chapter.

In Section 5.2, a variational formulation is provided for the simplified strain gradient model suggested by Altan and Aifantis (1992, 1997) by using the principle of minimum total potential energy, which leads to the complete determination of the governing equations and boundary conditions in a simultaneous manner. The boundary conditions obtained here differ from those suggested by Altan and Aifantis (1997), although the equilibrium equations are the same. Also, a displacement formulation of the simplified strain gradient theory is presented in Section 5.3 to complement the stress formulation. As a direct application of the newly developed displacement form of the theory, the pressurized thick-walled cylinder problem is solved in Section 5.4. Numerical results are also provided there to illustrate the current strain gradient theory based solution and to compare it with the well known Lamé's solution in classical elasticity. The chapter concludes with a summary in Section 5.5.

5.2. VARIATIONAL FORMULATION

The strain energy density function for an isotropic, gradient-dependent, linearly elastic material may be written as (e.g., Altan and Aifantis, 1997)

$$w = w(\varepsilon_{ij}, \varepsilon_{ij,k}) = \frac{1}{2}\lambda\varepsilon_{ii}\varepsilon_{jj} + \mu\varepsilon_{ij}\varepsilon_{ij} + c\left(\frac{1}{2}\lambda\varepsilon_{ii,k}\varepsilon_{jj,k} + \mu\varepsilon_{ij,k}\varepsilon_{ij,k}\right), \tag{5.1}$$

where λ and μ are the Lamé constants, c is a strain gradient coefficient with the dimension of length squared, and ε_{ij} are the strain components given by

$$\varepsilon_{ij} = \frac{1}{2}(u_{i,j} + u_{j,i}). \tag{5.2}$$

Then, the strain energy U in a region Ω occupied by the elastically deformed material can be readily shown to be

$$U = \int_{\Omega} w\, dv = \frac{1}{2}\int_{\Omega} (\tau_{ij}\varepsilon_{ij} + \mu_{ijk}\kappa_{ijk})\, dv, \tag{5.3}$$

where the Cauchy stress τ_{ij}, the double stress μ_{ijk} and the strain gradient κ_{ijk} are,

respectively, given by

$$\tau_{ij} = \frac{\partial w}{\partial \varepsilon_{ij}} = \lambda \varepsilon_{ll} \delta_{ij} + 2\mu \varepsilon_{ij} = \tau_{ji}, \tag{5.4}$$

$$\mu_{ijk} = \frac{\partial w}{\partial \kappa_{ijk}} = c(\lambda \varepsilon_{ll} \delta_{ij} + 2\mu \varepsilon_{ij}),_k = c\tau_{ij},_k = \mu_{jik}, \tag{5.5}$$

$$\kappa_{ijk} = \varepsilon_{ij,k} = \frac{1}{2}(u_{i,jk} + u_{j,ik}). \tag{5.6}$$

The work done by external forces is

$$W = \int_\Omega f_i u_i \, dv + \int_{\partial\Omega} (t_i u_i + q_i Du_i) \, da, \tag{5.7}$$

where f_i, t_i and q_i are, respectively, the body force, Cauchy stress traction vector and double force traction vector, respectively, $\partial\Omega$ is the surface of Ω, and Du_i is the normal (directional) derivative of the displacement u_i defined by

$$Du_i = n_l u_{i,l}, \tag{5.8}$$

with n_l being the outward unit vector normal to $\partial\Omega$.

Using Eqs. (5.3) and (5.7) then gives the total potential energy Π as

$$\Pi = U - W = \frac{1}{2}\int_\Omega (\tau_{ij}\varepsilon_{ij} + \mu_{ijk}\kappa_{ijk}) \, dv - \int_\Omega f_i u_i \, dv - \int_{\partial\Omega} (t_i u_i + q_i Du_i) \, da. \tag{5.9}$$

Taking the first variation of Π yields, with the symmetry properties of ε_{ij}, τ_{ij}, μ_{ijk} and κ_{ijk} indicated in Eqs. (5.2) and (5.4)-(5.6),

$$\delta\Pi = \delta U - \delta W = \int_\Omega (\tau_{ij}\delta\varepsilon_{ij} + \mu_{ijk}\delta\kappa_{ijk} - f_i\delta u_i) \, dv - \int_{\partial\Omega} (t_i \delta u_i + q_i Du_i) \, da. \tag{5.10}$$

Using Eqs. (5.2) and (5.6) and the symmetry of τ_{ij} and μ_{ijk} shown in Eqs. (5.4) and (5.5) leads to

$$\int_\Omega (\tau_{ij}\delta\varepsilon_{ij} + \mu_{ijk}\delta\kappa_{ijk} - f_i\delta u_i) dv = \int_\Omega (\tau_{ij}\delta u_{i,j} + \mu_{ijk}\delta u_{i,jk} - f_i\delta u_i) dv. \tag{5.11}$$

Applying the chain rule to the right hand side of Eq. (5.11) results in

$$\int_\Omega (\tau_{ij}\delta u_{i,j} + \mu_{ijk}\delta u_{i,jk} - f_i\delta u_i) dv = \int_\Omega \{[(\tau_{ij} - \mu_{ijk,k})\delta u_i],_j - (\tau_{ij} - \mu_{ijk,k}),_j \delta u_i - f_i\delta u_i + (\mu_{ijk}\delta u_{i,j}),_k\} dv. \tag{5.12}$$

Note that the total stress σ_{ij} is defined by (e.g., Altan and Aifantis, 1992; Li et al., 2004)

$$\sigma_{ij} \equiv \tau_{ij} - \mu_{ijk,k} = \tau_{ij} - c\tau_{ij,kk}. \tag{5.13}$$

Using Eq. (5.13) in Eq. (5.12) then gives

$$\int_\Omega (\tau_{ij}\delta u_{i,j} + \mu_{ijk}\delta u_{i,jk} - f_i\delta u_i)dv = \int_\Omega [(\sigma_{ij}\delta u_i)_{,j} - (\sigma_{ij,j} + f_i)\delta u_i + (\mu_{ijk}\delta u_{i,j})_{,k}]dv. \quad (5.14)$$

Applying the divergence theorem to Eq. (5.14) yields

$$\int_\Omega (\tau_{ij}\delta u_{i,j} + \mu_{ijk}\delta u_{i,jk} - f_i\delta u_i)dv = \int_{\partial\Omega} \sigma_{ij} n_j \delta u_i \, da - \int_\Omega (\sigma_{ij,j} + f_i)\delta u_i \, dv + \int_{\partial\Omega} \mu_{ijk} n_k \delta u_{i,j} \, da. \quad (5.15)$$

Note that the integrand of the third integral on the right hand side of Eq. (5.15) can be written as (e.g., Mindlin, 1964)

$$n_k \mu_{ijk}\delta u_{i,j} = n_k \mu_{ijk} D_j \delta u_i + n_k n_j \mu_{ijk} D\delta u_i, \quad (5.16)$$

where $D_j\delta u_i$ is the surface gradient of the displacement on $\partial\Omega$ (with the outward unit normal vector $\mathbf{n} = n_i\mathbf{e}_i$) given by

$$D_j \delta u_i = (\delta_{jl} - n_j n_l)\delta u_{i,l}. \quad (5.17)$$

Note that according to the chain rule the first term of the right hand side of Eq. (5.16) can be written as

$$n_k \mu_{ijk} D_j \delta u_i = D_j(n_k \mu_{ijk}\delta u_i) - D_j(n_k \mu_{ijk})\delta u_i, \quad (5.18)$$

where

$$D_j(n_k \mu_{ijk}\delta u_i) = (D_l n_l) n_k n_j \mu_{ijk}\delta u_i + n_q \varepsilon_{qpm}(\varepsilon_{mlj} n_l n_k \mu_{ijk}\delta u_i)_{,p}, \quad (5.19)$$

which is similar to an identity used by Mindlin (1964) and is proved in Appendix B.

Using Eqs. (5.16) – (5.19) in Eq. (5.15) then gives

$$\begin{aligned}\int_\Omega (\tau_{ij}\delta u_{i,j} + \mu_{ijk}\delta u_{i,jk} - f_i\delta u_i)dv &= -\int_\Omega (\sigma_{ij,j} + f_i)\delta u_i dv + \int_{\partial\Omega} n_k n_j \mu_{ijk} D\delta u_i da \\ &+ \int_{\partial\Omega} [\sigma_{ij} n_j - D_j(n_k \mu_{ijk}) + (D_l n_l) n_k n_j \mu_{ijk}]\delta u_i da + \int_{\partial\Omega} n_q \varepsilon_{qpm}(\varepsilon_{mlj} n_l n_k \mu_{ijk}\delta u_i)_{,p} da,\end{aligned} \quad (5.20)$$

where the third term on the right hand side can be rewritten as, with the help of Eq. (5.17),

$$\int_{\partial\Omega} \{\sigma_{ij} n_j - (n_{k,j}\mu_{ijk} + n_k \mu_{ijk,j} - n_j n_l n_{k,l}\mu_{ijk} - n_j n_l n_k \mu_{ijk,l}) + n_{l,l} n_k n_j \mu_{ijk}\}\delta u_i da, \quad (5.21)$$

and the fourth term on the right hand side is given by Stokes' theorem as

$$\int_{\partial\Omega} n_q \varepsilon_{qpm}(\varepsilon_{mlj} n_l n_k \mu_{ijk}\delta u_i)_{,p} ds = \oint_\Gamma [[n_k m_j \mu_{ijk}]]\delta u_i dl, \quad (5.22)$$

where Γ is the edge between two smooth sub-surfaces belonging to $\partial\Omega$, and m_j is the

outer co-normal vector satisfying the following relation:

$$m_j = \varepsilon_{jml} s_m n_l \,, \tag{5.23}$$

with s_m being the unit vector tangent to the edge Γ. The double brackets in Eq. (5.22) indicate that the enclosed quantity is the difference between the values on the two sides of the edge. If the entire surface $\partial\Omega$ is smooth, then the last term of Eq. (5.20) vanishes.

Finally, substituting Eqs. (5.20) – (5.22) into Eq. (5.10) results in

$$\begin{aligned}\delta\Pi = &-\int_\Omega (\sigma_{ij,j} + f_i)\delta u_i dv - \int_{\partial\Omega} \{t_i - [\sigma_{ij} n_j - (\mu_{ijk} n_k)_{,j} + (\mu_{ijk} n_k n_l)_{,l} n_j]\}\delta u_i da \\ &- \int_{\partial\Omega} (q_i - \mu_{ijk} n_j n_k) D\delta u_i da + \oint_\Gamma [[\mu_{ijk} m_j n_k]]\delta u_i dl \,.\end{aligned} \tag{5.24}$$

By applying the principle of minimum total potential energy, i.e., $\delta\Pi = 0$ for the stable equilibrium (e.g., Steigmann, 1992), and the fundamental lemma of the calculus of variation (e.g., Gao and Mall, 2001), Eq. (5.24) then gives

$$\sigma_{ij,j} + f_i = 0 \qquad \text{in } \Omega \tag{5.25}$$

as the governing (equilibrium) equations, and

$$\left.\begin{aligned} &\sigma_{ij} n_j - (\mu_{ijk} n_k)_{,j} + (\mu_{ijk} n_k n_l)_{,l} n_j = \bar{t}_i \quad or \quad u_i = \bar{u}_i \\ &\mu_{ijk} n_j n_k = \bar{q}_i \quad or \quad u_{i,l} n_l = \overline{\frac{\partial u_i}{\partial n}} \end{aligned}\right\} \text{ on } \partial\Omega \text{ (smooth part)} \tag{5.26a,b}$$

$$[[\mu_{ijk} m_j n_k]] = 0 \quad \text{or} \quad u_i = \bar{u}_i \qquad \text{on } \Gamma \tag{5.26c}$$

as the boundary conditions. In Eqs. (5.26a,b,c), the overbar represents a prescribed value.

It should be mentioned that Eqs. (5.25) and (5.26b) derived here are the same as those reported in Altan and Aifantis (1997) without derivations, whereas the traction boundary condition listed in Eq. (5.26a) differs from that given in Altan and Aifantis (1997), where terms involving gradients of the unit normal vector were missing, and the edge boundary condition obtained in Eq. (5.26c) was totally ignored in their paper.

5.3. DISPLACEMENT FORMULATION

To facilitate the application of the simplified strain gradient elasticity to problems that favor treating the displacement components as basic unknowns, a displacement

formulation is provided in this section. All expressions are presented in tensor forms and are therefore coordinate-invariant.

Using Eqs. (5.2) and (5.4) in Eq. (5.13) gives

$$\boldsymbol{\sigma} = (1 - c\nabla^2)[\lambda(\nabla \cdot \mathbf{u})\mathbf{I} + \mu\{\nabla\mathbf{u} + (\nabla\mathbf{u})^{\mathrm{T}}]. \tag{5.27}$$

Taking the divergence on the both sides of Eq. (27) yields

$$\nabla \cdot \boldsymbol{\sigma} = (1 - c\nabla^2)[(\lambda + \mu)\nabla(\nabla \cdot \mathbf{u}) + \mu\nabla^2\mathbf{u}], \tag{5.28}$$

where ∇^2 is the Laplacian. Upon the use of the identity $\nabla^2\mathbf{u} = \nabla(\nabla \cdot \mathbf{u}) - \mathrm{curl}(\mathrm{curl}\mathbf{u})$, Eq. (5.28) becomes

$$\nabla \cdot \boldsymbol{\sigma} = (1 - c\nabla^2)[(\lambda + 2\mu)\nabla(\nabla \cdot \mathbf{u}) - \mu\,\mathrm{curl}(\mathrm{curl}\mathbf{u})]. \tag{5.29}$$

Substituting Eq. (5.29) into Eq. (5.25) then gives

$$(1 - c\nabla^2)[(\lambda + 2\mu)\nabla(\nabla \cdot \mathbf{u}) - \mu\,\mathrm{curl}(\mathrm{curl}\mathbf{u})] + \mathbf{f} = \mathbf{0} \tag{5.30}$$

as the equilibrium equations in terms of the displacement vector $\mathbf{u}$.

In tensor forms, the boundary conditions obtained in Eqs. (5.26a-c) are now given by

$$\left.\begin{aligned} &\boldsymbol{\sigma}\mathbf{n} - \nabla \cdot (\boldsymbol{\mu}\mathbf{n}) + (\nabla \cdot \mathbf{n})(\boldsymbol{\mu} : \mathbf{n} \otimes \mathbf{n}) + (\nabla\boldsymbol{\mu} : \mathbf{n} \otimes \mathbf{n})\mathbf{n} + \boldsymbol{\mu} : [\mathbf{n} \otimes \{(\nabla\mathbf{n})\mathbf{n}\}] = \bar{\mathbf{t}} \quad \text{or} \quad \mathbf{u} = \bar{\mathbf{u}} \\ &\boldsymbol{\mu} : (\mathbf{n} \otimes \mathbf{n}) = \bar{\mathbf{q}} \quad \text{or} \quad (\nabla\mathbf{u})\mathbf{n} = \overline{\frac{\partial \mathbf{u}}{\partial n}} \end{aligned}\right\} \text{on } \partial\Omega \text{ (smooth part)} \tag{5.31a,b}$$

$$[[\boldsymbol{\mu} : (\mathbf{m} \otimes \mathbf{n})]] = \mathbf{0} \quad \text{or} \quad \mathbf{u} = \bar{\mathbf{u}} \qquad \text{on } \Gamma \tag{5.31c}$$

where

$$\boldsymbol{\mu} = c\nabla[\lambda(\nabla \cdot \mathbf{u})\mathbf{I} + \mu\{\nabla\mathbf{u} + (\nabla\mathbf{u})^{\mathrm{T}}] \tag{5.32}$$

is the double stress $\boldsymbol{\mu}$ in terms of the displacement $\mathbf{u}$, whose component form is given in Eq. (5).

5.4. SOLUTION OF A PRESSURIZED THICK-WALLED CYLINDER

The classical elasticity based solution for the problem of a thick-walled cylinder subjected to an internal and/or an external pressure is due to Lamé (1852) and is essential for pressure vessel design and shrink-fit analysis. However, this solution does not contain any material length scale parameter and cannot explain the material microstructure-dependent effects. To account for such effects, the cylinder problem is

solved in this section by directly using the simplified strain gradient theory discussed earlier in this chapter.

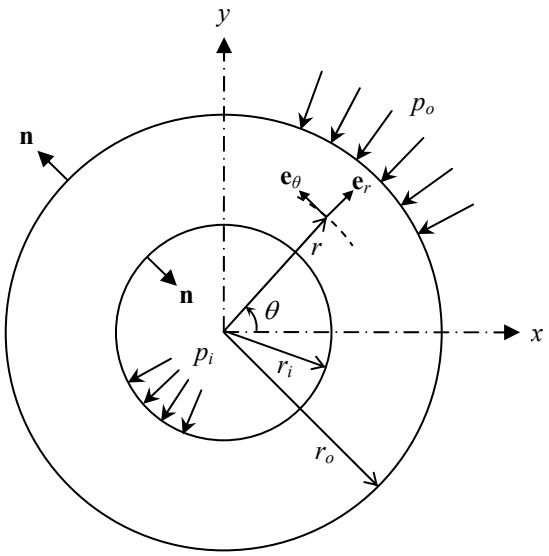

Fig. 5.1. A pressurized thick-walled cylinder.

Consider a pressurized cylinder that is undergoing a plane strain deformation. The cylinder has the inner radius r_i and outer radius r_o and is subjected to the internal pressure p_i and external pressure p_o, as shown in Fig. 5.1. The usual polar cylindrical coordinate system (r, θ, z) will be adopted, and the displacement method discussed in Section 5.3 will be used in the formulation below.

Due to the geometrical and loading symmetry, the displacement field $\mathbf{u}$ is taken to be

$$\mathbf{u} = u(r)\mathbf{e}_r, \tag{5.33}$$

where u is the only non-vanishing, radial displacement component, depending on the radial coordinate r only. It then follows from Eq. (5.33) that

$$\nabla \cdot \mathbf{u} = \frac{du}{dr} + \frac{u}{r}, \tag{5.34b}$$

$$\text{curl}\mathbf{u} = \mathbf{0}. \tag{5.34b}$$

Using Eq. (5.34a,b) in Eq. (5.30) gives the equilibrium equations in the absence of body force (i.e., $\mathbf{f}=\mathbf{0}$) as

$$\nabla(\nabla\cdot\mathbf{u})-c\nabla^2[\nabla(\nabla\cdot\mathbf{u})]=\mathbf{0}\,, \tag{5.35}$$

where

$$\nabla(\nabla\cdot\mathbf{u})=\left(\frac{d^2u}{dr^2}+\frac{1}{r}\frac{du}{dr}-\frac{1}{r^2}u\right)\mathbf{e}_r\,, \tag{5.36}$$

$$\nabla^2[\nabla(\nabla\cdot\mathbf{u})]=\left(\frac{d^4u}{dr^4}+\frac{2}{r}\frac{d^3u}{dr^3}-\frac{3}{r^2}\frac{d^2u}{dr^2}+\frac{3}{r^3}\frac{du}{dr}-\frac{3}{r^4}u\right)\mathbf{e}_r\,. \tag{5.37}$$

Substituting Eqs. (5.36) and (5.37) into Eq. (5.35) results in

$$\left(\frac{d^2u}{dr^2}+\frac{1}{r}\frac{du}{dr}-\frac{1}{r^2}u\right)-c\left(\frac{d^4u}{dr^4}+\frac{2}{r}\frac{d^3u}{dr^3}-\frac{3}{r^2}\frac{d^2u}{dr^2}+\frac{3}{r^3}\frac{du}{dr}-\frac{3}{r^4}u\right)=0\,. \tag{5.38}$$

Note that the second term on the left hand side of Eq. (5.38) can be written as

$$\frac{d^4u}{dr^4}+\frac{2}{r}\frac{d^3u}{dr^3}-\frac{3}{r^2}\frac{d^2u}{dr^2}+\frac{3}{r^3}\frac{du}{dr}-\frac{3}{r^4}u=\left(\frac{d^2}{dr^2}+\frac{1}{r}\frac{d}{dr}-\frac{1}{r^2}\right)\left(\frac{d^2u}{dr^2}+\frac{1}{r}\frac{du}{dr}-\frac{1}{r^2}u\right). \tag{5.39}$$

Define the linear differential operator L as

$$L\equiv\frac{d^2}{dr^2}+\frac{1}{r}\frac{d}{dr}-\frac{1}{r^2}\,. \tag{5.40}$$

Using Eqs. (5.39) and (5.40) in Eq. (5.38) then gives

$$L(1-cL)u=0 \tag{5.41}$$

as the governing equation of the cylinder problem based on the simplified strain gradient theory. Eq. (5.41) is a fourth-order ordinary differential equation for the general case with $c\neq 0$.

When $c = 0$, Eq. (5.41) reduces to, after using Eq. (5.40),

$$Lu\equiv\frac{d^2u}{dr^2}+\frac{1}{r}\frac{du}{dr}-\frac{u}{r^2}=0, \tag{5.42}$$

which is a homogeneous second-order ordinary differential equation of the Euler type. The solution of Eq. (5.42) can be readily obtained as

$$u_0=Ar+\frac{B}{r}\,, \tag{5.43}$$

where A and B are two constants to be determined from boundary conditions. This is the well-known solution of Lamé (1852) in classical elasticity, thereby indicating that

Lamé's solution is included in the current gradient elasticity solution as a special case with $c = 0$. When $c \neq 0$, a comparison of Eqs. (5.41) and (5.42) shows that solving Eq. (5.41) is equivalent to solving

$$(1 - cL)\, u = u_0 , \tag{5.44}$$

where u_0 is given in Eq. (5.43). Using Eqs. (5.40) and (5.43) in Eq. (5.44) yields

$$\frac{d^2 u}{dr^2} + \frac{1}{r}\frac{du}{dr} - \left(\frac{1}{r^2} + \frac{1}{c}\right) u = -\frac{1}{c}\left(Ar + \frac{B}{r}\right). \tag{5.45}$$

The homogeneous part of Eq. (5.45) is a second-order ordinary differential equation of the Bessel type, whose solution, $u_h(r)$, is given by (McLachlan, 1941)

$$u_h(r) = CI_1(\tfrac{1}{\sqrt{c}} r) + DK_1(\tfrac{1}{\sqrt{c}} r) , \tag{5.46}$$

where C and D are two constants, and $I_1(\cdot)$ and $K_1(\cdot)$ are, respectively, the modified Bessel functions of the first and second kinds of order 1given by

$$I_1(\tfrac{1}{\sqrt{c}} r) = \sum_{k=0}^{\infty} \frac{(\tfrac{1}{2\sqrt{c}} r)^{1+2k}}{k!\Gamma(k+2)} , \tag{5.47a}$$

$$K_1(\tfrac{1}{\sqrt{c}} r) = \frac{\pi}{2\sin\pi}\left\{I_{-1}(\tfrac{1}{\sqrt{c}} r) - I_1(\tfrac{1}{\sqrt{c}} r)\right\}, \tag{5.47b}$$

with $I_{-1}(\cdot)$ being the modified Bessel function of the first kind of order −1 which satisfies

$$I_{-1}(\tfrac{1}{\sqrt{c}} r) = I_1(\tfrac{1}{\sqrt{c}} r). \tag{5.48}$$

A particular solution of Eq. (5.45) is found to be

$$u_p(r) = Ar + \frac{B}{r} , \tag{5.49}$$

which happens to be the same as that given in Eq. (5.43). Combining Eqs. (5.46) and (5.49) then gives the general solution of Eq. (5.45), and thus of Eq. (5.41) or Eq. (5.38), as

$$u(r) = Ar + \frac{B}{r} + CI_1(\tfrac{1}{\sqrt{c}} r) + DK_1(\tfrac{1}{\sqrt{c}} r) . \tag{5.50}$$

Using Eq. (5.50) in Eq. (5.33) will yield the displacement field in the cylinder wall. It then follows from Eqs. (5.2), (5.33) and (5.50) that the strain field is

$$\boldsymbol{\varepsilon}(r)=\frac{du}{dr}\mathbf{e}_r\otimes\mathbf{e}_r+\frac{u}{r}\mathbf{e}_\theta\otimes\mathbf{e}_\theta\,. \tag{5.51}$$

Substituting Eq. (5.51) into Eq. (5.4) gives the Cauchy stress as

$$\boldsymbol{\tau}(r)=\left[(\lambda+2\mu)\frac{du}{dr}+\lambda\frac{u}{r}\right]\mathbf{e}_r\otimes\mathbf{e}_r+\left[\lambda\frac{du}{dr}+(\lambda+2\mu)\frac{u}{r}\right]\mathbf{e}_\theta\otimes\mathbf{e}_\theta+\left(\lambda\frac{du}{dr}+\lambda\frac{u}{r}\right)\mathbf{e}_z\otimes\mathbf{e}_z\,. \tag{5.52}$$

In component form, Eq. (5.52) becomes

$$\tau_{rr}=(\lambda+2\mu)\frac{du}{dr}+\lambda\frac{u}{r},\ \tau_{\theta\theta}=\lambda\frac{du}{dr}+(\lambda+2\mu)\frac{u}{r},\ \tau_{zz}=\lambda\frac{du}{dr}+\lambda\frac{u}{r}. \tag{5.53}$$

The total stress $\boldsymbol{\sigma}$ in terms of the components of the Cauchy stress $\boldsymbol{\tau}$ is obtained from Eq. (5.13) as

$$\begin{aligned}\boldsymbol{\sigma}=&\left[\tau_{rr}-c\left(\tau_{rr}''+\frac{\tau_{rr}'}{r}-\frac{2\tau_{rr}}{r^2}+\frac{2\tau_{\theta\theta}}{r^2}\right)\right]\mathbf{e}_r\otimes\mathbf{e}_r+\left[\tau_{\theta\theta}-c\left(\tau_{\theta\theta}''+\frac{\tau_{\theta\theta}'}{r}-\frac{2\tau_{\theta\theta}}{r^2}+\frac{2\tau_{rr}}{r^2}\right)\right]\mathbf{e}_\theta\otimes\mathbf{e}_\theta\\&+\left[\tau_{zz}-c\left(\tau_{zz}''+\frac{\tau_{zz}'}{r}\right)\right]\mathbf{e}_z\otimes\mathbf{e}_z,\end{aligned} \tag{5.54}$$

where use has been made of the Laplacian of the Cauchy stress $\boldsymbol{\tau}$**,** whose derivation is provided in Appendix C. Using Eqs. (5.50) and (5.53) in Eqs. (5.54), the expression of $\boldsymbol{\sigma} = \boldsymbol{\sigma}(r)$ will be determined. Here and in the sequel, the single and double prime denote, respectively, the first- and second-order derivatives with respect to r.

The double stress $\boldsymbol{\mu}$ in terms of the components of the Cauchy stress $\boldsymbol{\tau}$ is determined from Eqs. (5.5) as

$$\begin{aligned}\boldsymbol{\mu}=&c\left[\tau_{rr}'\mathbf{e}_r\otimes\mathbf{e}_r\otimes\mathbf{e}_r+\frac{1}{r}(\tau_{rr}-\tau_{\theta\theta})\mathbf{e}_r\otimes\mathbf{e}_\theta\otimes\mathbf{e}_\theta+\frac{1}{r}(\tau_{rr}-\tau_{\theta\theta})\mathbf{e}_\theta\otimes\mathbf{e}_r\otimes\mathbf{e}_\theta\right]\\&+c\left(\tau_{\theta\theta}'\mathbf{e}_\theta\otimes\mathbf{e}_\theta\otimes\mathbf{e}_r+\tau_{zz}'\mathbf{e}_z\otimes\mathbf{e}_z\otimes\mathbf{e}_r\right),\end{aligned} \tag{5.55}$$

whose derivation is given in Appendix C. Using Eqs. (5.50) and (5.53) in Eqs. (5.55), the expression of $\boldsymbol{\mu} = \boldsymbol{\mu}(r)$ will be obtained.

The boundary conditions of the current problem are given by

$$-\left\{\tau_{rr}-c\left[\tau_{rr}''+\frac{1}{r}(\tau_{rr}'-\tau_{\theta\theta}')-\frac{2}{r^2}(\tau_{rr}-\tau_{\theta\theta})\right]\right\}_{r=r_i}\mathbf{e}_r=p_i\mathbf{e}_r\,, \tag{5.56a}$$

$$\left\{\tau_{rr}-c\left[\tau''_{rr}+\frac{1}{r}(\tau'_{rr}-\tau'_{\theta\theta})-\frac{2}{r^2}(\tau_{rr}-\tau_{\theta\theta})\right]\right\}_{r=r_o}\mathbf{e}_r=-p_o\mathbf{e}_r, \tag{5.56b}$$

$$c\tau'_{rr}\big|_{r=r_i}\mathbf{e}_r=\mathbf{0}, \tag{5.56c}$$

$$c\tau'_{rr}\big|_{r=r_o}\mathbf{e}_r=\mathbf{0}. \tag{5.56d}$$

Eqs. (5.56a) and (5.56b) follow from the traction boundary conditions given in Eq. (5.31a), with the prescribed traction being $\bar{\mathbf{t}}=p_i\mathbf{e}_r$ on the inner surface $r=r_i$ and $\bar{\mathbf{t}}=-p_o\mathbf{e}_r$ on the outer surface $r=r_o$. Eqs. (5.56c) and (5.56d) are obtained from the double force traction boundary conditions specified in Eq. (5.31b), with the prescribed double force traction being $\mathbf{0}$ (i.e., $\bar{\mathbf{q}}=\mathbf{0}$) on both the inner surface $r=r_i$ and the outer surface $r=r_o$. The edge boundary conditions in Eq. (5.31c) are automatically satisfied, since the boundary $\partial\Omega$ consisting of the inner surface $r=r_i$ and the outer surface $r=r_o$ is round (smooth) here. Also, Eqs. (5.54) and (5.55) have been used in reaching Eqs. (5.56a-d).

Using Eqs. (5.50) and (5.53) in Eqs. (5.56a-d) then results in

$$\begin{aligned}&(-2\lambda-2\mu)A+\left(\frac{2\mu}{r_i^2}+\frac{4c\mu}{r_i^4}\right)B+\left[-\frac{2\sqrt{c}\mu}{r_i^2}I_0(\tfrac{1}{\sqrt{c}}r_i)-\left(\frac{\lambda}{r_i}-\frac{4c\mu}{r_i^3}\right)I_1(\tfrac{1}{\sqrt{c}}r_i)\right]C\\&+\left[\frac{2\sqrt{c}\mu}{r_i^2}K_0(\tfrac{1}{\sqrt{c}}r_i)-\left(\frac{\lambda}{r_i}-\frac{4c\mu}{r_i^3}\right)K_1(\tfrac{1}{\sqrt{c}}r_i)\right]D=p_i,\end{aligned} \tag{5.57a}$$

$$\begin{aligned}&(-2\lambda-2\mu)A+\left(\frac{2\mu}{r_o^2}+\frac{4c\mu}{r_o^4}\right)B+\left[-\frac{2\sqrt{c}\mu}{r_o^2}I_0(\tfrac{1}{\sqrt{c}}r_o)-\left(\frac{\lambda}{r_o}-\frac{4c\mu}{r_o^3}\right)I_1(\tfrac{1}{\sqrt{c}}r_o)\right]C\\&+\left[\frac{2\sqrt{c}\mu}{r_o^2}K_0(\tfrac{1}{\sqrt{c}}r_o)-\left(\frac{\lambda}{r_o}-\frac{4c\mu}{r_o^3}\right)K_1(\tfrac{1}{\sqrt{c}}r_o)\right]D=p_o,\end{aligned} \tag{5.57b}$$

$$\begin{aligned}&\frac{4\mu}{r_i^3}B+\left[-\frac{2\mu}{\sqrt{c}r_i}I_0(\tfrac{1}{\sqrt{c}}r_i)+\left(\frac{\lambda+2\mu}{c}+\frac{4\mu}{r_i^2}\right)I_1(\tfrac{1}{\sqrt{c}}r_i)\right]C\\&+\left[\frac{2\mu}{\sqrt{c}r_i}K_0(\tfrac{1}{\sqrt{c}}r_i)+\left(\frac{\lambda+2\mu}{c}+\frac{4\mu}{r_i^2}\right)K_1(\tfrac{1}{\sqrt{c}}r_i)\right]D=0,\end{aligned} \tag{5.57c}$$

$$\frac{4\mu}{r_o^3}B+\left[-\frac{2\mu}{\sqrt{c}r_o}I_0(\tfrac{1}{\sqrt{c}}r_o)+\left(\frac{\lambda+2\mu}{c}+\frac{4\mu}{r_o^2}\right)I_1(\tfrac{1}{\sqrt{c}}r_o)\right]C$$
$$+\left[\frac{2\mu}{\sqrt{c}r_o}K_0(\tfrac{1}{\sqrt{c}}r_o)+\left(\frac{\lambda+2\mu}{c}+\frac{4\mu}{r_o^2}\right)K_1(\tfrac{1}{\sqrt{c}}r_o)\right]D=0. \tag{5.57d}$$

Eqs. (5.57a-d) form a system of four linear algebraic equations for determining the four constants A, B, C and D, which depend on the material properties λ, μ (Lamé's constants) and c (the strain gradient coefficient), the geometry parameters r_i and r_o, and the applied pressures p_i and p_o. The matrix form of Eqs. (5.57a-d) is

$$\begin{bmatrix} M_{11} & M_{12} & M_{13} & M_{14} \\ M_{21} & M_{22} & M_{23} & M_{24} \\ M_{31} & M_{32} & M_{33} & M_{34} \\ M_{41} & M_{42} & M_{43} & M_{44} \end{bmatrix}\begin{Bmatrix} A \\ B \\ C \\ D \end{Bmatrix}=\begin{Bmatrix} p_i \\ p_o \\ 0 \\ 0 \end{Bmatrix}, \tag{5.58}$$

where the components of the four by four coefficient matrix are given by

$$M_{11}=M_{21}=-2\lambda-2\mu\,,$$

$$M_{12}=\frac{2\mu}{r_i^2}+\frac{4c\mu}{r_i^4}\,,$$

$$M_{13}=-\frac{2\sqrt{c}\mu}{r_i^2}I_0(\tfrac{1}{\sqrt{c}}r_i)-\left(\frac{\lambda}{r_i}-\frac{4c\mu}{r_i^3}\right)I_1(\tfrac{1}{\sqrt{c}}r_i)\,,$$

$$M_{14}=\frac{2\sqrt{c}\mu}{r_i^2}K_0(\tfrac{1}{\sqrt{c}}r_i)-\left(\frac{\lambda}{r_i}-\frac{4c\mu}{r_i^3}\right)K_1(\tfrac{1}{\sqrt{c}}r_i)\,,$$

$$M_{22}=\frac{2\mu}{r_o^2}+\frac{4c\mu}{r_o^4}\,,$$

$$M_{23}=-\frac{2\sqrt{c}\mu}{r_o^2}I_0(\tfrac{1}{\sqrt{c}}r_o)-\left(\frac{\lambda}{r_o}-\frac{4c\mu}{r_o^3}\right)I_1(\tfrac{1}{\sqrt{c}}r_o)\,,$$

$$M_{24}=\frac{2\sqrt{c}\mu}{r_o^2}K_0(\tfrac{1}{\sqrt{c}}r_o)-\left(\frac{\lambda}{r_o}-\frac{4c\mu}{r_o^3}\right)K_1(\tfrac{1}{\sqrt{c}}r_o)\,,$$

$$M_{31}=M_{41}=0\,,$$

$$M_{32} = \frac{4\mu}{r_i^3},$$

$$M_{33} = -\frac{2\mu}{\sqrt{c}r_i} I_0(\tfrac{1}{\sqrt{c}} r_i) + \left(\frac{\lambda + 2\mu}{c} + \frac{4\mu}{r_i^2} \right) I_1(\tfrac{1}{\sqrt{c}} r_i),$$

$$M_{34} = \frac{2\mu}{\sqrt{c}r_i} K_0(\tfrac{1}{\sqrt{c}} r_i) + \left(\frac{\lambda + 2\mu}{c} + \frac{4\mu}{r_i^2} \right) K_1(\tfrac{1}{\sqrt{c}} r_i),$$

$$M_{42} = \frac{4\mu}{r_o^3},$$

$$M_{43} = -\frac{2\mu}{\sqrt{c}r_o} I_0(\tfrac{1}{\sqrt{c}} r_o) + \left(\frac{\lambda + 2\mu}{c} + \frac{4\mu}{r_o^2} \right) I_1(\tfrac{1}{\sqrt{c}} r_o),$$

$$M_{44} = \frac{2\mu}{\sqrt{c}r_o} K_0(\tfrac{1}{\sqrt{c}} r_o) + \left(\frac{\lambda + 2\mu}{c} + \frac{4\mu}{r_o^2} \right) K_1(\tfrac{1}{\sqrt{c}} r_o). \tag{5.59}$$

For given values of λ, μ, c, r_i, r_o, p_i and p_o, Eq. (5.58) can be readily solved to obtain the four constants A, B, C and D. The displacement field $u = u(r)$ will then be determined from Eqs. (5.33) and (5.50), and the Cauchy stress, total stress and double stress from Eqs. (5.52), (5.54) and (5.55), respectively.

To illustrate the newly derived solution of the cylinder problem, some numerical results have been obtained and presented in Fig. 5.2, where the stress distributions along the cylinder wall given by both the current strain gradient solution and Lamé's solution in classical elasticity are shown. The material properties used in the calculations are taken to be E = 135 GPa, ν = 0.3, and c = 0.05 μm^2, which are the same as those used by Li et al. (2004). For comparison, two other values of the strain gradient coefficient c (depending on the underlying material microstructure) are also used in the calculations shown in Fig. 5.2. The geometric parameters used are r_i = 1 μm and r_o = 5 μm, and the pressures are set to be p_i = 10 MPa, p_o = 0 MPa.

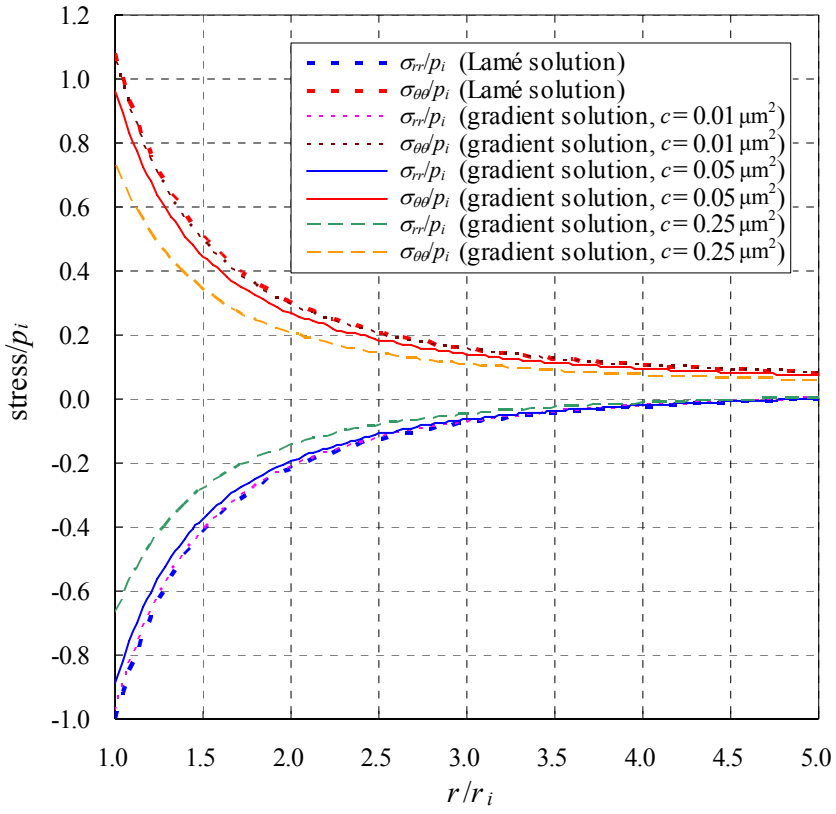

Fig. 5.2. Stress distributions along the cylinder wall.

Clearly, it is seen from Fig. 5.2 that the magnitudes of both $\sigma_{\theta\theta}$ and σ_{rr} given by the strain gradient solution are smaller than those given by the classical elasticity solution in all cases considered. Also, Fig. 5.2 shows that the differences between the current strain gradient solution and Lamé's solution are negligibly small when c is very small (e.g., c = 0.01 μm^2 here), but are significant when c becomes bigger (e.g., c = 0.25 μm^2 here). This indicates that the effect of material microstructures can be large and Lamé's solution may not be accurate for materials that exhibit significant microstructural effects.

5.5. SUMMARY

A variational formulation is provided for a simplified strain gradient elasticity theory by using the principle of minimum total potential energy, which leads to the

simultaneous determination of the governing equations and the complete boundary conditions for the first time. Also, the displacement form of the simplified strain gradient theory is derived here and directly used to solve the problem of a pressurized thick-walled cylinder. A comparison with Lamé's solution in classical elasticity shows that the newly derived strain gradient solution contains an additional material length scale parameter and can account for the microstructural effects, while Lamé's solution does not have the same capability.

CHAPTER VI

CONCLUSIONS

In this dissertation research, variational formulations are provided for two simple higher order elasticity theories – the modified couple stress theory proposed by Yang et al. (2002) and the simplified strain gradient elasticity theory suggested by Altan and Aifantis (1997), both of which contain only one additional material length scale parameter. In both cases, the governing equations and complete boundary conditions are determined simultaneously for the first time by using the principle of minimum total potential energy. Also, the displacement form is explicitly derived for each theory for the first time.

The modified couple stress theory is applied to solve a simple shear problem, to develop a new Bernoulli-Euler beam model, and to derive the constitutive relations for hexagonal honeycomb structures, while the simplified strain gradient elasticity theory is used to solve the pressurized thick-walled cylinder problem.

Numerical results obtained from the newly developed/derived models/solutions and the comparisons with their counterpart results in classical elasticity reveal that the higher order theory based models/solutions have the capacity to account for microstructural effects, whereas their counterparts in classical elasticity do not have the same capability. Nevertheless, the former are shown to recover the latter if the microstructural effects are suppressed or ignored.

More detailed summary is provided at the end of each chapter.

REFERENCES

Aifantis, E.C., 1996, Higher order gradients and size effects, In: Carpinteru, A. editor. *Size-scale effects in the failure mechanisms of materials and structures*, London: E&FN Spon, 231-242.

Altan, B.S. and Aifantis, E.C., 1992, On the structure of the mode III crack-tip in gradient elasticity, *Scripta Met.*, **26**, 319-324.

Altan, B.S. and Aifantis, E.C., 1997, On some aspects in the special theory of gradient elasticity, *J. Mech. Behavior Mater*., **8** (3), 231-282.

Anthoine, A., 2000, Effect of couple-stresses on the elastic bending of beams, *Int. J. Solids Struct*., **37**, 1003-1018.

Casal, P., 1972, *La théorie du second gradient et la capillarité*, C. R. Acad. Sc. Paris A, **274**, 1571-1574.

Chen, J.Y., Huang, Y. and Ortiz, M., 1998, Fracture analysis of cellular materials: A strain gradient model, *J. Mech. Phys. Solids*, **46**, 789-828.

Diebels, S. and Steeb, H., 2002, The size effect in foams and its theoretical and numerical investigation. *Proc. R. Soc. Lond. A*, **458**, 2869-2883.

Diebels, S. and Steeb, H., 2003, Stress and couple stress in foams, *Comput. Mater. Sci.*, **28**, 714-722.

Eringen, A.C., 1983, On differential equations of nonlocal elasticity and solutions of screw dislocation and surface waves, *J. Appl. Phys*., **54**, 4703-4710.

Exadaktylos G.E. and Vardoulakis I., 1998, Surface instability in gradient elasticity with surface energy, *Int. J. Solids Struct.*, **35**, 2251-2281.

Gao, X.-L. and Mall, S., 2001, Variational solution for a cracked mosaic model of woven fabric composites, *Int. J. Solids Struct*., **38**, 855-874.

Gao, X.-L. and Rowlands, R.E., 2000, Hybrid method for stress analysis of finite three-dimensional elastic components. *Int. J. Solids Struct.*, **37**, 2727-2751.

Gibson, L.J. and Ashby, M.F., 1997, *Cellular solids: structure and properties*, Cambridge: Cambridge University Press.

Horstemeyer, M.F., Baskes, M.I., Prantil, V.C., Philliber, J. and Vonderheide, S., 2003, A multiscale analysis of fixed-end simple shear using molecular dynamics, crystal plasticity, and a macroscopic internal state variable theory. *Modelling Simul. Mater. Sci. Eng.*, **11**, 265-286.

Jacobs, J.A. and Kilduff, T.F., 2005, *Engineering materials technology: structures, processing, properties, and selection*, Upper Saddle River, New Jersey: Pearson Prentice Hall.

Koiter, W.T., 1964, Couple-stresses in the theory of elasticity: I and II, *Proc. K. Ned. Akad. Wet*., **B67** (1), 17-44.

Kumar, R. S. and McDowell, D.L., 2004, Generalized continuum modeling of 2-D periodic cellular solids, *Int. J. Solids Struct.*, **41**, 7399-7422.

Lam, D.C.C., Yang, F., Chong, A.C.M., Wang, J. and Tong, P., 2003, Experiments and theory in strain gradient elasticity, *J. Mech. Phys. Solids*, **51**, 1477-1508.

Lamé, G., 1852, *Leçons sur la théorie…de l'élasticité*, Paris: Gautheir-Villars.

Lazopoulos, K.A., 2004, On the gradient strain elasticity theory of plates, *Euro. J. Mech. A/Solids*, **23**, 843-852.

Li, K., Gao, X.-L. and Subhash, G., 2005, Effects of cell shape and cell wall thickness

variations on the elastic properties of two-dimensional cellular solids, *Int. J. Solids Struct.*, **42**, 1777-1795.

Li, S., Miskioglu, I., Altan, B.S., 2004, Solution to line loading of a semi-infinite solid in gradient elasticity, *Int. J. Solids Struct.*, **41**, 3395-3410.

Little, R.W., 1973, *Elasticity*, Englewood Cliffs, New Jersey: Prentice Hall.

McFarland, A.W. and Colton, J.S., 2005, Role of material microstructure in plate stiffness with relevance to microcantilever sensors, *J. Micromech. Microeng*., **15**, 1060-1067.

McLachlan N.W., 1941, *Bessel functions for engineers*, London: Oxford University Press.

Mindlin, R.D., 1963, Influence of couple-stresses on stress concentrations, *Exp. Mech*., **3**, 1-7.

Mindlin, R.D., 1964, Micro-structure in linear elasticity, *Arch. Ration. Mech. Anal.*, **16**, 51-78.

Mindlin R.D., 1965, Second gradient of strain and surface-tension in linear elasticity, *Int. J. Solids Struct.*, **1**, 417-438.

Mindlin, R.D. and Eshel, N.N., 1968, On first strain-gradient theories in linear elasticity, *Int. J. Solids Struct.*, **4**, 109-124.

Mindlin, R.D. and Tiersten, H. F., 1962, Effects of couple-stresses in linear elasticity, *Arch. Rational Mech. Anal*., **11**, 415-448.

Papargyri-Beskou, S., Tsepoura, K.G., Polyzos, D. and Beskos, D.E., 2003, Bending and stability analysis of gradient elastic beams, *Int. J. Solids Struct*., **40**, 385-400.

Park, S.K. and Gao, X.-L., 2006, Bernoulli-Euler beam model based on a modified couple stress theory. *J. Micromech. Microeng*., **16**, 2355-2359.

Park, S.K. and Gao, X.-L., 2006, Variational formulation of a modified couple stress theory and its application to a simple shear problem, *Z. Angew. Math. Phys.* (in press).

Peddieson, J., Buchanan, G.R. and McNitt, R.P., 2003, Application of nonlocal continuum models to nanotechnology, *Int. J. Eng. Sci*., **41**, 305-312.

Pei, J., Tian, F. and Thundat, T., 2004, Glucose biosensor based on the microcantilever, *Analytical Chem*., **76**, 292-297.

Pereira, R.S., 2001, Atomic force microscopy as a novel pharmacological tool, *Biochem. Pharmacology*, **62**, 975–983.

Ru, C.Q. and Aifantis, E.C., 1993, A simple approach to solve boundary-value problems in gradient theory, *Acta Mech.*, **101**, 59-68.

Shames, I.H., 1985, *Energy and finite element methods in structural mechanics*, New York: Hemisphere.

Slaughter, W.S., 2002, *The linearized theory of elasticity*, Boston: Birkhäuser.

Steigmann, D. J., 1992, Equilibrium of prestressed networks, *IMA J. Appl. Math.*, **48**, 195-215.

Tekoglu, C., Onck, P.R., 2005, Size effects in the mechanical behavior of cellular materials. *J. Mater. Sci*., **40**, 5911-5917.

Teneketzis Tenek, L. and Aifantis, E.C., 2001, On some applications of gradient elasticity to composite materials, *Compos. Struct.*, **53**, 189-197.

Timoshenko, S.P. and Goodier, J.N., 1970, *Theory of elasticity*, 3rd edition, New York: McGraw-Hill.

Toupin, R.A., 1962, Elastic materials with couple stresses, *Arch. Rational Mech. Anal*., **11**, 385-414.

Toupin, R.A., 1964, Theories of elasticity with couple stress. *Arch. Rational Mech. Anal*., **17**, 85-112.

Vardoulakis, I. and Giannakopoulos, A.E., 2006, An example of double forces taken from structural analysis, *Int. J. Solids Struct*., **43**, 4047-4062.

Vardoulakis, I. and Sulem, J., 1995, *Bifurcation analysis in geomechanics*, London: Blackie/Chapman and Hall.

Wang, X.L. and Stronge, W.J., 1999, Micropolar theory for two-dimensional stresses in elastic honeycomb, *Proc. R. Soc. Lond.*, **455**, 2091-2116.

Warren, E.W. and Byskov, E., 2002, Three-fold symmetry restrictions on two-dimensional micropolar materials, *Eur. J. Mech. A-Solids*, **21**, 779-792.

Yang, F., Chong, A.C.M., Lam, D.C.C. and Tong, P., 2002, Couple stress based strain gradient theory for elasticity, *Int. J. Solids Struct*., **39**, 2731-2743.

Yang, J.F.C. and Lakes, R.S., 1982, Experimental study of micropolar and couple stress elasticity in compact bone in bending, *J. Biomechanics*, **15**, 91-98.

APPENDIX A

COMPARISON OF VARIOUS HIGHER ORDER ELASTICITY THEORIES

Table 1 presents various higher order theories, and their constitutive equations and equilibrium equations with their displacement forms if applicable.

Table 1. Higher order elasticity theories with material constants

Model	Strain energy density function/Constitutive equation /Equilibrium equation with displacement form	Material constants
Cosserat's model (1909)	$W=\frac{1}{2}\lambda\varepsilon_{ii}\varepsilon_{jj}+\mu\varepsilon_{ij}\varepsilon_{ij}+\frac{1}{2}\kappa\varepsilon_{ij}\varepsilon_{ijk}(r_k-\phi_k)+\frac{1}{2}(\alpha\phi_{i,i}\phi_{j,j}+\beta\phi_{i,j}\phi_{i,j}+\gamma\phi_{i,j}\phi_{j,i})$ $\sigma_{ij}=\lambda\varepsilon_{kk}\delta_{ij}+2\mu\varepsilon_{ij}+\kappa\varepsilon_{ijk}(r_k-\phi_k),\quad m_{ij}=\alpha\phi_{k,k}\delta_{ij}+\beta\phi_{i,j}+\gamma\phi_{j,i}$ $\sigma_{ji,j}+f_i=0,\quad m_{ji,j}+\varepsilon_{ijk}\sigma_{jk}+y_i=0\qquad(r_i=\frac{1}{2}\varepsilon_{ijk}u_{k,j})$	$\lambda,\mu,\kappa,$ α,β,γ
Koiter's couple stress model (1964)	$W=\frac{1}{2}\lambda\varepsilon_{ii}\varepsilon_{jj}+\mu\varepsilon_{ij}\varepsilon_{ij}+2\mu l^2(\chi_{ij}\chi_{ij}+\eta\chi_{ij}\chi_{ji}),\quad \chi_{ij}\neq\chi_{ji}$ $\sigma_{ij}=\lambda\varepsilon_{kk}\delta_{ij}+2\mu\varepsilon_{ij},\quad m_{ij}=4\mu l^2(\chi_{ij}+\eta\chi_{ji})$ $\sigma_{ij,j}+\frac{1}{2}\varepsilon_{ijk}(m_{kl,lj}+y_{k,j})+f_i=0\qquad(\chi_{ij}=\theta_{i,j},\quad\theta_i=\frac{1}{2}\varepsilon_{ijk}u_{k,j})$ $\mu[u_{i,jj}+\frac{1}{1-2\nu}u_{j,ji}-l^2(u_{i,jj}-u_{j,ji}),_{kk}]+\frac{1}{2}\varepsilon_{ijk}y_{k,j}+f_i=0$ (η is omitted.)	$\lambda,\mu,l,$ η
Mindlin's second strain gradient model (1965)	$W=\frac{1}{2}\lambda\varepsilon_{ii}\varepsilon_{jj}+\mu\varepsilon_{ij}\varepsilon_{ij}+a_1\varepsilon_{iik}\varepsilon_{ikk}+a_2\varepsilon_{iik}\varepsilon_{kjj}+a_3\varepsilon_{iik}\varepsilon_{jjk}+a_4\varepsilon_{ijk}\varepsilon_{ijk}$ $+a_5\varepsilon_{ijk}\varepsilon_{kji}+b_1\varepsilon_{iijj}\varepsilon_{kkll}+b_2\varepsilon_{ijkk}\varepsilon_{ijll}+b_3\varepsilon_{iijk}\varepsilon_{jkll}+b_4\varepsilon_{iijk}\varepsilon_{llkj}$ $+b_5\varepsilon_{iijk}\varepsilon_{lljk}+b_6\varepsilon_{ijkl}\varepsilon_{ijkl}+b_7\varepsilon_{ijkl}\varepsilon_{jkli}+c_1\varepsilon_{ii}\varepsilon_{jjkk}+c_2\varepsilon_{ij}\varepsilon_{ijkk}$ $+c_3\varepsilon_{ij}\varepsilon_{kkij}+b_0\varepsilon_{iijj}$ $\varepsilon_{ij}=\frac{1}{2}(u_{i,j}+u_{j,i}),\ \varepsilon_{ijk}=u_{i,jk},\ \varepsilon_{ijkl}=u_{i,jkl}$	$\lambda,\mu,$ $a_1\sim a_5,$ $b_0\sim b_7,$ $c_1\sim c_3$
Mindlin and Eshel's first strain gradient model (1968)	$W=\frac{1}{2}\lambda\varepsilon_{ii}\varepsilon_{jj}+\mu\varepsilon_{ij}\varepsilon_{ij}+c_1\varepsilon_{ij,j}\varepsilon_{ik,k}+c_2\varepsilon_{ii,k}\varepsilon_{jk,j}+c_3\varepsilon_{ii,k}\varepsilon_{jj,k}+c_4\varepsilon_{ij,k}\varepsilon_{ij,k}$ $+c_5\varepsilon_{ij,k}\varepsilon_{jk,i}$ $\tau_{ij}=\lambda\varepsilon_{kk}\delta_{ij}+2\mu\varepsilon_{ij},$ $\mu_{ijk}=c_1(\lambda\delta_{kl}\varepsilon_{lj,l}+\delta_{kl}\varepsilon_{li,l})+\frac{1}{2}c_2(\delta_{kl}\varepsilon_{ll,j}+\delta_{kl}\varepsilon_{ll,i}+2\delta_{ij}\varepsilon_{lk,j})+2c_3\delta_{ij}\varepsilon_{ll,k}$ $+2c_4\varepsilon_{ij,k}+c_5(\varepsilon_{ij,i}+\varepsilon_{ik,j})$ $\{\lambda\delta_{ij}\varepsilon_{kk}+2\mu\varepsilon_{ij}-(c_1+c_5)(\varepsilon_{lj,i}+\varepsilon_{li,j}),_l-c_2(\varepsilon_{ll,ij}+\delta_{ij}\varepsilon_{lk,kl})\},_j$ $-2(c_3\delta_{ij}\varepsilon_{kk,ll}+c_4\varepsilon_{ij,kk}),_j=0$	$\lambda,\mu,$ $c_1\sim c_5$
Altan and Aifantis's model (1997)	$W=\frac{1}{2}\lambda\varepsilon_{ii}\varepsilon_{jj}+\mu\varepsilon_{ij}\varepsilon_{ij}+c(\frac{1}{2}\lambda\varepsilon_{ii,k}\varepsilon_{jj,k}+\mu\varepsilon_{ij,k}\varepsilon_{ij,k})$ $\tau_{ij}=\lambda\varepsilon_{kk}\delta_{ij}+2\mu\varepsilon_{ij},\quad\mu_{ijk}=c(\lambda\varepsilon_{kk}\delta_{ij}+2\mu\varepsilon_{ij}),_j$ $\sigma_{ij,j}+f_i=(\tau_{ij}-\mu_{ijk}),_j+f_i=0$	λ,μ,c
Yang et al.'s model (2002)	$W=\frac{1}{2}\lambda\varepsilon_{ii}\varepsilon_{jj}+\mu\varepsilon_{ij}\varepsilon_{ij}+\mu l^2\chi_{ij}\chi_{ij},\quad\chi_{ij}=\chi_{ji}$ $\sigma_{ij}=\lambda\varepsilon_{kk}\delta_{ij}+2\mu\varepsilon_{ij},\quad m_{ij}=2l^2\mu\chi_{ij}$ $\sigma_{ij,j}+\frac{1}{2}\varepsilon_{ijk}(m_{kl,lj}+y_{k,j})+f_i=0\qquad(\chi_{ij}=\frac{1}{2}(\theta_{i,j}+\theta_{j,i}),\quad\theta_i=\frac{1}{2}\varepsilon_{ijk}u_{k,j})$	λ,μ,l

APPENDIX B

PROOF OF AN IDENTITY

Included in this appendix is a proof of the identity

$$D_j(n_k\mu_{ijk}\delta u_i) = (D_l n_l)n_k n_j \mu_{ijk}\delta u_i + n_q \varepsilon_{qpm}(\varepsilon_{mlj} n_l n_k \mu_{ijk}\delta u_i),_p, \tag{B.1}$$

where

$$D_j(\cdot) = (\delta_{jl} - n_j n_l)(\cdot),_l. \tag{B.2}$$

is the surface gradient (Mindlin, 1964).

Proof. Note that Eq. (B.1) can be rewritten as

$$n_q \varepsilon_{qpm}\varepsilon_{mlj}(n_l n_k \mu_{ijk}\delta u_i),_p = D_j(n_k\mu_{ijk}\delta u_i) - (D_l n_l)n_k n_j \mu_{ijk}\delta u_i, \tag{B.3}$$

where ε_{ijk} *is* the permutation symbol. By using the identity $\varepsilon_{qpm}\varepsilon_{mlj} = \delta_{ql}\delta_{pj} - \delta_{qj}\delta_{pl}$, the left hand side of Eq. (B.3) becomes

$$n_q \varepsilon_{qpm}\varepsilon_{mlj}(n_l n_k \mu_{ijk}\delta u_i),_p = n_q\delta_{ql}\delta_{pj}(n_l n_k \mu_{ijk}\delta u_i),_p - n_q\delta_{qj}\delta_{pl}(n_l n_k \mu_{ijk}\delta u_i),_p, \tag{B.4}$$

which, upon invoking the properties of the Kronecker delta δ_{ij}, changes to

$$n_q \varepsilon_{qpm}\varepsilon_{mlj}(n_l n_k \mu_{ijk}\delta u_i),_p = n_l(n_l n_k \mu_{ijk}\delta u_i),_j - n_j(n_l n_k \mu_{ijk}\delta u_i),_l. \tag{B.5}$$

Using the chain rule to expand Eq. (B.5) gives

$$\begin{aligned} n_q \varepsilon_{qpm}\varepsilon_{mlj}(n_l n_k \mu_{ijk}\delta u_i),_p &= n_l n_{l,j} n_k \mu_{ijk}\delta u_i + n_l n_l n_{k,j}\mu_{ijk}\delta u_i + n_l n_l n_k \mu_{ijk,j}\delta u_i \\ &+ n_l n_l n_k \mu_{ijk}\delta u_{i,j} - n_j n_{l,l} n_k \mu_{ijk}\delta u_i - n_j n_l n_{k,l}\mu_{ijk}\delta u_i - n_j n_l n_k \mu_{ijk,l}\delta u_i - n_j n_l n_k \mu_{ijk}\delta u_{i,l} \end{aligned} \tag{B.6}$$

Note that $\mathbf{n} = n_l\mathbf{e}_l$ is a unit vector with

$$\mathbf{n}\cdot\mathbf{n} = n_l n_l = 1. \tag{B.7}$$

Inserting Eq. (B.7) into Eq. (B.6) then leads to

$$\begin{aligned} n_q \varepsilon_{qpm}\varepsilon_{mlj}(n_l n_k \mu_{ijk}\delta u_i),_p &= n_l n_{l,j} n_k \mu_{ijk}\delta u_i + n_{k,j}\mu_{ijk}\delta u_i + n_k \mu_{ijk,j}\delta u_i + n_k \mu_{ijk}\delta u_{i,j} \\ &- n_j n_{l,l} n_k \mu_{ijk}\delta u_i - n_j n_l n_{k,l}\mu_{ijk}\delta u_i - n_j n_l n_k \mu_{ijk,l}\delta u_i - n_j n_l n_k \mu_{ijk}\delta u_{i,l} \end{aligned} \tag{B.8}$$

From the identity for two arbitrary vectors **u** and **v**:

$$(u_i v_i),_j = u_{i,j}v_i + u_i v_{i,j} \quad \text{or} \quad \nabla(\mathbf{u}\cdot\mathbf{v}) = (\nabla\mathbf{u})^{\mathrm{T}}\mathbf{v} + (\nabla\mathbf{v})^{\mathrm{T}}\mathbf{u}, \tag{B.9}$$

it follows that

$$(n_l n_l)_{,j} = 2n_{l,j} n_l = 0 \quad \text{or} \quad \nabla(\mathbf{n}\cdot\mathbf{n}) = 2(\nabla\mathbf{n})^{\mathrm{T}}\mathbf{n} = 0\,. \tag{B.10}$$

Using Eq. (B.10) in Eq. (B.8) then gives

$$\begin{aligned} n_q \varepsilon_{qpm}\varepsilon_{mlj}(n_l n_k \mu_{ijk}\delta u_i)_{,p} &= n_{k,j}\mu_{ijk}\delta u_i + n_k \mu_{ijk,j}\delta u_i + n_k \mu_{ijk}\delta u_{i,j} - n_j n_{l,l} n_k \mu_{ijk}\delta u_i \\ &- n_j n_l n_{k,l}\mu_{ijk}\delta u_i - n_j n_l n_k \mu_{ijk,l}\delta u_i - n_j n_l n_k \mu_{ijk}\delta u_{i,l}\,. \end{aligned} \tag{B.11}$$

Now, applying Eq. (B.2) to the first term of the right hand side of Eq. (B.3) yields

$$D_j(n_k \mu_{ijk}\delta u_i) = \delta_{jl}(n_k \mu_{ijk}\delta u_i)_{,l} - n_j n_l (n_k \mu_{ijk}\delta u_i)_{,l}\,, \tag{B.12}$$

which, upon the use of chain rule, becomes

$$\begin{aligned} D_j(n_k \mu_{ijk}\delta u_i) &= n_{k,j}\mu_{ijk}\delta u_i + n_k \mu_{ijk,j}\delta u_i + n_k \mu_{ijk}\delta u_{i,j} - n_j n_l n_{k,l}\mu_{ijk}\delta u_i \\ &- n_j n_l n_k \mu_{ijk,l}\delta u_i - n_j n_l n_k \mu_{ijk}\delta u_{i,l}\,. \end{aligned} \tag{B.13}$$

Similarly, applying Eq. (B.2) to the second term of Eq. (B.3) and using the chain rule will result in

$$(D_l n_l) n_k n_j \mu_{ijk}\delta u_i = n_{l,l}\, n_k n_j \mu_{ijk}\delta u_i - n_l n_m n_{l,m}\, n_k n_j \mu_{ijk}\delta u_i\,. \tag{B.14}$$

Using Eq. (B.10) in Eq. (B.14) gives

$$(D_l n_l) n_k n_j \mu_{ijk}\delta u_i = n_{l,l}\, n_k n_j \mu_{ijk}\delta u_i\,. \tag{B.15}$$

Combining Eqs. (B.13) and (B.15) then leads to

$$\begin{aligned} D_j(n_k \mu_{ijk}\delta u_i) - (D_l n_l) n_k n_j \mu_{ijk}\delta u_i &= n_{k,j}\mu_{ijk}\delta u_i + n_k \mu_{ijk,j}\delta u_i + n_k \mu_{ijk}\delta u_{i,j} - n_j n_l n_{k,l}\mu_{ijk}\delta u_i \\ &- n_j n_l n_k \mu_{ijk,l}\delta u_i - n_j n_l n_k \mu_{ijk}\delta u_{i,l} n_{l,l}\, n_k n_j \mu_{ijk}\delta u_i\,. \end{aligned} \tag{B.16}$$

A comparison of Eqs. (B.11) and (B.16) immediately shows that (B.3) is true, thereby proving the identity given in Eq. (B.1).

APPENDIX C

GRADIENTS OF SECOND AND THIRD ORDER TENSORS

It is shown here that the total stress has the following expression (see Eq. (5.54)):

$$\boldsymbol{\sigma} = \left[\tau_{rr} - c\left(\tau''_{rr} + \frac{\tau'_{rr}}{r} - \frac{2\tau_{rr}}{r^2} + \frac{2\tau_{\theta\theta}}{r^2} \right) \right] \mathbf{e}_r \otimes \mathbf{e}_r + \left[\tau_{\theta\theta} - c\left(\tau''_{\theta\theta} + \frac{\tau'_{\theta\theta}}{r} - \frac{2\tau_{\theta\theta}}{r^2} + \frac{2\tau_{rr}}{r^2} \right) \right] \mathbf{e}_\theta \otimes \mathbf{e}_\theta$$
$$+ \left[\tau_{zz} - c\left(\tau''_{zz} + \frac{\tau'_{zz}}{r} \right) \right] \mathbf{e}_3 \otimes \mathbf{e}_3, \tag{C.1}$$

and the double stress can be expressed as (see Eq. (5.55))

$$\begin{aligned} \boldsymbol{\mu} = c\Big[& \tau'_{rr} \mathbf{e}_r \otimes \mathbf{e}_r \otimes \mathbf{e}_r + \frac{1}{r}(\tau_{rr} - \tau_{\theta\theta}) \mathbf{e}_r \otimes \mathbf{e}_\theta \otimes \mathbf{e}_\theta + \frac{1}{r}(\tau_{rr} - \tau_{\theta\theta}) \mathbf{e}_\theta \otimes \mathbf{e}_r \otimes \mathbf{e}_\theta \Big] \\ & + c\left(\tau'_{\theta\theta} \mathbf{e}_\theta \otimes \mathbf{e}_\theta \otimes \mathbf{e}_r + \tau'_{zz} \mathbf{e}_3 \otimes \mathbf{e}_3 \otimes \mathbf{e}_r \right), \end{aligned} \tag{C.2}$$

Proof. Note that Eq. (5.52) can be rewritten as

$$\tau(r) = \tau_{rr}(r) \mathbf{e}_r \otimes \mathbf{e}_r + \tau_{\theta\theta}(r) \mathbf{e}_\theta \otimes \mathbf{e}_\theta + \tau_{zz}(r) \mathbf{e}_3 \otimes \mathbf{e}_3, \tag{C.3}$$

where the stress components are given in Eq. (5.53). Then, it follows from Eq. (C.3) that

$$\begin{aligned} \nabla \boldsymbol{\tau}(r) &= \nabla(\tau_{rr} \mathbf{e}_r \otimes \mathbf{e}_r) + \nabla(\tau_{\theta\theta} \mathbf{e}_\theta \otimes \mathbf{e}_\theta) + \nabla(\tau_{zz} \mathbf{e}_3 \otimes \mathbf{e}_3) \\ &= (\mathbf{e}_r \otimes \mathbf{e}_r) \otimes \nabla \tau_{rr} + \tau_{rr} \nabla(\mathbf{e}_r \otimes \mathbf{e}_r) + (\mathbf{e}_\theta \otimes \mathbf{e}_\theta) \otimes \nabla \tau_{\theta\theta} + \tau_{\theta\theta} \nabla(\mathbf{e}_\theta \otimes \mathbf{e}_\theta) \\ &\quad + (\mathbf{e}_3 \otimes \mathbf{e}_3) \otimes \nabla \tau_{zz} + \tau_{zz} \nabla(\mathbf{e}_3 \otimes \mathbf{e}_3), \end{aligned} \tag{C.4}$$

where use has been made of the identity:

$$\nabla(\phi \mathbf{A}) = \mathbf{A} \otimes \nabla \phi + \phi \nabla \mathbf{A}, \tag{C.5}$$

with ϕ being a scalar field and $\mathbf{A}$ being a second-order tensor field. After tedious derivations involving the coordinate transformations between the polar cylindrical coordinate system with the base vectors $\{\mathbf{e}_r, \mathbf{e}_\theta, \mathbf{e}_3\}$ and the Cartesian coordinate system with the base vectors $\{\mathbf{e}_1, \mathbf{e}_2, \mathbf{e}_3\}$, it can be shown that Eq. (C.4) eventually becomes

$$\nabla \boldsymbol{\tau}(r) = \tau'_{rr} \mathbf{e}_r \otimes \mathbf{e}_r \otimes \mathbf{e}_r + \left(\frac{\tau_{rr}}{r} - \frac{\tau_{\theta\theta}}{r} \right) \mathbf{e}_r \otimes \mathbf{e}_\theta \otimes \mathbf{e}_\theta + \left(\frac{\tau_{rr}}{r} - \frac{\tau_{\theta\theta}}{r} \right) \mathbf{e}_\theta \otimes \mathbf{e}_r \otimes \mathbf{e}_\theta$$
$$+ \tau'_{\theta\theta} \mathbf{e}_\theta \otimes \mathbf{e}_\theta \otimes \mathbf{e}_r + \tau'_{zz} \mathbf{e}_3 \otimes \mathbf{e}_3 \otimes \mathbf{e}_r. \tag{C.6}$$

This gives the gradient of the Cauchy stress in the polar cylindrical coordinate system, which is a third-order tensor. Using Eq. (C.6) in Eq. (5.5) will immediately give the expression for the double stress $\boldsymbol{\mu}$ listed above in Eq. (C.2).

Similarly, after very lengthy derivations the gradient of the third-order tensor $\nabla\boldsymbol{\tau}$ can be determined from Eq. (C.6) to be

$$\nabla\nabla\boldsymbol{\tau}(r) = \tau''_{rr}\mathbf{e}_r\otimes\mathbf{e}_r\otimes\mathbf{e}_r\otimes\mathbf{e}_r + \left(\frac{\tau'_{rr}}{r} - \frac{2\tau_{rr}}{r^2} + \frac{2\tau_{\theta\theta}}{r^2}\right)\mathbf{e}_r\otimes\mathbf{e}_r\otimes\mathbf{e}_\theta\otimes\mathbf{e}_\theta$$

$$+\left(\frac{\tau'_{rr}}{r} - \frac{\tau'_{\theta\theta}}{r} - \frac{\tau_{rr}}{r^2} + \frac{\tau_{\theta\theta}}{r^2}\right)\mathbf{e}_r\otimes\mathbf{e}_\theta\otimes\mathbf{e}_r\otimes\mathbf{e}_\theta + \left(\frac{\tau'_{rr}}{r} - \frac{\tau'_{\theta\theta}}{r} - \frac{\tau_{rr}}{r^2} + \frac{\tau_{\theta\theta}}{r^2}\right)\mathbf{e}_r\otimes\mathbf{e}_\theta\otimes\mathbf{e}_\theta\otimes\mathbf{e}_r$$

$$+\left(\frac{\tau'_{rr}}{r} - \frac{\tau'_{\theta\theta}}{r} - \frac{\tau_{rr}}{r^2} + \frac{\tau_{\theta\theta}}{r^2}\right)\mathbf{e}_\theta\otimes\mathbf{e}_r\otimes\mathbf{e}_r\otimes\mathbf{e}_\theta + \left(\frac{\tau'_{rr}}{r} - \frac{\tau'_{\theta\theta}}{r} - \frac{\tau_{rr}}{r^2} + \frac{\tau_{\theta\theta}}{r^2}\right)\mathbf{e}_\theta\otimes\mathbf{e}_r\otimes\mathbf{e}_\theta\otimes\mathbf{e}_r$$

$$+\tau''_{\theta\theta}\mathbf{e}_\theta\otimes\mathbf{e}_\theta\otimes\mathbf{e}_r\otimes\mathbf{e}_r + \left(\frac{\tau'_{\theta\theta}}{r} + \frac{2\tau_{rr}}{r^2} - \frac{2\tau_{\theta\theta}}{r^2}\right)\mathbf{e}_\theta\otimes\mathbf{e}_\theta\otimes\mathbf{e}_\theta\otimes\mathbf{e}_\theta$$

$$+\tau''_{zz}\mathbf{e}_z\otimes\mathbf{e}_z\otimes\mathbf{e}_r\otimes\mathbf{e}_r + \frac{\tau'_{zz}}{r}\mathbf{e}_z\otimes\mathbf{e}_z\otimes\mathbf{e}_\theta\otimes\mathbf{e}_\theta\,. \tag{C.7}$$

It then follows from Eq. (C.7) that

$$\nabla^2\boldsymbol{\tau}(r) = \nabla\cdot\nabla\boldsymbol{\tau}(r) = \left(\tau''_{rr} + \frac{\tau'_{rr}}{r} - \frac{2\tau_{rr}}{r^2} + \frac{2\tau_{\theta\theta}}{r^2}\right)\mathbf{e}_r\otimes\mathbf{e}_r + \left(\tau''_{\theta\theta} + \frac{\tau'_{\theta\theta}}{r} - \frac{2\tau_{\theta\theta}}{r^2} + \frac{2\tau_{rr}}{r^2}\right)\mathbf{e}_\theta\otimes\mathbf{e}_\theta$$

$$+\left(\tau''_{zz} + \frac{\tau'_{zz}}{r}\right)\mathbf{e}_3\otimes\mathbf{e}_3\,. \tag{C.8}$$

Using Eqs. (C.3) and (C.8) in Eq. (5.13) will immediately give Eq. (C.1).

VITA

Sung Kyoon Park graduated from Sungbo High school in Seoul, Korea in 1993. He entered the Mechanical Engineering program at Kookmin University in Seoul, Korea in March 1993 and received his Bachelor of Engineering degree in February 2000. He entered the Machine and Production Engineering program at Hanyang University in Seoul, Korea in March 2000 and received his Master of Science degree in February 2002. The title of his master thesis is "Structural Analysis and Optimum Design of a Micro-Gyroscope." He started his doctoral studies in the Department of Mechanical Engineering at Texas A&M University in August 2003 and received his Ph.D. in December 2006.

Sung Kyoon Park's permanent address is

1634-49 Shillim 1-Dong,
Kwanak-Gu, Seoul 151-900, Korea.
E-mail: parksungkyoon@yahoo.co.kr.